INTERNAL FRICTION AND HIGH TEMPERATURE

MEASUREMENTS ON REFRACTORY MATERIALS

by

JOHN MICHAEL PELMORE

Submitted for the degree of Doctor of Philosophy

at

The University of Aston in Birmingham

August 1975

SUMMARY

A new method for measuring internal friction has been developed. It is particularly suitable for high temperature work, and has been applied to measurements in the 1000°C-2000°C temperature range. Grain boundary and background damping results for a number of refractory materials are given for the 100 kHz region and compared with existing 1 Hz data where available. A new internal friction peak in hot pressed silicon nitride at 1160°C with a half width corresponding to 2.5eV and a height of 0.075 is reported.

The method uses a resonator made of the specimen material, coupled to a magnetostrictive transducer by means of a long acoustic transmission line. The resonator is excited by bursts of oscillation fed into the transducer and echoes received from the resonator are analysed to yield information about the specimen. Various methods of extracting internal friction data from the echo are considered in detail and tests to validate the method using pure polycrystalline copper are described. An important pre-requisite is the fabrication of good acoustic joints and particulars of these are given.

The application of the results to ultrasonic thermometer probe design is discussed. Two prototype test probes made of iridium and sapphire showed good results up to 2000°C and 1900°C respectively in a flame.

A preliminary study of an internal friction method for the trace analysis of oxygen in liquid sodium showed the feasibility of a direct reading instrument to detect oxygen levels of 1ppm.

ACKNOWLEDGEMENTS

CONTENTS

LIST OF ILLUSTRATIONS

LIST OF SYMBOLS

A   amplitude, area of cross section, pre-exponential factor

A_o initial amplitude

c   rod velocity of ultrasonic waves, concentration

D   diameter of transmission line

E   echo amplitude, Youngs modulus, activation energy

E_o initial echo amplitude

E_∞ asymptotic value of amplitude of echo signal

E_e end echo amplitude

E_s shoulder echo amplitude

ΔE_o 'true' activation energy in Schoek formula

f   frequency, force

f_o resonant frequency

G   shear modulus

ΔG free energy change

Δ_G relaxation strength per atom %

J   junction echo amplitude

K   see equ. 4.30

k   Boltzmann constant, damping coefficient

l   length

M   dynamic Youngs modulus

M_u unrelaxed modulus

M_R relaxed modulus

$\overline{M}$ complex modulus

m   mass, mode number

Δm relaxation strength (twice the peak height)

n   frequency dependence factor (see equ. 2.41)

n_o oscillations to crossover for $Q_m^{-1} = 0$

n_x oscillations to crossover

P   force

Q   Q value

Q_c coupling Q

Q_m^{-1}, Q^{-1} internal friction (material loss)

Q_T 'total Q' $(Q_T^{-1} = Q_c^{-1} + Q_m^{-1})$

R   reflection amplitude, universal gas constant

S   strain

T   temperature measured in degrees K, stress, transmission coefficient

t   time

u   atomic displacement

W   energy

$W_{\frac{1}{2}}$ half width

$X = E_s/E_e$ for zero attenuation

$Z = \rho c A$ acoustic impedance

Z_l line impedance

Z_r resonator impedance

α attenuation coefficient

β distribution function

ϕ loss angle, potential energy

ρ density

σ Poisson's ratio

θ temperature in °C, phase angle

τ relaxation time

τ_o pre-exponential factor

τ_s strain relaxation time

τ_T stress relaxation time

ω angular frequency

ω_o resonant or relaxation frequency

ω_n natural resonant frequency

ω_s transmitter frequency

Useful constants

$1 \text{ eV} = 96.49 \text{ kJ mole}^{-1} = 23.05 \text{ kcal mole}^{-1}$

$k = 8.65 \times 10^{-5} \text{ eV}$

$N = 6.024 \times 10^{23} \text{ molecule mole}^{-1}$

$R = 8.314 \text{ J k}^{-1} \text{ mole}^{-1} = 1.987 \text{ cal K}^{-1} \text{mole}^{-1}$

CHAPTER 1 : GENERAL INTRODUCTION

The usefulness of internal friction in the study of the
defect structure of solids has become recognised over the
last twenty years. There are also several industrial
applications, an example being the use of internal friction
methods to determine the quantity of interstitial solutes
in metals, which can grossly affect the metallurgical
properties. Instrumentation applications lie in the field
of vibrating transducers, an example being the ultrasonic
thermometer. The use of the internal friction technique
at very high temperatures has been a rather neglected area
of the subject, partly due to experimental difficulties.
This thesis describes measurements in the 1000°C-2000°C
temperature range and grain boundary and background damping
data are reported for a frequency of the order of 100 kHz,
the results being compared with 1 Hz data where available.

A new method, particularly suited to high temperature work,
has been developed for these measurements. It consists in
essence of a resonant specimen coupled to a long acoustic
transmission line. The other end is terminated with a
transducer which is thus remote from the specimen in the
furnace. Bursts of energy are applied to the transducer to
excite resonances in the specimen. From analysis of the
echoes received from the resonator the properties of the
specimen, including internal friction can be deduced.

In the final chapters two technical applications of the
results are described. The ultrasonic thermometer employs
a resonator whose frequency changes with temperature. The

design of these thermometers thus requires the detailed knowledge of its elastic properties. Two complete prototype high temperature probes have been made and shown good results in a flame up to 2000°C.

A second application is the measurement of traces of oxygen in liquid sodium by an internal friction method. A vanadium ultrasonic probe absorbs oxygen from the sodium and the concentration can be estimated from the height of the internal friction peak. This is capable of making a direct reading instrument.

Some useful general texts are:

Metallurgy: Smallman (1971), Reed Hill (1964)
Acoustics: Stephens and Bate (1966), Morse (1948)
Acoustic properties of solids: Mason (1958), Kolsky (1967)
High temperature technology: Campbell and Sherwood (1967)

The electronic instrumentation has not been described in detail, the text being confined to block diagrams but the full circuits are given appendix B.

CHAPTER 2:   INTERNAL FRICTION AND ELASTICITY

2.1   Introduction

Internal friction and elastic properties of materials have
been measured for many years, both for direct engineering
use and as a means of studying material structure.   The
elastic constants are obviously required for the calculation
of deformation of a structure under load and the frequencies
of vibrational modes.   These elastic properties are also
dependent on material structure - for example when a
material undergoes a phase change the elastic moduli will
change.

Internal friction is very highly structure sensitive and this
accounts for its importance.   This property can also be
described as mechanical damping or Q.   Materials with low
internal friction like aluminium are sonorous.   Lead has
very high internal friction at room temperature and is not
sonorous.   Cooling it down in liquid nitrogen enables it to
ring like a bell - an example of the frequently observed
strong temperature dependence of internal friction.   Defects
in crystals such as dislocations, interstitial and sub-
stitutional solutes, and grain boundaries markedly affect
internal friction.   Thus this method forms one of a battery
of techniques, including electron microscopy and x-ray
diffraction for studying defects in solids.   The defects
in turn affect mechanical properties such as hardness and
creep.   It is also able to provide some thermodynamic data
and can be used as a method of chemical analysis.   A more
direct use is the calculation of vibration amplitudes in

acoustic transducers and machinery. In acoustic transducers resonance is desirable (e.g. the ultrasonic thermometer) and the internal friction must be low. The very low internal friction of quartz finds an application in the highly stable quartz crystal oscillator. In machinery vibration is unwanted and high internal friction is desirable. Special high damping alloys (e.g. manganese copper) can be designed so that the frequency of vibration coincides with an internal friction peak.

In this chapter a brief review will be given of the elastic and anelastic properties of materials.

2.2 Young's modulus

Young's modulus is defined:

$$\text{Young's modulus E} = \frac{\text{stress}}{\text{strain}}$$

Discussion in this chapter will be confined to small strain behaviour. Young's modulus varies quite widely between different metals - for iridium it is 52×10^9 Nm^{-2} and for lead it is 1.6×10^9 Nm^{-2}. The differences in the magnitude of Young's modulus for different materials are connected with the strength of the bonds holding the atoms together. Strong bonds, as in tungsten produce properties such as high melting point, latent heat of fusion and Young's modulus. In randomly orientated polycrystalline materials Young's modulus is an isotropic property. For single crystals, grain orientated materials and fibre and laminar composites it will be anisotropic. Two example are given below:

copper (fcc) $\dfrac{E_{111}}{E_{100}} = 2.8$

aluminium (fcc) $\dfrac{E_{111}}{E_{100}} = 1.2$

Defects such as dislocations tend to reduce Young's modulus so that annealing a cold worked material will increase its Young's modulus as well as improving its ductility. More exactly Young's modulus is related to the dependence of potential energy on atomic separation (Hall 1968, Hearman 1946)

$$f = \frac{d\phi(u)}{du}$$

f = force

ϕ = potential energy

u = atomic displacement

Expressing the potential energy as a Taylor series,

$$\phi(u) = \phi_0 + \left(\frac{d\phi}{du}\right)_0 u + \left(\frac{d^2\phi}{du^2}\right) \frac{u^2}{2}$$

Let the potential energy minimum occur when U = 0. At this point,

$$\frac{d\phi}{du} = 0$$

Hence

$$\phi(u) \simeq \phi_0 + \left(\frac{d^2\phi}{du^2}\right)_0 \frac{u^2}{2}$$

and

$$f \simeq \frac{d\phi(u)}{du} \simeq \left(\frac{d^2\phi}{du^2}\right)_0 (u)$$

i.e. force = const x strain

If $\phi(u)$ is known for an atom in a crystal Young's modulus can be calculated. This is only known in a very few cases, but where it is known there is good agreement with the experimental value.

So far only the static value of Young's modulus has been defined but a dynamic value can be similarly defined, which may be frequency dependent. Under the action of an alternating stress T the strain S may have a phase lag expressed by:

$$T = T_o \exp iwt \qquad\qquad 2.1$$

$$S = (S_1 - iS_2)\exp iwt \qquad\qquad 2.2$$

Two new moduli may now be defined:

Dynamic modulus $M = \dfrac{T_o}{S_1}$

$$\qquad\qquad 2.3$$

Complex modulus $\overline{M} = \dfrac{T_o}{S_1 - iS_2}$

$$\qquad\qquad 2.4$$

Putting $\dfrac{S_2}{S_1} = \tan \phi$ for small ϕ (= loss angle)

$$\overline{M} \rightleftharpoons M(1 + i\phi) \qquad\qquad 2.5$$

ϕ is a measure of the damping or internal friction. At sufficiently low frequencies the dynamic modulus is the same as the static modulus, often known as the relaxed modulus M_R. At high frequencies the dynamic modulus may increase to a value known as the unrelaxed modulus M_u. This frequency variation will be dealt with in more detail in 2.3a.

Young's modulus decreases with increasing temperature

(examples of exceptions to this rule are graphite and pyrex glass) and the value near the melting point can be as low as half the room temperature value. The temperature variation is illustrated in figure 2.1. . A noticeable feature is the knee in the curve for a polycrystalline material, occurring at about half the melting point if it is pure. At this temperature(the recrystallisation temperature) the grain boundaries become mobile giving easier deformation of the material, and there is a large associated internal friction peak. When this or any other internal friction peak is traversed there will be an unrelaxed modulus - relaxed modulus transition (see 2.3a). Another feature that sometimes occurs for cold worked materials is a sudden trough in the Young's modulus - temperature characteristic, without an associated internal friction peak. For examples see the results for copper (figure 4.16) and rhenium (figure 5.9). This is due to a recovery process in which slip is taking place (e.g. Batist 1972 p.260).

2.3 Internal friction

If a resonant system such as a tuning fork is set vibrating then in the absence of a driving force the oscillations will die away. The tuning fork loses some of its energy by radiation through the air as sound and some of its energy is lost by internal friction in the material. This can be measured by observing the exponential decay of the oscill-ations. In the case of an ordinary musical tuning fork, the experiment would have to be performed in vacuum to eliminate the radiation loss.

Internal friction is defined in terms of 'Q'

$$Q = \frac{\text{energy stored}}{\text{energy lost per radian}} = \frac{2\pi W}{\Delta W} \qquad 2.6$$

ΔW = energy loss per cycle

Converting to amplitudes the expression for the exponential decay is:

$$A_2 = A_1 \exp - \pi n/Q \qquad 2.7$$

Where A_1 is an initial amplitude and A_2 is the amplitude after a number of oscillations n.

The Q of some materials is given below:

Quartz crystal $\qquad\qquad 10^7$

Aluminium (commercial) $\quad 3 \times 10^4$

Pyrex glass $\qquad\qquad 2 \times 10^3$

Lead (commercial) $\qquad 3 \times 10^2$

The data given is for room temperature, kHz frequencies and small vibration amplitude.

The most commonly used unit of internal friction is the quantity Q^{-1} (dimensionless). Other measures are:

log decrement $\delta \qquad Q^{-1} = \frac{\delta}{\pi} = \frac{1}{\pi} \ln(A_n/A_{n+1})$

damping factor Δ
or capacity $\qquad\qquad Q^{-1} = \frac{\Delta}{2\pi} = \frac{1}{2\pi} (\Delta W/W)$

loss angle $\phi \qquad\qquad Q^{-1} = \tan \phi \simeq \phi$

hysteretic constant h $\qquad Q^{-1} = \frac{h}{\pi}$

attenuation coefficient $\alpha \qquad Q^{-1} = \frac{c\alpha}{\pi f}$

$\qquad\qquad c$ = group velocity

the numerical conversion factor is given by:

$$Q^{-1} = \frac{0.115}{\pi} \frac{\alpha}{f} \qquad .$$

α = attenuation coefficient dB μS^{-1}

f = frequency MHz

There are four main factors which affect the internal friction of a given material:

1. microstructure
2. temperature
3. frequency
4. strain amplitude

Internal friction measurements are usually made as a function of increasing temperature and a number of peaks will be seen together with an increasing background loss, illustrated for iron in figure 2.2. In the next section internal friction will be treated on a phenomenological basis, making use of mechanical models and in later sections the physical basis will be described.

2.3a Phenomenological approach to internal friction

Internal friction is often measured by means of a resonant system of some kind and the subject will be introduced by this means.

viscous damping force $k\dot{x}$

SPRING MODULUS M
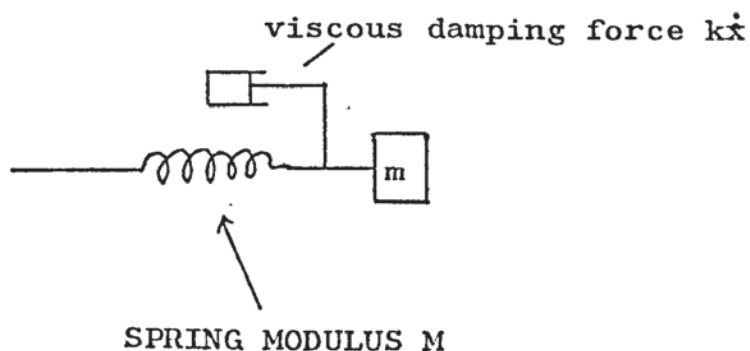
The spring, dashpot and mass represent the material but the mass m may include a large external mass to bring the resonant frequency down to a low value as in the case of a torsion pendulum. In the case of the bar resonator the mass is exclusively that of the material.

The equation of motion of a damped system is:

$$m\ddot{x} + k\dot{x} + Mx = P_o \exp i\omega t \qquad 2.8$$

k is assumed independent of x, $\dot{x}$

Considering first the transient solution if the system is displaced and released it will oscillate with decaying amplitude according to:

$$x = x_o \exp - \pi n k \omega_n / M \qquad 2.9$$

where $\omega_n \simeq \omega_o = \sqrt{\dfrac{M}{m}}$ for small damping $\quad 2.10$

working out the energy loss per cycle, we may calculate the Q of the system Q_s

$$\frac{\Delta W}{W} = \frac{2\pi k \omega_o}{M} = 2\pi Q_s^{-1}$$

$$\text{i.e.} \quad Q_s = \frac{M}{k\omega_o}$$

By using different masses m the resonant frequency of the system may be altered and the Q of the material Q_m is given generally by:

$$Q_m^{-1} = k\omega/M \qquad 2.11$$

Notice that the material loss increases with frequency with the simple spring-dashpot representation, and that the definition of Q_m does not depend on the mass. The electrical

equivalent of the spring and dashpot is a capacitor in parallel with a resistor.

Considering now forced oscillating the solution is:

$$x = \frac{P_o \cos(\omega t - \Theta)}{m\sqrt{(\omega_o^2 - \omega^2) + \frac{\omega^2 k^2}{m^2}}}$$

2.12

where Θ is the phase angle between the driving force and displacement, and is given by:

$$\tan \Theta = \frac{k\omega}{m(\omega_o^2 - \omega^2)}$$

2.13

There are two useful ways of determining the internal friction from the forced oscillations. In the sub-resonance method (useful for high damping) ω is made much less than ω_o and the phase angle Θ is measured.

From equations 2.10, 2.11, 2.13,

$$\tan \Theta = \frac{k\omega_o^2 \omega}{m(\omega_o^2 - \omega^2)} = Q_m^{-1} \frac{\omega_o^2}{(\omega_o^2 - \omega^2)} \rightleftharpoons Q_m^{-1} = \tan \phi$$

2.14

Thus measurement of $\tan \Theta$ gives Q_m^{-1} directly. The phase angle under these conditions ($\omega \ll \omega_o$) is equal to the loss angle ϕ. This is also the method used for determining dielectric loss in a capacitor.

When the damping is small the determination of the width of the resonance is a better method. For the half power points (or $\frac{1}{2}\sqrt{2}$ amplitude points)

$$Q_s^{-1} \rightleftharpoons \frac{\Delta\omega}{\omega_o} \rightleftharpoons Q_m^{-1} \qquad \text{for small } \Delta\omega$$

2.15

Equation 2.8 can be rewritten in the form:

$$m\ddot{x} + M(1+i\phi)x = P_o \exp i\omega t \qquad 2.16$$

$$\text{where } M\phi = kw \quad \text{and} \quad Q_m^{-1} = \tan\phi$$

In the forgoing analysis the damping parameter k has been assumed constant. Amplitude dependence will not be considered here but it is described by De Batist (1972). One consequence is that the resonant frequency becomes a function of the driving force and the resonance curve is distorted. These effects have been shown to occur in a dramatic form in lead single crystals (Baker 1972) and are a general feature of dislocation damping.

In the system discussed the internal friction will be proportional to frequency (see equation 2.11). In physical terms this means as the mass m is reduced increasing the resonant frequency, the internal friction increases. This corresponds to a model known as the Voigt linear solid.

The frequency dependence of internal friction can be classified into three important types.

1. Hysteretic damping - the damping is independent of frequency.

2. Viscous damping - the internal friction is proportional to frequency.

3. Anelastic damping - an internal friction peak is seen at a certain frequency.

Hysteretic damping will first be briefly disposed of:

The system may be represented thus:
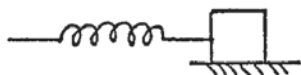
frictional force F
independent of velocity
but may depend on dis-
placement
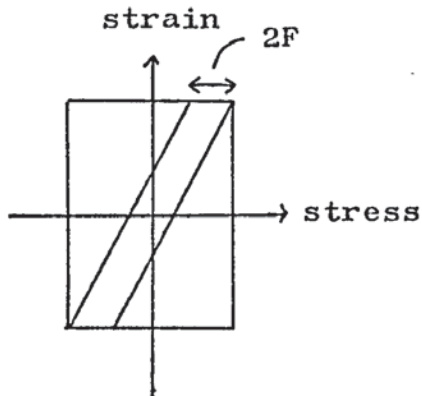
This model gives an energy loss per cycle that is independent
of frequency. The amplitude dependence can be complicated,
depending on how F varies with displacement. If F is zero
for small amplitude and then increases, the internal friction
will increase with amplitude - this phenomenon is observed
in disolocation damping. If F is proportional to displace-
ment the internal friction will be amplitude independent.

Anelastic damping will now be considered in some detail.
Viscous damping forms a special case of anelastic damping.
The mechanical model is shown below.

spring 1

spring 2
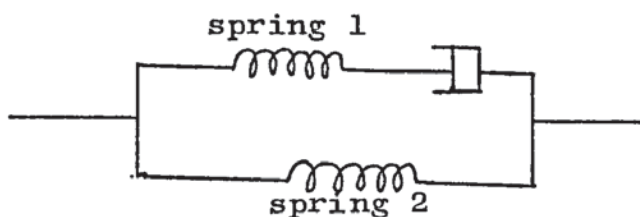
The mass m put in the model of the mechanical resonator has
been omitted - it merely serves to fix the resonant frequency.

This model is known as the standard linear solid and is due
to Zener. The treatment here follows that of De Batist (1972)

and is given in an abbreviated form. The stress strain relationship can be written:

$$aT + b\dot{T} = cS + d\dot{S} \qquad 2.14$$

$$T = \text{stress} \quad S = \text{strain} \quad a,b,c,d \text{ are constants}$$

Now consider some 'static' cases which will serve to express the constants in terms of some physical qualities.

Suppose $S = \dot{S} = 0$

$$aT + b\dot{T} = 0$$

$$T = T_0 \exp(-at/b)$$

put $\dfrac{b}{a} = \gamma_s$ relaxation time for constant strain 2.15

Similarly, if $T = \dot{T} = 0$

$$S = S_0 \exp(-ct/d)$$

$$\gamma_T = \frac{d}{c} \qquad 2.16$$

Now consider the effect of a constant strain S,

$$aT + b\dot{T} = cS_0$$

$$T = \frac{c}{a} S_0 + (T_0 - \frac{c}{a} S_0) \exp(-t/\gamma_s) \qquad 2.17$$

When relaxed i.e. the stress has achieved a constant value,

$$T = \frac{c}{a} S_0$$

We may define a relaxed modulus M_R

$$M_R = \frac{c}{a} \qquad 2.18$$

Similarly we may consider the effect of a constant stress

$$S = M_R^{-1} T_0 + (S_0 - M_R^{-1} T_0) \exp(-t/\gamma_T) \qquad 2.19$$

Now consider the effect of a sudden stress ΔT, integrating 2.19,

$$\tau_s \, \Delta T = M_R \, \tau_T \, \Delta S \qquad\qquad 2.20$$

Hence we may define an unrelaxed ('instantaneous') modulus M_u

$$M_u = \frac{\Delta T}{\Delta S} = M_R \frac{\tau_T}{\tau_s} \qquad\qquad 2.21$$

Physically the strain can only increase with time so,

$$M_R \leqslant M_u \quad \text{and} \quad \tau_T \geqslant \tau_s$$

Now suppose a harmonic stress is applied to the system,

$$(1 + i\omega\tau_s)T_o = M_R(1 + i\omega\tau_T)S_o \qquad\qquad 2.22$$

and the dynamic modulus (see equs. 2.3, 2.5)

$$M = \frac{T_o}{S_o} = M_R \frac{1 + \omega^2 \tau_T \tau_s}{1 + \omega^2 \tau_s^2} \qquad\qquad 2.23$$

Note now that the dynamic modulus is a function of frequency. Considering the internal friction;

$$Q^{-1} = \tan\phi = \frac{\omega(\tau_T - \tau_s)}{1 + \omega^2 \tau_T \tau_s} \qquad\qquad 2.24$$

If we put $\sqrt{M_u M_R} = M_o$ and $\sqrt{\tau_s \tau_T} = \tau$ then

$$Q^{-1} = \frac{M_u - M_R}{M_o} \cdot \frac{\omega\tau}{1+(\omega\tau)^2} = \frac{\Delta m \, \omega\tau}{1+(\omega\tau)^2} \qquad\qquad 2.25$$

where Δm = relaxation strength, τ = relaxation time.

This is the well known Debye relaxation function first applied to dielectrics in 1929. The internal friction rises

to a maximum when the drive frequency $\omega = \frac{1}{\gamma}$.

Thus the modulus and the internal friction are strongly frequency dependent.

Equation 2.23 can be rearranged, using the relationships between γ_s, γ_T, M_R, M_u to give,

$$M = M_u + \frac{M_R - M_u}{1 + (\omega\gamma_s)^2} \qquad\qquad 2.26$$

and making the approximation $\gamma_s = \gamma_T = \gamma$ (because experimentally $M_u \sim M_R$ and see 2.21).

$$M = M_u - \frac{M_u - M_R}{1 + (\omega\gamma)^2} \qquad\qquad 2.27$$

At low frequencies the dynamic modulus is equal to the relaxed or static modulus and at high frequencies to the unrelaxed modulus. The difference between the moduli and the internal friction peak height are directly related for an anelastic process. Putting $w = 1/\gamma$ in equation 2.25.

$$Q^{-1}_{max} = \tfrac{1}{2} \left(\frac{M_u - M_R}{M_o}\right) = \tfrac{1}{2} \frac{\Delta M}{M} \qquad\qquad 2.28$$

$\frac{\Delta M}{M}$ is known as the modulus defect and is equal to the relaxation strength Δm. Thus the internal friction peak height can also be obtained from measurements of elastic modulus and this provides a useful cross check that the process is an anelastic one.

Before considering the frequency dependence of internal friction, two extreme cases of the standard linear solid

will be considered. If spring no.2 is removed the model is known as the Maxwell linear solid and the equation is:

$$aT + b\dot{T} = \dot{S} \qquad\qquad 2.29$$

The results of the analysis are given in figure 2.3 The frequency dependence $Q^{-1} \propto \frac{1}{\omega}$ is rather unusual physically and the static behaviour corresponds to creep.

The other extreme case occurs when spring no.1 is removed and results in the Voigt linear solid (already discussed). The frequency dependence $Q^{-1} \propto \omega$ does occur physically (in "polymer" materials) but the quasi static behaviour is not realised physically because this model results in instantaneous strain being impossible.

Anelastic behaviour will now be considered in more detail centering on the Debye equation

$$Q^{-1} = \frac{\Delta m. \omega \tau}{1 + \omega^2 \tau^2} \qquad\qquad 2.30$$

In terms of the drive frequency ω, this peak is rather broad and to go from one half amplitude point to another requires the frequency to be changed by a factor of 11. Experimentally, it is normally very difficult to achieve the wide frequency variation required to trace out a peak but fortunately the relaxation time τ is very sensitive to the temperature.

Experimentally the relaxation time can usually be described by the Arrhenius relationship:

$$\tau = \tau_0 \exp \Delta E/kT \qquad\qquad 2.31$$

k = Boltzmann constant   T = temperature $^\circ$K

ΔE is the activation energy of the process. The pre-exponential factor γ_o is more difficult to interpret. Mathematically it corresponds to the relaxation time at infinite temperature - it is sometimes pictured as the reciprocal of an attempt frequency or the mean time of stay of a particle in a potential well. Substituting for γ in 2.27 gives:

$$Q^{-1} = \frac{\Delta m \, \omega \gamma_o \, \exp \Delta E/kT}{1 + \omega^2 \gamma_o^2 (\exp \Delta E/kT)^2} \qquad 2.32$$

Q^{-1} is now very sensitive to temperature and a change of 100°C will almost always give a good tracing of the peak. Experimentally this is the usual method of examining a peak and a relatively small change in frequency will give all the necessary additional information for the characterisation of a peak.

A plot of Q^{-1} against $1/T$ will yield a symmetrical curve of half width given by:

$$\Delta E = 2.28 \times 10^{-4}/W_{\frac{1}{2}} \qquad 2.33$$

ΔE = activation energy   eV   (If ΔE is in J then the constant of proport-
$W_{\frac{1}{2}}$ = half width $\text{deg}^{-1}K$ ionality is 22.1)

Usually practical peaks are rather broader than a Debye peak so that ΔE as calculated from this equation will be too small.

As the drive frequency is increased the peak will move to a higher temperature because a smaller relaxation time is required. The temperature dependence is given by (from 2.31)

$$\frac{1}{T_2} = \frac{-k}{\Delta E} \ln \frac{\omega_1}{\omega_2} + \frac{1}{T_1} \qquad\qquad 2.34$$

Thus a plot of ln $(1/\omega)$ against $1/T$ will give a straight line:

$$\text{gradient} = \frac{Rk}{\Delta E} \qquad\qquad 2.35$$

This gives a much more reliable value for ΔE than the half width but it may be difficult to make the required changes in frequency. Fig. 2.4 shows the variation of peak temperature with frequency for different activation energies.

Another method of determining ΔE is due to Wert and Marx (1953) and relies on the fact that γ_0 is fairly constant for a particular type of process. Using equation 2.31 and making the reciprocal drive frequency γ = const. we see that:

$$\Delta E = kT2.3 \log \gamma/\gamma_0 = \text{const x T}$$

The constant is determined by the drive frequency and γ_0

$\gamma_0 \sim 10^{-15}$ s   for a point defect

$\gamma_0 \sim 10^{-12}$ s   for a line defect

$\gamma_0 \sim 10^{-10}$ s   for a point defect - dislocation interaction.

Thus a simple determination of the peak temperature at a known frequency can be used to give an approximate value for ΔE. The method is illustrated in figure 2.5.

Frequently a peak does not fit the simple Debye relation but may still be analysed in this way. For example two or more relaxation peaks may overlap and the resultant peak may be analysed into components. In other cases there may be a continuum of peaks with a distribution of relaxation times.

Two types of distribution function that have been used are
the square (box) function and the Gaussion (lognormal)
function. Adjustment of the distribution parameters can
give good computer fits to experimental data.

The Debye relation can also be used to fit data when no
peak is seen at all.

From equation 2.28,

$$\text{when } \omega \ll \frac{1}{\gamma} \quad Q^{-1} = \Delta m . \omega \gamma , \quad M \simeq M_R$$

$$\text{when } \omega \gg \frac{1}{\gamma} \quad Q^{-1} = \frac{\Delta m}{\omega \gamma} , \quad M \simeq M_u$$

Thus these cases of frequency dependence can be explained
by the anelastic process but this type of explanation does
not necessarily have any physical reality.

2.3b <u>General classification of internal friction phenomenon</u>

If a material is heated up at a constant frequency a number
of internal friction peaks will be seen together with some
background damping which increases rapidly at high temperatures.

In internal friction measurement the background damping has
to be subtracted to give the peak shapes.

A list of the important internal friction effects is given
below:

1. <u>Bordoni peak</u> - a low temperature peak produced by cold
    work in fcc metals.

2. <u>Dislocation damping</u> - damping at room temperature due to
    glissile dislocations. Amplitude dependent. Currently

explained in terms of the vibrating string model Granato and Lücke (1956)

3. <u>Snoek peak</u> - caused by interstitial solutes in bcc metals.

4. <u>Zener peak</u> - observed in binary and ternary substitutional alloys. Due to stress induced ordering of solute atom pairs.

5. <u>Grain boundary peak</u> - due to grain boundary motion. Observed at approximately half the melting point for polycrystalline but not single crystal materials.

6. <u>High temperature background</u> - internal friction increases rapidly at high temperatures and obeys the Arrhenius relationship

$$Q^{-1} = A \exp -\Delta E/kT$$

The Snoek, grain boundary peaks and the high temperature background will now be discussed in more detail.

2.4 <u>Snoek peaks</u>

These well characterised peaks are due to the presence of atomically small interstitial solutes (carbon, nitrogen, oxygen and hydrogen) in body centred cubic (bcc) metals - principally iron, niobium, tantalum and vanadium. These peaks were first observed by Snoek (1941) for carbon in α iron. The peak temperature was about 40°C at 1 Hz. Some examples of Snoek peaks are shown in Chapter 5.

For a bcc lattice there are two types of hole in which the interstitial can settle. Figure 2.7 illustrates the octahedral and tetrahedral sites. Both types of site have tetragonal symmetry but the tetrahedral sites are larger.

Snoek explained his results by the hypothesis that the carbon was in the octahedral sites and that under stress the energy of some sites was reduced while for others it became larger. Hence the relaxation was due to jumping of the interstitials between octahedral sites, the time constant corresponding to the time constant of the redistribution of the interstitials. From consideration of the effect of stress on the crystal it can be shown (Nowick and Berry 1972) that the maximum relaxation will occur when the stress is in the 100 direction and there will be no relaxation for the 111 direction. ,the reason being that all octahedral sites are equally inclined to this direction. This was confirmed by Dijkstra (1947) and in more detail by Hoffman and Wert (1966). In other systems it appears that tetrahedral-tetrahedral, octahedral-tetrahedral and tetrahedral-octahedral jumps may occur. Snoek peaks of hydrogen in iron, tantalum and niobium have been observed but they all occur at low temperatures ($<100°K$ for 1 Hz).

The Snoek peak generally has a half width only slightly greater than that of a Debye peak and the frequency dependence may be calculated from the usual formula (equation 2.31). The results are shown in Figure 2.6.

An important application of the Snoek peak is the measurement of the concentration of interstitials. An example is the study of the precipitation of carbon.

The relationship between peak height and concentration is given approximately by:

$$2Q^{-1}_{max} = \Delta m = \Delta_G . C \qquad\qquad 2.37$$

Δm = relaxation strength

Δ_G = relaxation strength parameter per atom %

C = concentration atom %

Δ_G for the different solute - solvent systems is shown in Figure 2.7. The data is for polycrystalline materials - for single crystals Δ_G is a function of direction. It is also varies slightly with grain size. As the solute concentration increases the peaks can broaden and the relaxation times alter. This may be interpreted in terms of a solute-solute interaction peak whose height is proportional to the square of the solute concentration. Also if two solutes are present an intermediate interaction peak results.

The temperature dependence of the relaxation strength is given by Polder (1945)

$$\Delta_G = \frac{T}{T_o} \left(\frac{1}{T-\alpha T_c}\right) \qquad\qquad 2.38$$

$\alpha = 1$ T_c = critical temperature for ordering

For iron $T_c \sim 0°K$ but for the oxygen-tantalum system Powers and Doyle (1959) have determined T_c to be 77°K.

2.5 Grain Boundary Peaks

Early theoretical work on grain boundary peaks was due to Zener (1941). He predicted a grain boundary relaxation due to viscous sliding between two adjacent crystals and further-more made some quantitative statements. Firstly, the relaxation strength would be independent of the grain size d provided this was less than the sample dimensions. He calculated the ratio of the shear moduli G_R/G_u to be approximately 0.61 for

all metals leading to the result that the relaxation strength should be the same for all peaks. This assumed that sliding occurred across the whole of the grain boundary. Finally, the relaxation time γ_o was proportional to the grain diameter d.

The first detailed experimental work was done by Kê (1947   ) who largely confirmed Zener's predictions. He used 99.99% pure aluminium specimens and established the following results (see Figure 2.1). A polycrystalline sample gave a peak $(Q^{-1}_{max} = 0.09)$ at 300°C for a driving frequency of 1 Hz while a single crystal did not. The peak height was in accordance with Zener's theory and also independent of grain size even when the diameter approached the sample diameter. For larger diameters the peak height decreased. $\gamma_o \, \alpha \, d$ again as predicted. The activation energy as determined from the frequency shift of the peak was very close to the activation energy for self diffusion but the half width was about three times the width of a Debye peak.

Subsequent work mainly on gold, copper and silver has showed more complexity than Kê's results. These metals showed broader and less intense peaks $(Q^{-1}_{max} \sim 0.02 - 0.05)$, and also double peaks were frequently observed, e.g. gold - Mash and Hall (1953), nickel - Datsko and Pavlov (1963) and copper - De Morton and Leak (1966), Williams and Leak (1967). The experiments on copper showed the high temperature peak only when some grain boundaries extended right across the specimen and was only fully developed for the 'bamboo' structure. This peak had an activation energy of 4.6eV compared to 2.0eV for self diffusion, and was thought to be due to grain boundary sliding rather than migration.

The work of Barrand (1966) on double peaks in the iron chromium system is particularly important. The pure metal shows a low temperature 'PM' peak. As the solute (chromium) concentration is increased a high temperature solid solution (SS) peak appears and the PM peak disappears. The SS peak has a peak height of $Q^{-1} \sim 0.08 - .12$ and an activation energy similar to that of self diffusion. The SS peak seems to be more of a true grain boundary peak as it disappears for coarse grained materials. It appears likely that Kê's work on aluminium was in fact for an SS peak.

Later experiments on the effect of grain size conflicted with Kê's result of $\tau \propto d$ and gave results of $\tau \propto d^2$ (see Starr 1953 for aluminium and Leak 1967 for iron). Peters (1964) using 99.99% pure copper fitted the grain boundary peaks to a log normal distribution and found the distribution parameter β increased with grain size but the relaxation strength did not. Thus the increase in grain size gave a broader lower peak.

As a result of this experimental work further suggestions have been made about the mechanism of grain boundary damping since Zener's theory. Leak (1967) suggested that the PM peak might be due to grain boundary migration on the atomic scale which has a lower activation energy than self diffusion. The SS peak was due to sliding. Machlin and Weining (unpublished but reported in Nowick and Berry (1972)) have pointed out that a grain boundary is a ledge like structure, as shown by field ion microscopy (Brandon 1964). Thus sliding can only occur if smoothing by local migration first occurs. To explain the phenomena they postulate an activation energy for sliding E_s midway between the activation energy for self

diffusion Esd and migration Em (Em $\sim$ 0.5 Esd). In a pure metal sliding is the rate limiting step so the PM peak has an activation energy of Es. Addition of a solute increases Em to Esd giving the SS peak.

In conclusion it may be said that in contrast to the Snoek relaxation, the grain boundary relaxation is not very well understood and to quote Nowick and Berry 1972 "....clearly more work is required, of both experimental and theoretical nature, before it can be stated that the phenomenon of grain-boundary relaxation is well understood".

2.6   Background damping

In general background damping obeys the Arrhenius relationship

$$Q^{-1} = A \exp -\Delta E/kT \qquad\qquad 2.39$$

where A is an experimentally determined constant and
ΔE is an activation energy.

The value of ΔE is generally rather larger above the grain boundary peak than below it. Background damping below the grain boundary peak may be explained in terms of dislocations. The number of (thermally) unpinned dislocations increases with temperature, with the usual Boltzman relationship, and gives a corresponding increase in internal friction. Normally background damping is found to be amplitude independent (up to 10^{-4}) and fairly independent of frequency.

The interpretation of the high temperature background is controversial. It can be described as an anelastic process with a broad spectrum of relaxation times or as a visco-

elastic process (Maxwell model). The value of ΔE measured from fitting data to equation 2.39 is sometimes close to the activation energy of self diffusion and sometimes well below it and this has resulted in the use of other equations. Pearson and Rotherham (1956) took the view that the Maxwell model is the correct one, and proposed the equation:

$$Q^{-1} = \frac{A}{\omega} \exp -\Delta E/kT \qquad\qquad 2.40$$

Schoek et al. (1964) emphasise the need to take the frequency dependence into account when calculating the activation energy and using the anelastic model proposed the equation:

$$Q^{-1} = A\omega^{-n} \exp -n\Delta E_o/RT \qquad\qquad 2.41$$

Thus the true activation energy from the gradient of an Arrhenius plot is given by:

$$\Delta E_o = \frac{\Delta E}{n} \qquad\qquad 2.42$$

Pines and Karmazin (1966) measured the frequency dependence and temperature dependence in ten metals and in all cases the values of ΔE_o came to within 10% of the value for self diffusion. The values of n were in the range 0.15-0.4. However, when other authors data is examined such close agreement is not always found.

Quasi static experiments by Kê and Zener (1950) have pointed to the anelastic explanation for the lower temperature range of background damping. At higher temperatures creep occurs involving vacancy motion and from calculations of Nabarro-Herring creep Friedel (1961) has shown that the internal friction due to this mechanism should obey the law:

$$Q^{-1} = \frac{\Lambda}{\omega^n T} \exp \Delta E/kT$$

where n = 1 at low frequencies

n = $\frac{1}{2}$ at high (kHz) frequencies

To summarise it may be said that the high temperature background is the composite result of several mechanisms involving the high temperature behaviour of dislocations. Again quoting Nowick and Berry (1972) "...it seems very probable that a more active interest in this phenomenon could give further insight into high temperature dislocation behaviour in much the same way that studies of the Bordoni peak and high frequency attenuation measurements have given information about the behaviour of dislocations at low temperatures".

2.7. Internal friction in ceramics and glasses

An important feature of non metallic materials is that they are electrical insulators and this brings the possibility of further internal friction effects due to ionic forces. Furthermore dielectric loss measurements can complement internal friction data.

The main high temperature feature of a polycrystalline ceramic is the grain boundary peak as for the metal. Single crystals have very low internal friction at high temperatures because they contain fewer dislocations than metals. Glasses show a rapid rise in internal friction at the softening point but have nothing corresponding to a grain boundary peak. At lower temperatures various ionic anelastic effects are present in ceramics and glasses (broadly analogous to the Snoek and Zener peaks in metals). Additionally in glasses there are peaks due

to deformation of the network but these effects are much
more marked in polymers.

Ceramics

At moderate temperatures peaks occur due to point defects
such as interstitials and impurity atoms. Two examples will
be quoted. Calcium in sodium chloride produces a moderate
internal friction peak at 75°C (1Hz) (Dreyfus , Laibavitz 1964).
Ca^{++} ions enter the lattice substitutionally and create an equal
number of cation vacancies due to the double charge. The
substitutional atoms electrically attract the vacancies and
there is an anelastic effect. To take another example excess
oxygen in uranium dioxide gives a peak at 240°C at 1Hz due to
the interstitial atoms (Sócino 1967).

The use of the internal friction technique in the study of high
temperature properties is virtually non existant. Hornstra
(1965) and Spriggs (1969) discuss the role of grain boundaries
in high temperature creep and suggest that the internal friction
method is used. It seems also that this technique could be
very valuable as an additional method for the determination
of phase transformations at high temperatures (see for example
Foex 1968).

Glasses

Quite extensive work has been done on internal friction in the
inorganic glasses (Hopkins and Kurkjian 1965). The main
phenomena observed will be illustrated by reference to the
common sodium silicate glasses. At 50 kHz a peak at approxim-
ately 250°C is seen due to sodium ion migration and a second

peak at 500°C due to singly bonded oxygen ion motion. The magnitude of the peaks is roughly proportional to the sodium concentration. At -200°C there is a peak due to Si-O-Si bond bending.

Near the softening point there is an exponential rise in the internal friction with increasing temperature. Measurements on this are not very useful but in a composite material internal friction can be used to detect the softening of a glassy phase (see 5.12).

Aston University

Illustration removed for copyright restrictions

FIGURE 2.1 - Variation of Young's modulus
and internal friction with temp-
erature for polycrystalline and
single crystal aluminium. The
polycrystalline sample shows a
grain boundary peak (Reproduced
from Kê 1954).

FIGURE 2.2 - Internal friction spectrum of
iron (Reproduced from Beshers 1967)

	Maxwell	Voigt	Standard linear (Anelastic)	Hysteretic
Mechanical representation				
Defining equation	$aT + b\dot{T} = \dot{S}$	$T = cS + d\dot{S}$	$aT + b\dot{T} = cS + d\dot{S}$	$T(1 - k) = cS$
Frequency dependence of Q^{-1}	$Q^{-1} \propto 1/\omega$	$Q^{-1} \propto \omega$	$Q^{-1} \propto \dfrac{\omega\tau}{1+\omega^2\tau^2}$	independent
Frequency dependence of dynamic modulus	independent	independent	$M_R \to M_U$ $(M_R < M_U)$	independent
Amplitude dependence of Q^{-1}	independent	independent	independent	may be independent
strain response to a stress pulse				F independent of velocity
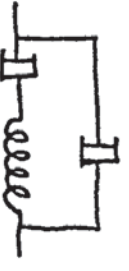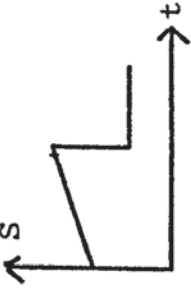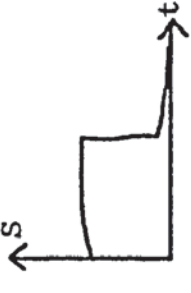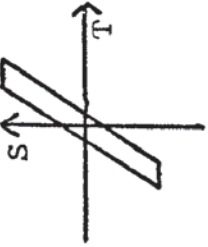
FIGURE 2.3 - Mechanical models of solids
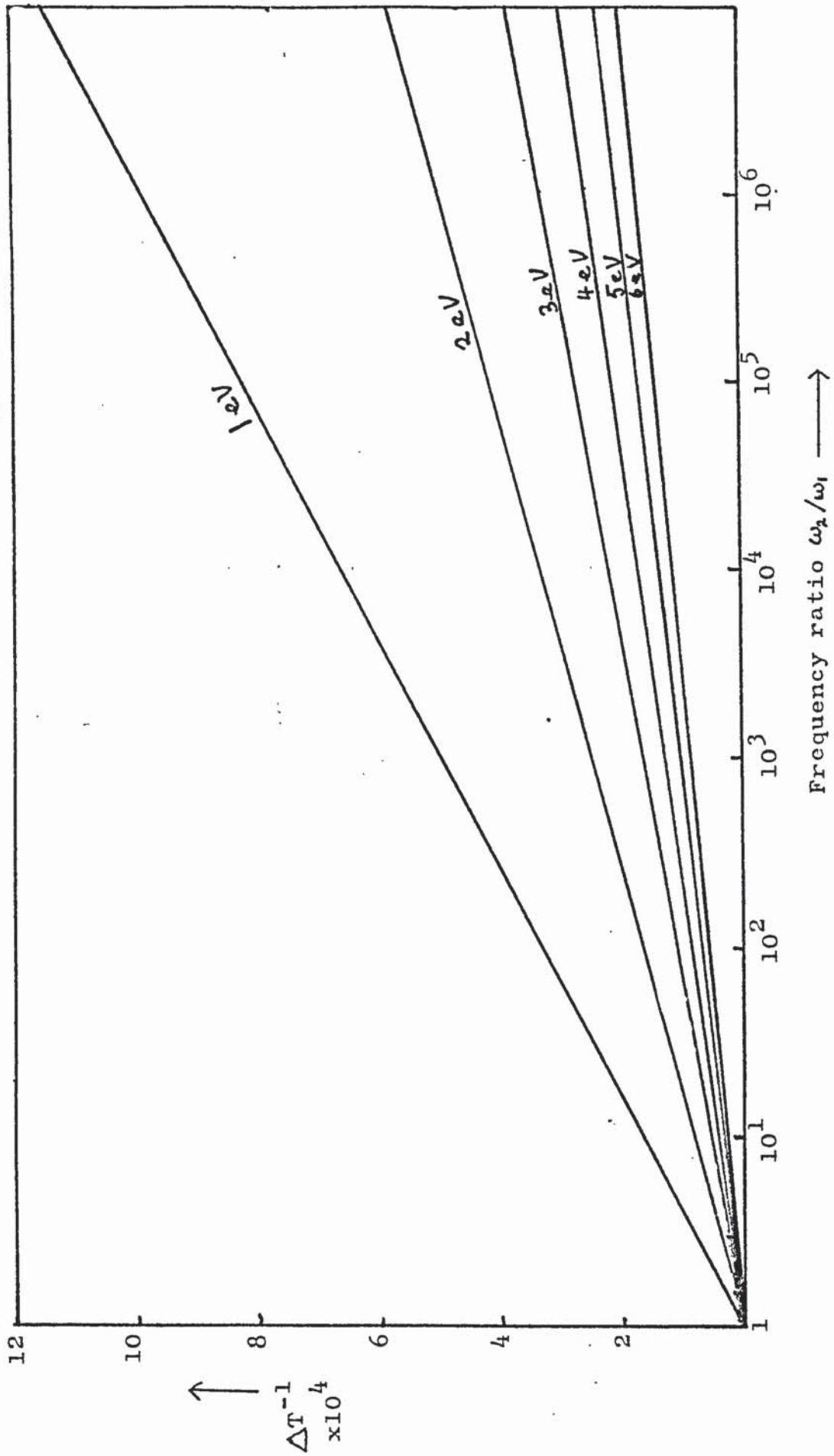
FIGURE 2.4 - This shows how the temperature of a peak shifts with frequency and the dependence on the activation energy.
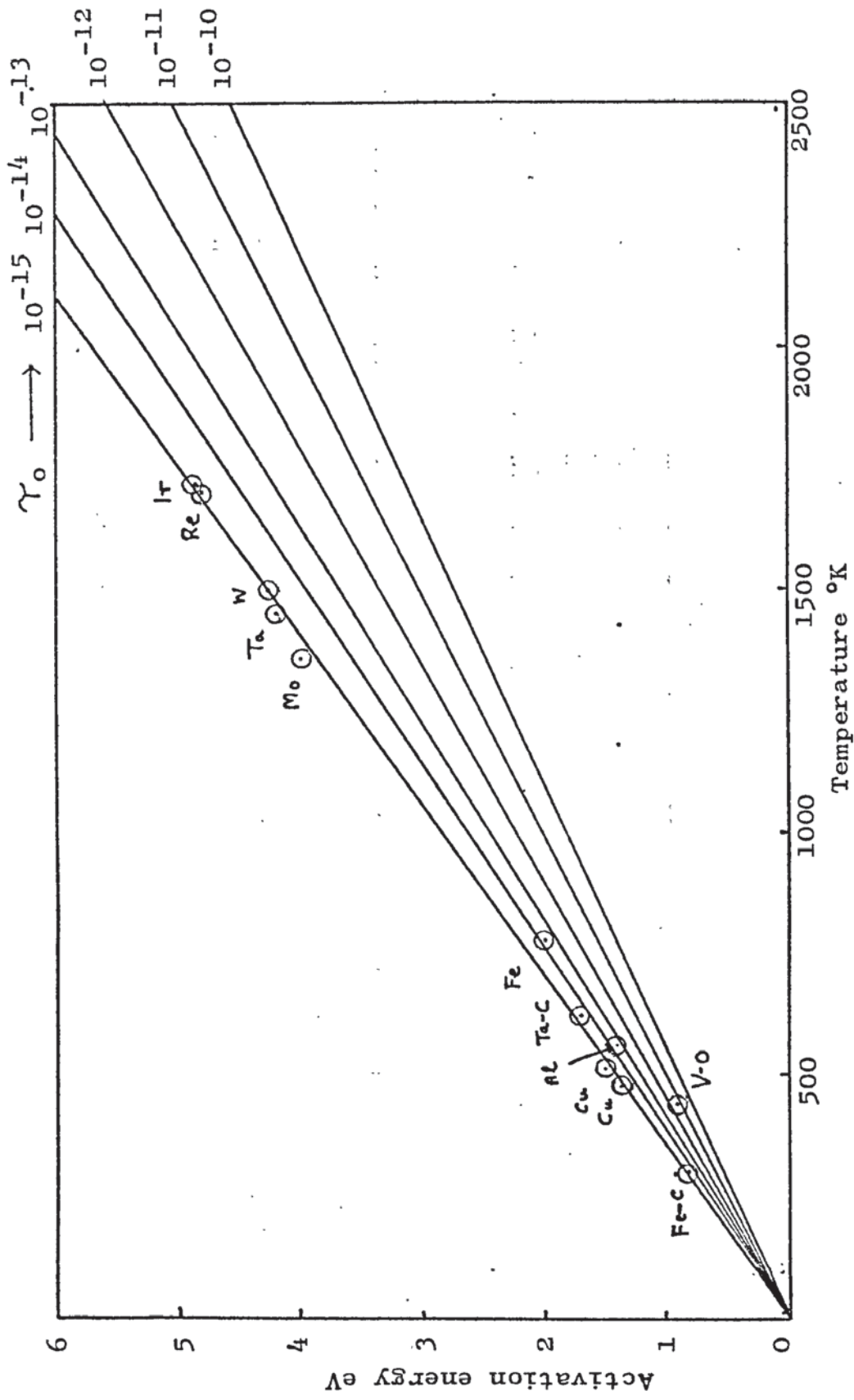
FIGURE 2.5 — Wert-Marx plot showing selected Snoek and grain-boundary peaks (1 Hz data). Because experimentally it is found that $\gamma_o \sim 10^{-14}-10^{-15}$ for these peaks, the peak temperature will give an approximate value for the activation energy. The diagram is also useful in predicting the approximate shift in peak temperature due to a change in frequency.
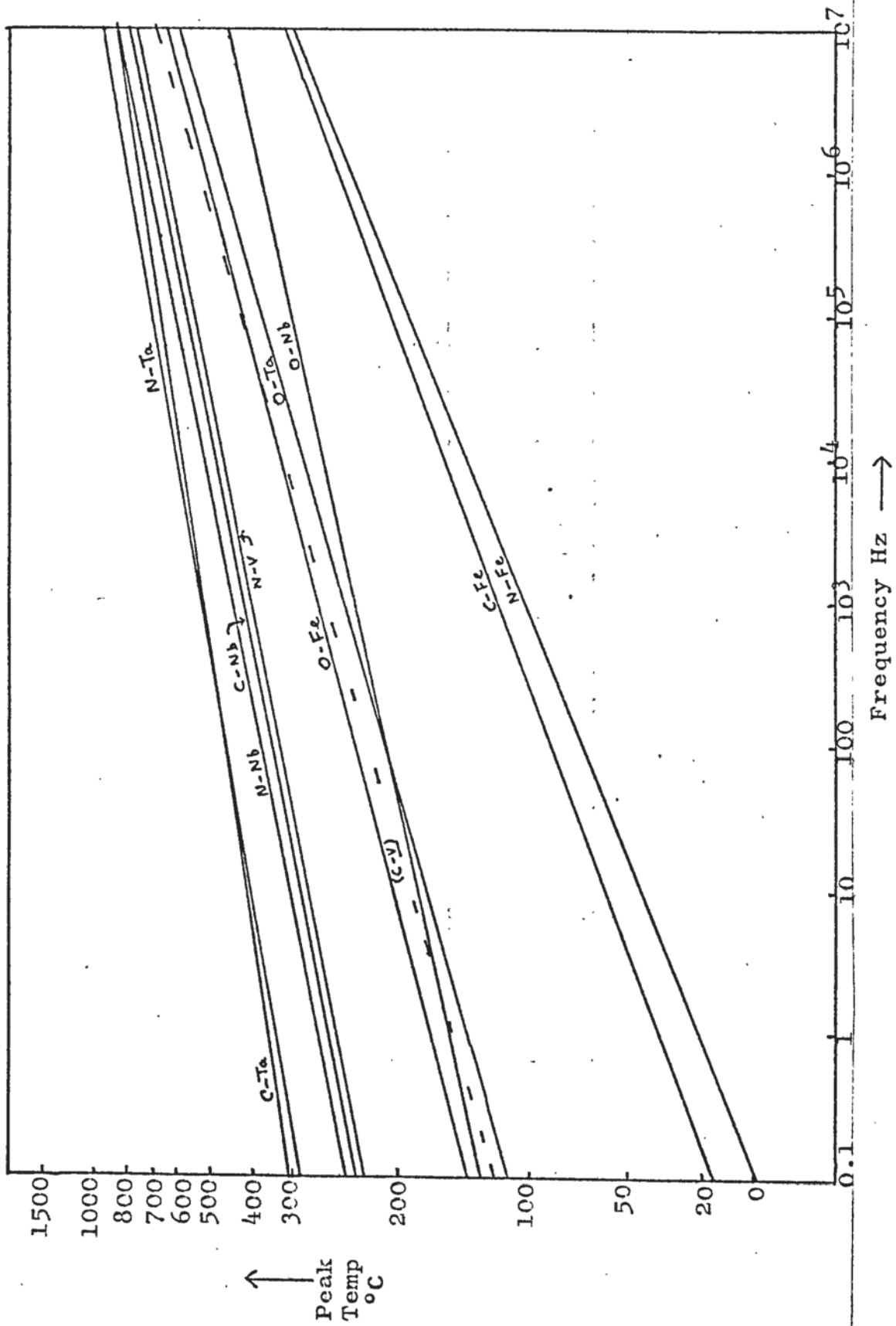
FIGURE 2.6 – This shows the variation in temperature of Snoek peaks with frequency (Extrapolated from Powers and Doyle 1959 data).
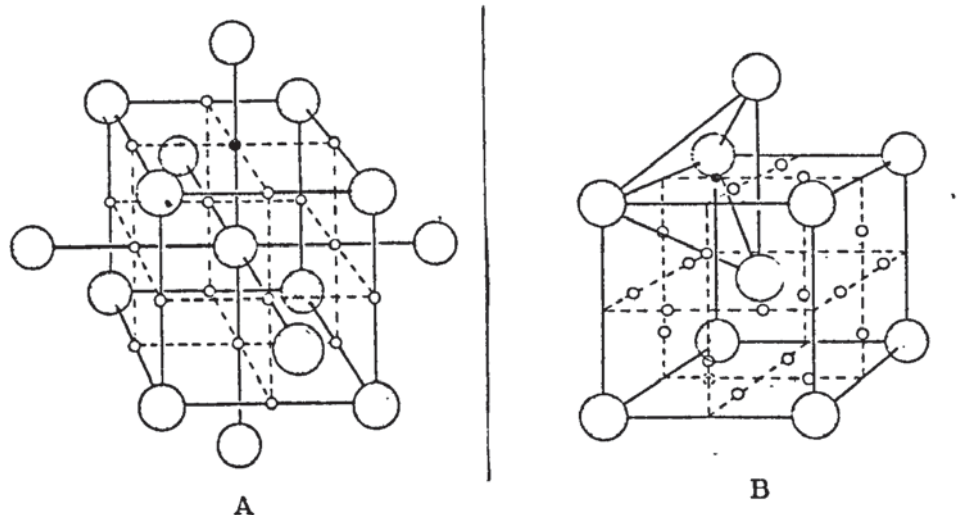
FIGURE 2.7A,B - Octahedral (A) and tetrahedral (B) holes in the bcc lattice. The small circles show the interstitial sites. (Reproduced from Nowick and Berry 1972)

Δm per atom %

	C	O	N
Fe	0.42	—	0.44
V	–	0.067	0.36
Nb	–	0.054	0.065
Ta	0.19	0.11	0.12

FIGURE 2.7C - Table showing values of relaxation strength (Δm) at 300°K for the Snoek peaks. Data taken from Powers and Doyle (1959).

CHAPTER 3:   METHODS

3.1   Introduction

Most methods of measuring internal friction can be used to measure Young's modulus and vice versa. Reviews of methods with the emphasis on internal friction are given by De Batist (1972) and Nowick and Berry (1972). A brief review of methods of measuring Young's modulus is given by Pugh (1967). Here the emphasis will be on internal friction. Few commercial instruments exist as yet and so internal friction experiments are more troublesome than they might be. The classical way of making internal measurements is the torsion pendulum illustrated in figure 3.2 This is the method Snoek (1941) used for his work on the Snoek peak and it is still very widely used.

Methods can be divided up into resonant methods, pulse methods and static methods. The table shown in figure 3.1. gives a summary of the techniques currently available. The limits on temperature etc.are approximate ones which have sometimes been exceeded, perhaps with great difficulty.

The torsion pendulum (figure 3.2) is a resonant method and the most common way of measuring internal friction. The specimen is in the form of a wire and is made to undergo torsional oscillations at a frequency of around 1 Hz. Normally the system is set oscillating and then the observation of free decay of the oscillations gives the internal friction, the damping due to the instrument

itself being negligible. Frequently an optical pick off
is used to drive a chart recorder, measurements being made
directly off the record. This apparatus has the advantage
of being simple and electronic instrumentation is inessential.
One objection to this apparatus is that the specimen is
always subjected to a static stress, which could cause
structural changes at high temperatures, but this is over-
come in the inverted torsion pendulum where the stress is
almost reduced to zero. Various automatic types of
pendulum (e.g. Brozel 1973) have been constructed
but use of these is not widespread.

The various other resonant methods use an electro-mechanical
transducer to excite the specimen and detect the oscill-
ations. These can be classified as piezo-electric, electro-
magnetic and electrostatic. The specimen usually takes the
form of a longitudinally driven bar but sometimes a
flexurally driven strip is used. In these methods the
frequency dependence of internal friction is measured by
use of the overtones as well as the fundamental. There
are three main ways of measuring the internal friction:

1. observation of free decay;

2. varying the oscillator frequency to measure
   the sharpness of tuning;

3. using a control loop to control the driving
   amplitude and measuring the amount of energy
   required to give constant amplitude.

Method 3 is a method for automating the torsion pendulum.
Common to the piezoelectric and electromagnetic (particul-
arly magnetostrictive) methods is that the transducer may

load the specimen affecting both the frequency and the damping, in contrast to the torsion pendulum where the damping is very low (Q^{-1} can be better than 10^{-7} in a vacuum) due to optical detection of the oscillations. Another problem with this group of methods is supporting the specimen. This is commonly achieved by supporting the specimen at the centre by means of needles. The contribution to the damping due to the supports is low at the fundamental but only the odd harmonics which give a node at the centre can be used. This gives only a few possible exciting frequencies. In the electrostatic method it can be difficult to excite the specimen sufficiently to give reasonable amplitude when the damping is high. A disadvantage of the piezo-electric method is that the crystal must be stuck on, this giving a composite oscillator. The effect of the adhesive bond is always a source of doubt and can produce supurious internal friction peaks. Ideally, the specimen and crystal should have the same resonant frequency, and this condition cannot be met over a wide temperature range.

The second type of method is the ultrasonic method which is more fully described in Chapter 4. A pulse is generated and the change in amplitude after travelling a known distance in the specimen gives the internal friction. Measurement of the velocity gives the Young's modulus. Use of this technique presupposes that the wavelength is small compared to the specimen length so that the frequencies used are generally 1 MHz (λ = 5mm in steel) and above. This technique is often applied where resonance techniques are

difficult - i.e. high damping, high frequency or high temperature. It, however, is not very accurate because pulse distortion makes accurate measurements difficult. A single pulse consists of a wide range of frequencies so that the frequency is not accurately known but this can be partly overcome by using a burst of oscillations. The band-width is equal to $2f/n$ where f is the oscillator frequency and n is the number of oscillations. Thus making $n = 10$ will give a bandwidth of 20% of the oscillator frequency. The strain amplitude is usually difficult to measure and can generally be adjusted over a smaller range than the resonant methods.

The third group are static methods. These essentially rely on the observation of a hysteresis loop during a conventional stress strain experiment. The frequency can vary from extremely low frequencies up to a few Hz. This is a good method for the measurement of high amplitude internal friction (e.g. Threader and Feltham 1973) but has not been very widely used because most of the interest lies in the low and medium amplitude region.

3.2 Choice of a method for high temperatures

The object of this section is to review the possible methods for work in the 1000-2000°C range. Clearly, some methods can be eliminated, namely any method using a piezo crystal or magnetostrictive transducer mounted directly on the specimen. However, these methods can be used if the drive unit is remote from the specimen but this is difficult for a resonant method. Electrostatic drive is certainly

feasible and so is the torsion pendulum. The most attract-
ive method is the pulsed ultrasonic one because the drive
can be very remote and there are no problems of feeding
the signal into the specimen. A survey of work in the high
temperature field showed that relatively little had been
done above 1000°C. This is partly because this temperature
range is thought to be of less interest by internal friction
workers and partly because of experimental difficulties.

The torsion pendulum has been used by Berlec (1970) up
to 2400°C in his study of tungsten. The specimen was used
as its own resistance heater. Other work has been done
by Murray (1968), Shestopal (1967) up to 1600°C, Ke (1949)
up to 600°C and Postnikov (1957) up to 700°C on his grain
boundary damping study of many metals. The disadvantage
of this method is that the specimen must be in the form
of a wire and it is unsuitable for brittle specimens such
as ceramics.

The electrostatic method has been used by Southgate (1959,
1966) for his work on doped single crystal magnesia up to
1200°C. The feature of this method is its ability to
measure low levels of damping at very high temperatures -
an essential feature for refractory single crystal work.
This method is suitable for a specimen in the form of a
longitudinally driven bar or a flexurally driven reed.
Methods employing magnetostrictive or piezo-electric
transducers coupled to the specimen by short rods or wires
have been successfully used for measuring Young's modulus,
(see e.g. Koster 1959, Kalugin 1966) but not very much for
internal friction because of the problem of spurious

effects due to the coupling leads.

Pulsed ultrasonic methods are much more satisfactory because the transducer can be very remote - several metres or more from the specimen, which is much longer than the wavelength of the pulse. In this way spurious coupling effects are avoided. The single pulse method has been used by a number of workers e.g. Bell (1957) up to 1000°C. The method used for the measurements in this thesis combines the advantages of the single pulse method with many of the advantages of the resonant method and is described in 3.4.

To sum up the following features are desirable in a high temperature method;

1. The ability to use a wide variety of specimen shapes and sizes.

2. To be able to use small specimens, say a few mm long. This makes for easier and cheaper specimen heating. Also, some materials are expensive, rare or difficult to prepare.

3. As little apparatus as possible should be in the hot zone. The ultrasonic methods have the advantage that the only substance present in the hot zone is the specimen material itself.

3.3 The single pulse attenuation method

A number of different types of apparatus using this principle are reviewed by Mason (1964) and De Batist (1972). One type of apparatus is shown in figure 3.3. A short pulse (usually 5μs or less) or sometimes a short burst of oscillations is

periodically fed into an acoustic transmission line which
carries the pulse to the specimen. In the method shown
in the diagram, the magnetostrictive transducer is also
used as the receiver. The pulse is reflected at the shoulder
and at the end of the specimen. As the attenuation in
the specimen increases (due to heating for example) the end
echo is reduced and so the attenuation in the specimen can
be measured by measuring the relative amplitudes of the end
and shoulder echoes on an oscilloscope display.

The amplitude of a wave travelling in a medium is given by

$$A = A_o \exp - \alpha l \qquad\qquad 3.1$$

where, $\quad Q_m^{-1} = \dfrac{\alpha c}{2\pi f}, \quad \alpha =$ attenuation coefficient $\qquad 3.2$

hence, $\quad \dfrac{E_e}{E_s} = X \exp(- \alpha l) \qquad\qquad 3.3$

where, E_e = amplitude of end echo. E_s = amplitude of shoulder
echo and X is the value of E_e/E_s when the attenuation is zero,

or, $\quad Q_m^{-1} = \dfrac{2.3c}{2\pi f \cdot l} \log_{10} \dfrac{X E_s}{E_e} \qquad\qquad 3.4$

In another type of apparatus another transmission line and
transducer receive echoes out of the far end of the specimen.
The received signal strength is thus a measure of the
attenuation in the specimen. In yet another method the
transducers are mounted directly on the specimen (e.g. Chick
1960).

The high temperature application of this method will now
be considered in a little more detail, concentrating on the
Bell (1957) type of apparatus. This method has been used

up to 2000°C by Lynnworth(1967) and has been embodied in a commercial instrument known as the 'Panatherm'. This instrument is used for measuring temperature and material properties. The immediate problem with this type of apparatus is the low sensitivity for a reasonable specimen length.

For the Young's modulus measurement,

$$t = \frac{2l}{c} \tag{3.5}$$

putting

$$c = \sqrt{\frac{E}{\rho}} \tag{3.6}$$

$$E = 4\rho c \left(\frac{l^2}{t^2}\right) \tag{3.7}$$

$$\frac{dE}{E} = -\frac{2dt}{t} \tag{3.8}$$

(the effect of thermal expansion has been neglected in this analysis).

For the internal friction measurement from equation 3.4

$$dQ^{-1} = \frac{3c}{2\pi f l} \left(\frac{dE_s E_s X}{E_s}\right) \tag{3.9}$$

or

$$\frac{dQ^{-1}}{Q^{-1}} = \frac{E_i}{2.3 \log_{10} E_s/E_e} \cdot \frac{dE_e}{E_e} \tag{3.10}$$

E_i = initial amplitude of shoulder echo.

Consider a typical experiment for steel where $c \sim 5 \times 10^3$ m s^{-1}, the specimen length l = 100 mm, frequency f = 300 kHz.

The time between the end and shoulder echoes will be 40μs. If the time can be measured to 0.1μs then dE/E = 0.5% which is not a very good sensitivity as compared with a typical

figure of 0.01% or better for the resonant methods. Consider now the internal friction.

Suppose using the oscilloscope display that E_s = 50 mm and X = 2,

For Q_m^{-1} = 10 x 10^{-3}(a typical value in a high temperature experiment)

E_e = 71.5 mm.

If this amplitude is measured to 1mm then using 3.6,

dQ^{-1} = 3.2 x 10^{-4}

or dQ^{-1}/Q^{-1} = 3%

This sensitivity is comparable with the resonant methods but the problem is that the frequency is not accurately known, and a further complication is pulse distortion. From the pulse width the centre frequency of the fourier transform is used as the 'effective frequency'. However, if this effective frequency varies during a temperature run then it would affect the observed internal friction curve because the variation of f in equation 3.4 would cause different values of Q^{-1}.

The outstanding advantage of this method is that no apparatus need be inside the furnace apart from the specimen material and thus the temperature limit is set by the melting point of the specimen. Typically the specimen is in the form of a rod a few mm in diameter shaped as shown in figure 3.3. The neck must be fairly thin to produce a good shoulder echo. For example a 3 mm diameter rod might require

machining down to 1 mm thickness. For ceramic specimens
a diamond wheel can be used while for many metals the use
of a hand file is satisfactory. The effective position of
the shoulder can be determined by measuring the time delay
between end and shoulder echoes for different lengths of
specimen (see Bell 1960).

3.4 The Bell (resonant) method

The basic system is shown in figure 3.6. This was originally
developed for resonant ultrasonic thermometry (Bell 1968,
1966). This thesis describes the application of this approach
for measuring internal friction. In essence the method
consists of a resonator made of the specimen material
coupled to a magnetostrictive transducer by means of a
long rigid mechanical coupling in the form of a rod or
wire which acts as an acoustic transmission line. The resonator
is periodically excited into oscillation by acoustic signals
sent along the transmission line and the signals received
back from the specimen via the transmission line are used
to measure the elastic moduli and internal friction. The
use of an acoustic transmission line many wavelengths long
avoids the problems of transducer-resonator interaction
that occur with many other methods, because the line presents
a resistive load to the resonator.

A burst of oscillations is fed into the transducer and an
echo is received from the resonator. This is shown in
figures 3.6, 3.7. The line must be adequately long to
prevent overlap between the transmitted signal and the echo.
The figure shows the echo for the case when the transmitter

frequency is at the fundamental resonator frequency. The
effect of mistuning is shown in figure 3.8. The resonator
frequency can thus be determined very accurately. The
effect of internal friction is shown in figure 3.9. Thus
the echo shape can be used to determine Q^{-1}.

3.4a Description of the echo

The echo can be divided into two parts - the first part is
referred to as the echo signal, and the second part, con-
sisting of decaying oscillations from the resonator is
called the echo decrement. For elementary purposes the
echo signal can be considered as the sum of a reflection
at the transmitter frequency from the line resonator
junction and a signal building up in the resonator. Thus
when the transmitter frequency is equal to the resonator
frequency the two signals will sum to zero at the crossover
point (n_x) but when off tune the two signals will not
because of the frequency difference. As the internal
friction increases the amplitude E_∞ decreases so n_x must
increase. The simple model explains the basic phenomena
and can be used to calculate n_x as a function of internal
friction etc. However, the details are not explained - for
example the complex signals obtained when off resonance.
The exact mathematical analysis is given by Sharp (1974)
who used a Laplace transform technique to solve the basic
equations of motion for the resonator coupled to the trans-
mission line. Detailed comparison of experimentally
observed echoes with the graphical computer output confirmed
the rigour of the solutions. This mathematical approach is
complicated but some of the echo phenomena cannot be explained
by less rigorous methods.

The echo can be used for precise determinations of the
resonator frequency thus enabling Young's modulus (or
other elastic moduli) of the specimen to be determined.
Referring to figure 3.8 an obvious way of doing this is
to tune the transmitter till a crossover is seen. This
is the simplest and most precise method. Another method
relies on the fact that at resonance there is a 180°
difference in phase between the early and late part of
the echo signal. When there is no crossover, there are
two methods available - tuning for minimum E_∞ or maximum
decrement amplitude. A fundamental method is to measure
the frequency of the echo decrement.

The simplest method of measuring internal friction is again
by use of the crossover. It may be calculated from the
increase in the number of oscillations to crossover over
the undamped case. Other methods are the measurement of
E_∞/E_o and observation of the logarithmic decrement.

Finally a special feature of the method must be discussed.

The resonator loses energy in three ways - by internal
friction in the material, by reradiation down the trans-
mission line, and by radiation to the medium surrounding
the resonator. This third type of loss is very small when
the resonator is in air and will be neglected.

$$Q_T^{-1} = Q_c^{-1} + Q_m^{-1} \qquad\qquad 3.11$$

Q_T = total 'Q' Q_c^{-1} = coupling loss

Q_m^{-1} = internal friction
(material loss)

Q_c^{-1} is of necessity quite large, normally being in the range 5×10^{-3} - 50×10^{-3}. This is an important feature of this method and means that low values of internal friction cannot be measured. However, Q_c^{-1} is constant throughout the experiment so that a Q_m^{-1} of 10% of Q_c^{-1} can easily be measured. Methods for the determination of Q_c^{-1} are described in 4.4c.

3.4b Summary of mathematical results

For the echo signal Sharp (1974) showed the following:

$$n_x \simeq \frac{Q_c Q_m}{\pi(Q_c + Q_m)} \ln (2 Q_m/[Q_m - Q_c]) \qquad 3.12$$

$$n_o \simeq \frac{Q_c}{\pi} \ln 2 \quad = \quad Q_c/4.55 \qquad 3.13$$

$$\frac{n_x}{n_o} \simeq \frac{\ln 2 - \ln(1 - Q_m^{-1}/Q_c^{-1})}{(\ln 2)(1 + Q_m^{-1}/Q_c^{-1})} \qquad 3.14$$

$$\frac{Q_m^{-1}}{Q_c^{-1}} = \frac{1 - E_\infty/E_o}{1 + E_\infty/E_o} \qquad 3.15$$

These results apply to the resonant condition when $n_x > 5$, resonant frequency > 1 kHz, $Q_m^{-1} < 5Q_c^{-1}$.

Thus the internal friction Q_m^{-1} can be obtained from measurements of n_x or E_∞/E_o. The phase of the late part of the echo signal relative to the early part is given by:

$$\delta\phi \simeq 3.65 \, Q_c \cdot \frac{\delta f}{f_o} \qquad 3.16$$

for small δf, $Q_m = \infty$.

For appreciable internal friction the 3.65 factor is
increased.

The behaviour of the echo decrement is well known

$$A_2 = A_1 \exp \pi n/Q_T \qquad\qquad 3.17$$

or $\quad Q_m^{-1} = \left\{0.73/(n_2-n_1)\right\} \log_{10}\left(A_1/A_2\right) - Q_c^{-1}$

$$3.18$$

Method	Frequency range	Amplitude range	Maximum operating temperature	Internal friction range q^{-1}	Specimen shape	Remarks
Torsion pendulum (Berlec 1970)	0.1 Hz - 1 kHz	$10^{-9}-10^{-4}$	2500°C	$10^{-6}-10^{-1}$	wire	The most popular method
Piezo-electrically driven resonator (Mason 1950)	10-200 kHz	$10^{-9}-10^{-4}$	500°C	$10^{-6}-10^{-1}$	rod	
Magnetostrictively driven resonator (Carnahan 1963)	10-200 kHz	$10^{-9}-10^{-4}$	200°C	$10^{-6}-10^{-1}$	rod	
Electrostatically driven resonator (Southgate 1966)	10-200 kHz	$10^{-9}-10^{-4}$	2000°C	$10^{-7}-10^{-2}$	rod, reed	Good for measuring low damping at high temps.
Pulse attenuation (Bell 1957)	200 kHz - 10 mHz	$10^{-7}-10^{-5}$	3000°C	10^{-3}	wire,thin or thick bar	
Quasi-static (Threader and Feltham 1973)	0.01 - 1 Hz	$10^{-4}-10^{-2}$	500°C	$10^{-4}-10^{-1}$	bar	
Bell	20 kHz - 500 kHz	$10^{-5}-10^{-4}$	3000°C+	$10^{-3}-0.2$	good variety e.g. rod wire strip bar disk	Very versatile

FIGURE 3.1 – Some methods of measuring internal friction. The references given refer to a recent user: In most cases several authors have made use of the method. The capabilities of the Bell method are given below for comparison.
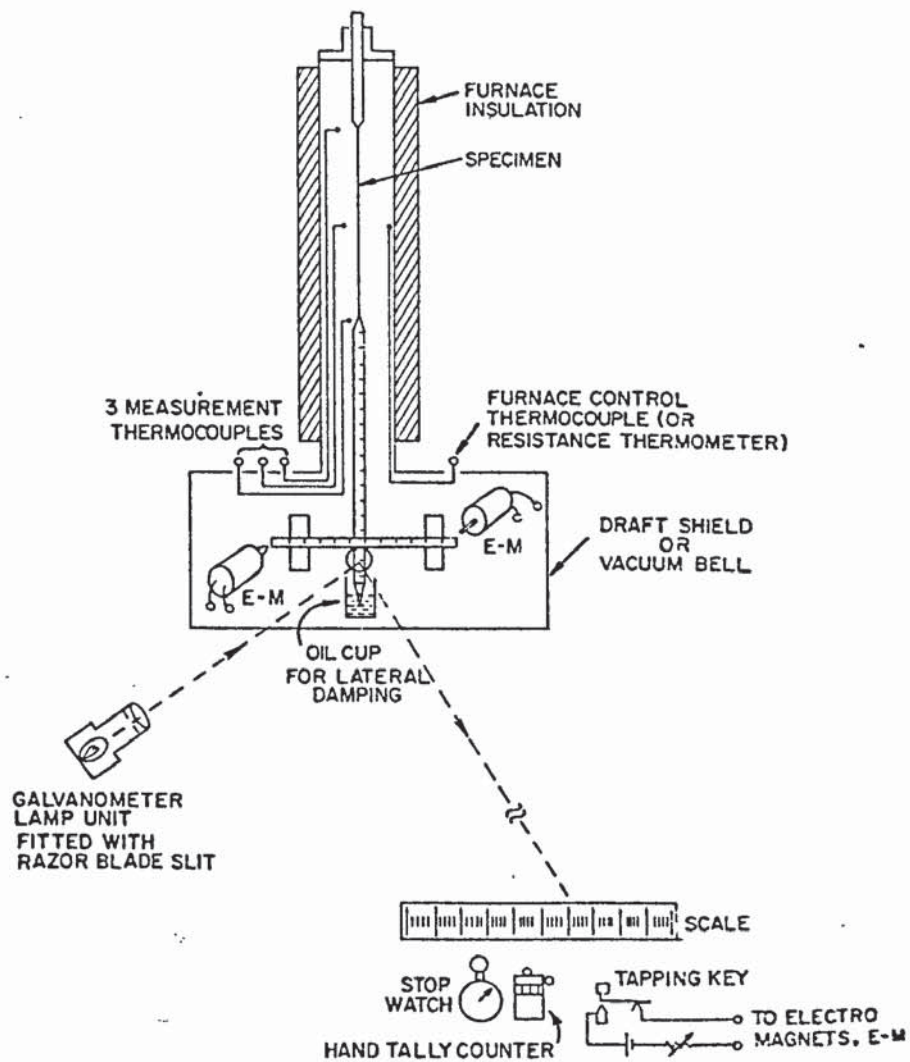
FIGURE 3.2 - Torsion pendulum of the type used by Kê

A convenient experimental procedure is to both count and time the number of cycles between two measured amplitudes so both decrement and frequency are determined simultaneously. In other types of apparatus the oscillations are recorded on a pen recorder for later analysis.
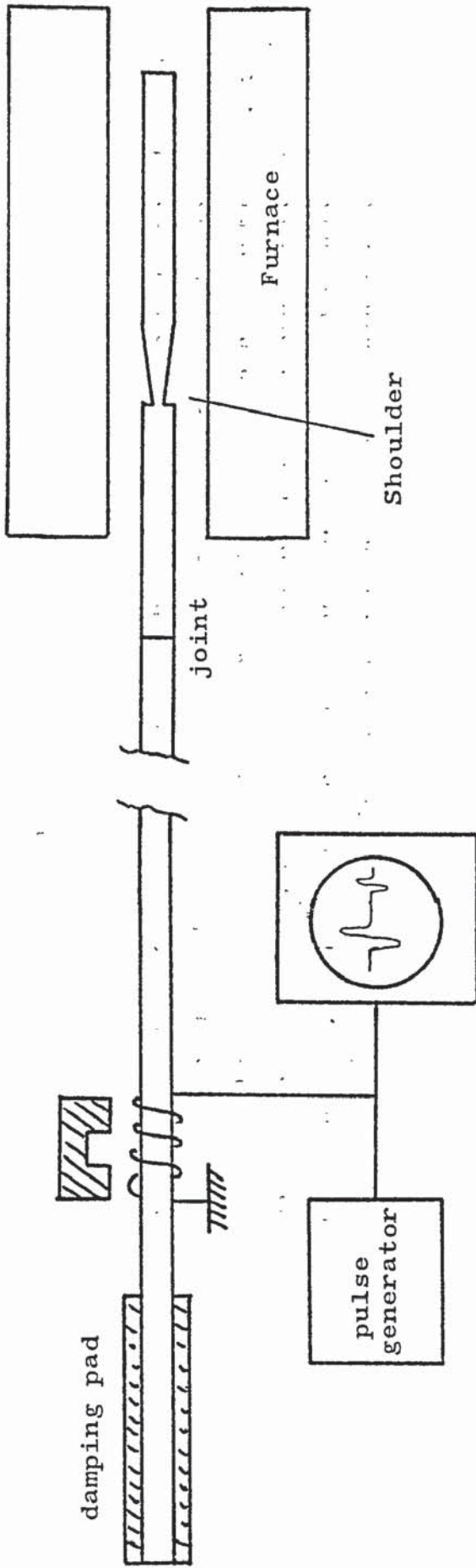
FIGURE 3.3 - The single pulse ultrasonic attenuation method. This is a simplified drawing of the apparatus used by Bell (1957). The time interval between the shoulder and end echoes gives velocity and the relative amplitude gives the attenuation. Various arrangements can be used to give much more accurate measurements than simple observation on the oscilloscope screen. A variant of the method uses a short burst of oscillations rather than a single pulse giving a more closely defined frequency.
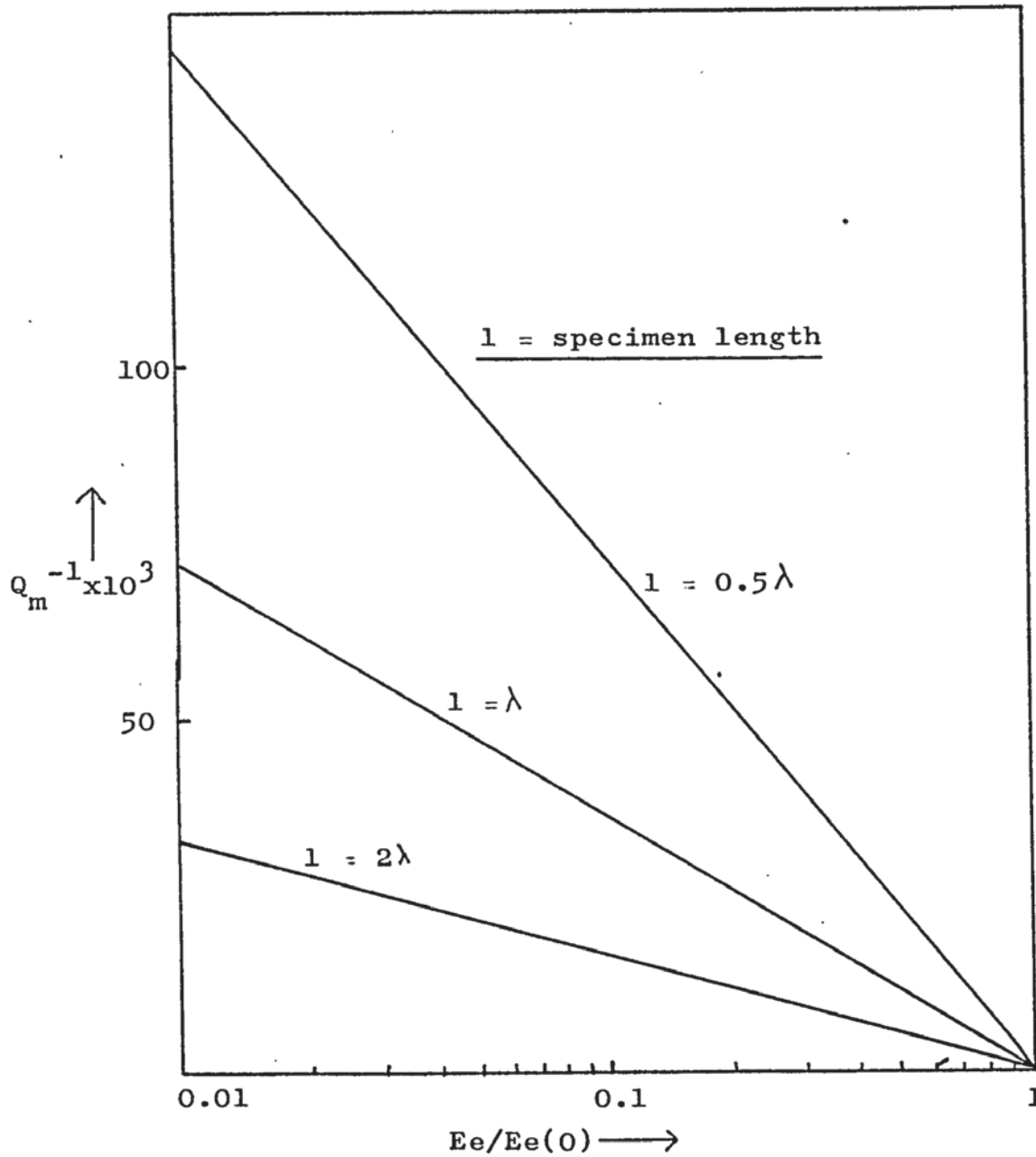
Ratio of echo amplitude:echo amplitude with zero
damping.

FIGURE 3.4 - Calibration curve for the single pulse
method showing the dependence of end echo
amplitude on internal friction and number
of wavelengths in the specimen.
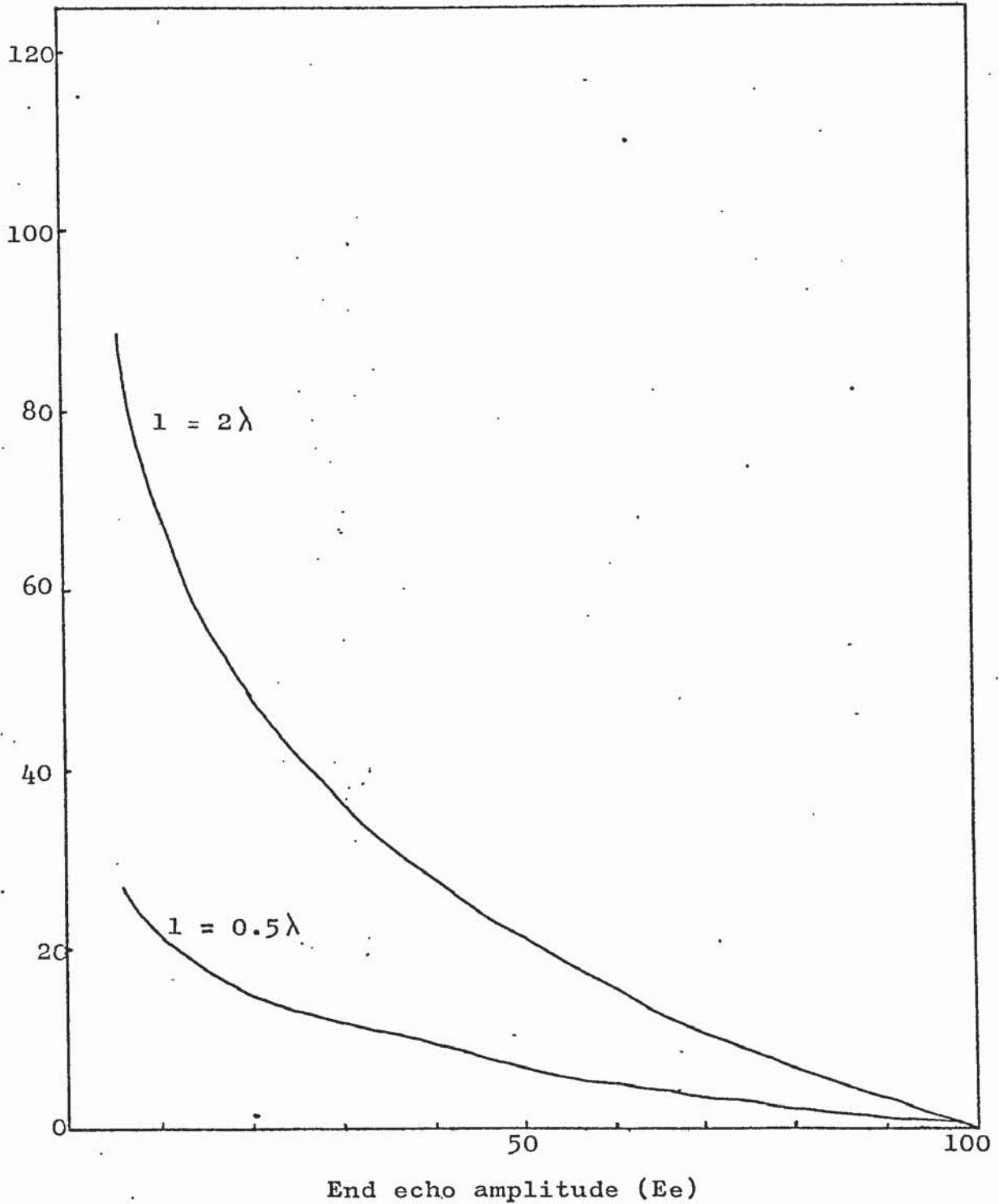
FIGURE 3.5 - Calibration curve for single pulse method. Figure 3.4 has been replotted on a linear scale to show the large errors possible when Ee becomes small.
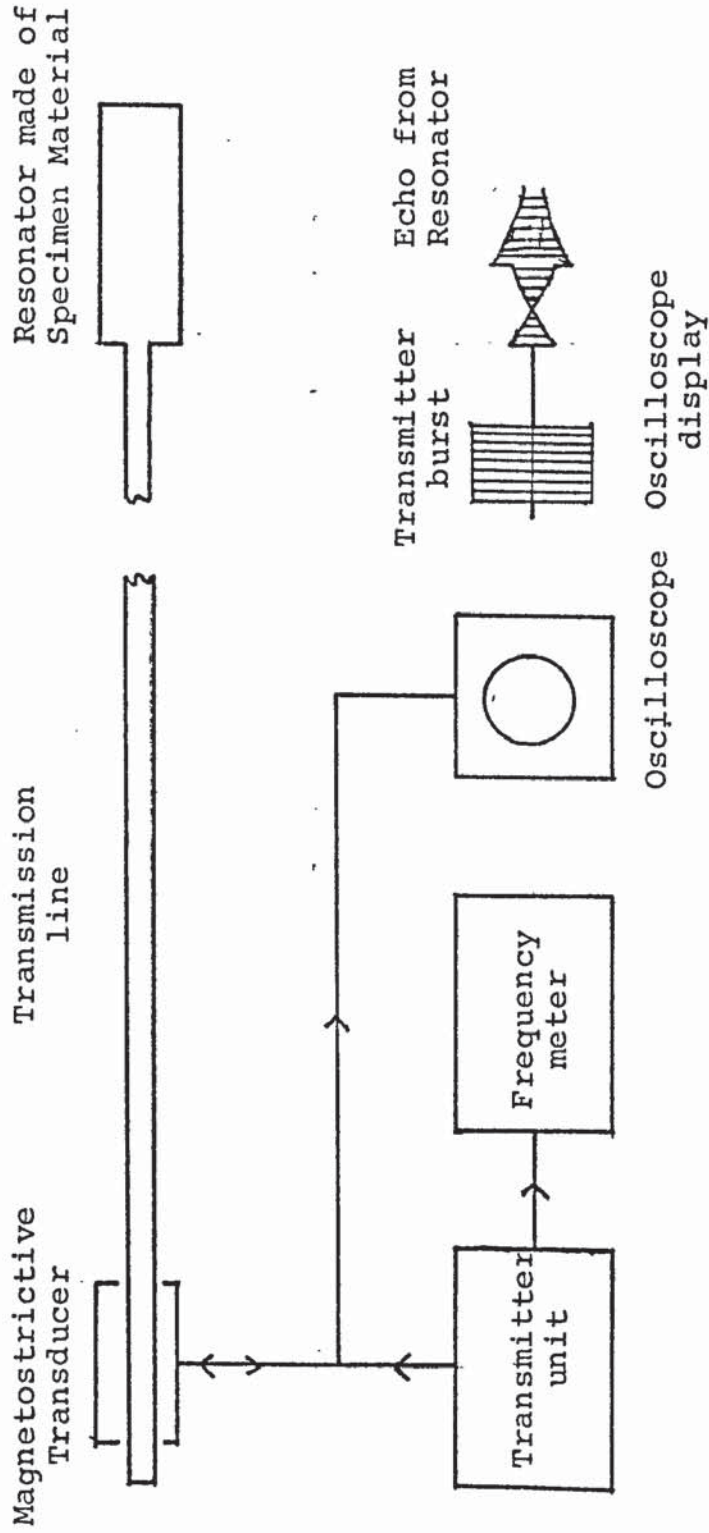
FIGURE 3.6 - Basic system for measurement of internal friction and elastic moduli by the Bell method.
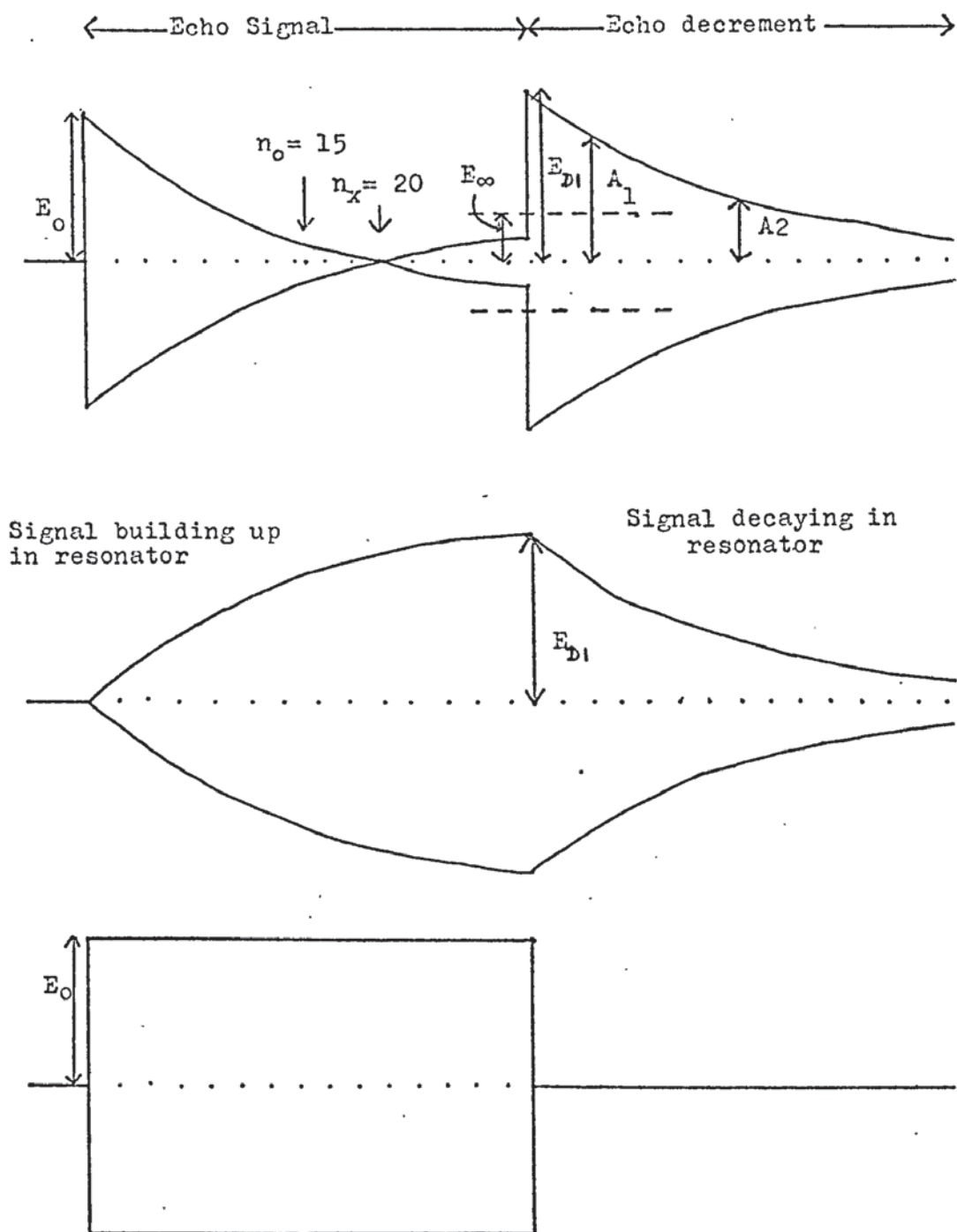
FIGURE 3.7 - A simple method of analysing the echo by splitting it into two components.
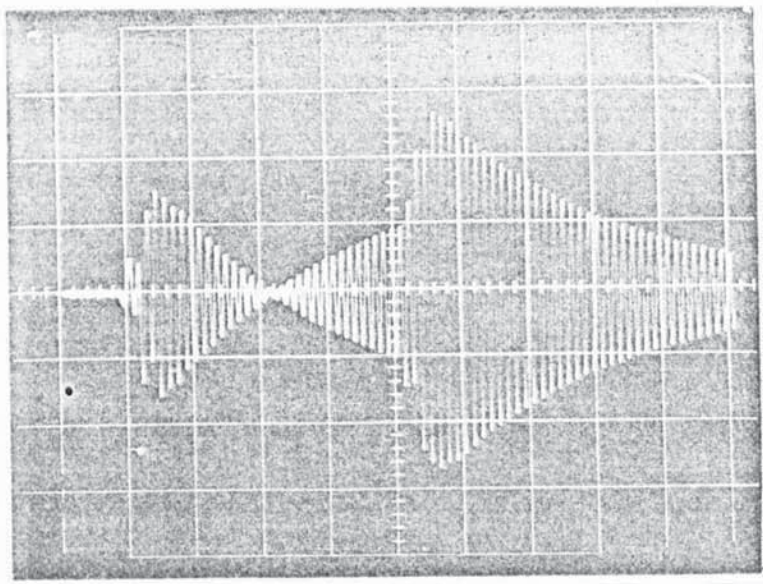
Transmitter tuned
to resonance
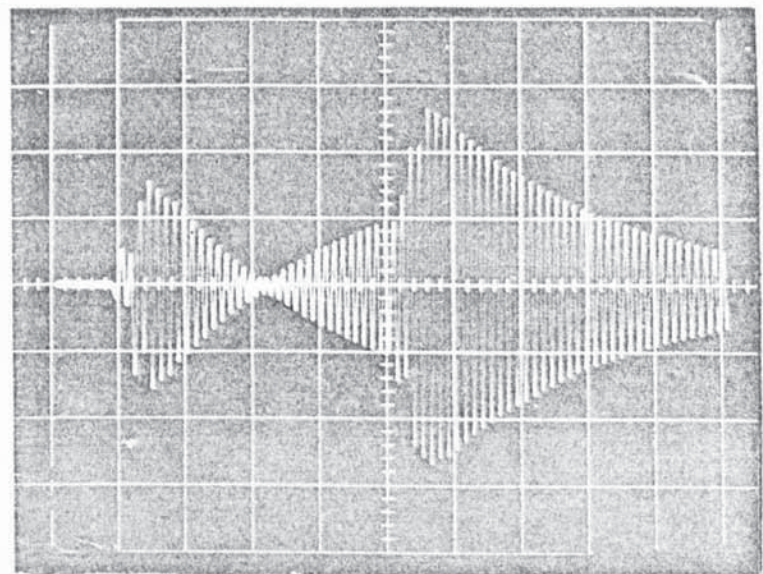
Transmitter frequency
increased by 0.1%
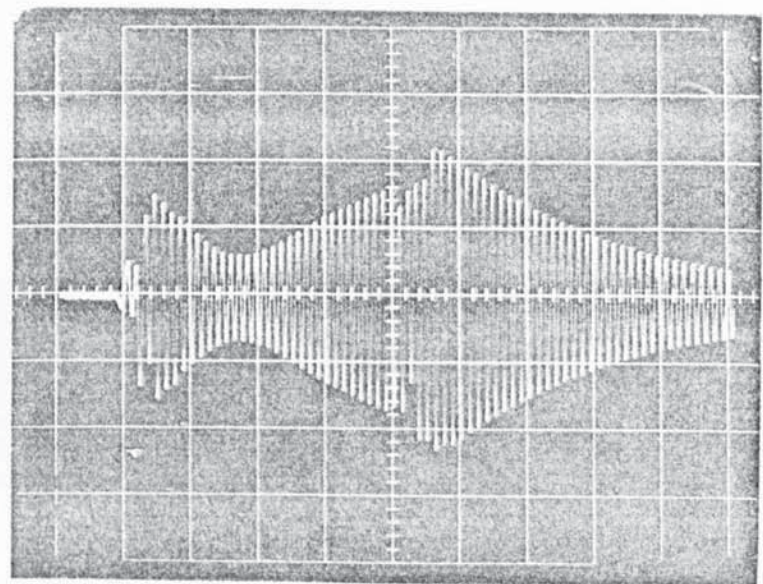
Transmitter frequency
increased by 1%

The decrease in the
amplitude of the echo
decrement is now
noticeable

10mm grid $Y = 20m$ V cm^{-1} $f_r = 98$ kHz

$n_o = 17$ $Q_c^{-1} = 12.9 \times 10^{-3}$

FIGURE 3.8 - Measurements of the resonator frequency using
the Bell method. The figure illustrates the
sensitivity of the 'crossover' method.
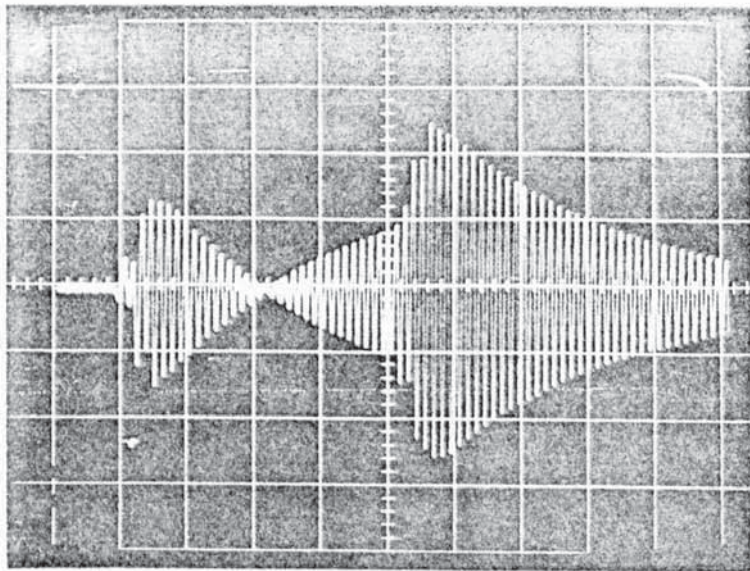
Internal friction
negligible

$Q_m^{-1} = 0$

$n_x = n_o = 17$
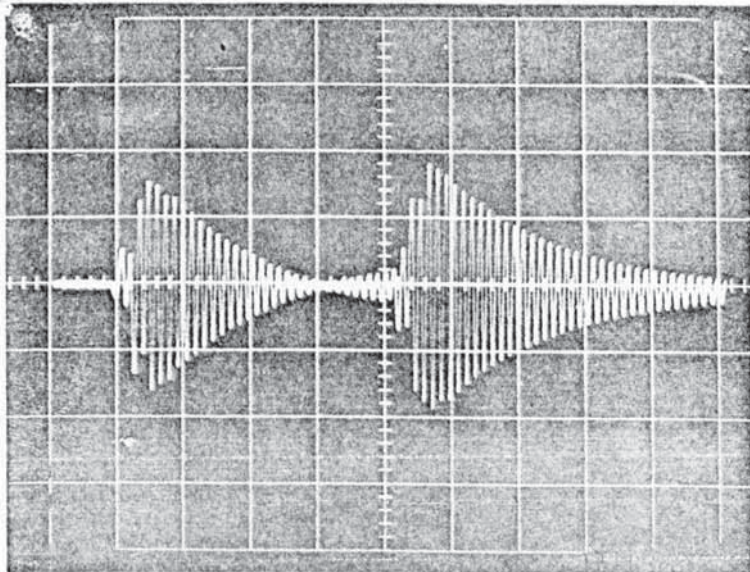
Internal friction apprec-
iable

$Q_m^{-1} = 7.4 \times 10^{-3} = 0.57 \, Q_c^{-1}$

$n_x = 24$

The crossover has 'moved
out' and the decrement
amplitude is noticeably
reduced.

E is now much less than E_0
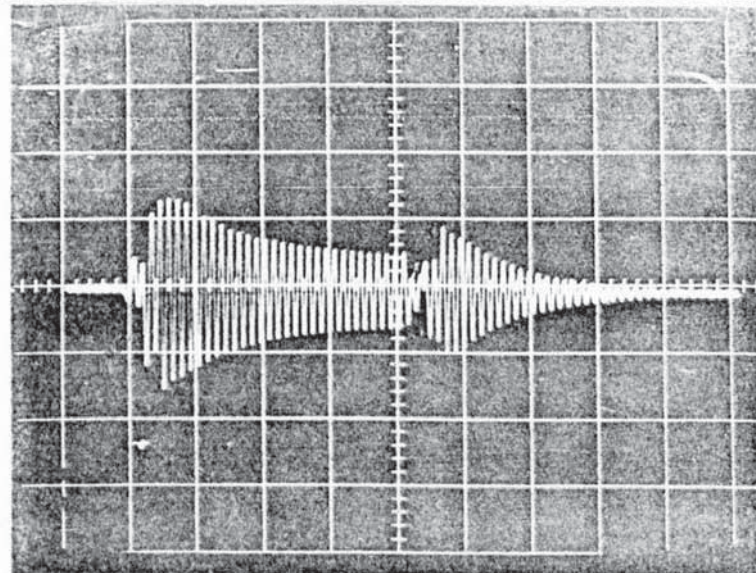
Internal friction now large

$Q_m^{-1} = 27.3 \times 10^{-3} = 2.12 Q_c^{-1}$

The crossover has now dis-
appeared and the echo
decrement is now small

10mm grid Y = 20mV cm^{-1}

$n_0 = 17$ $Q_c^{-1} = 12.9 \times 10^{-3}$

$f_r = 98$ kHz

FIGURE 3.9 – The effect of internal friction on the echo.
For this demonstration the specimen was artificially
damped by applying a thin film of grease so that
the frequencies remained constant. In a typical
furnace run a similar progression of echo shapes
will be seen accompanied by a fall in frequency.

CHAPTER 4:   APPARATUS AND PRELIMINARY EXPERIMENTS

4.1 Acoustics

The basic acoustic system, consisting of a magnetostrictive
transducer, a transmission line and a resonator has been
shown in Figure 3.6.

4.1a The transducer

The theory of the magnetostrictive transducer is given by
Kikuchi (1969) and Seth (1974). An electromagnetic coil
induces stress waves in the magnetostrictive wire. It is
necessary to apply a magnetic bias of half the saturation
value. Two transducers that were used are shown in
Figures 4.1, 4.22, which for these experiments consisted
of a few hundred turns of wire wound on a ceramic tube which
fitted closely round the magnetostrictive wire. For optimum
performance the length of the winding should be 0.4λ. Thus
a series of transducers was made to give good performance
in the range 40 to 200 kHz and for the different sizes of
transmission line used, the diameters being 0.5, 1.0 and
3.0 mm. The coil design is not at all critical and in an
experiment on a longitudinal resonator where modes up to
the fifth harmonic were measured the transducer was not
changed. Normally a horseshoe magnet was used to bias the
magnetostrictive material but for the 0.5 mm wire sometimes
a small ferrite ring magnet was used. No effort was directed
at optimising the performance of the transducer as it was
felt that this would not significantly improve the overall
result.

The transducer has to be tuned for maximum echo amplitude on

the oscilloscope. This involves tuning the capacitor in
the parallel resonant circuit and then mechanically tuning
it by adjusting the position over the magnetostrictive rod
so that the end is $\lambda/4$ from the centre of the coil. Thirdly
the bias magnet has to be adjusted for optimum bias. A
simple slide mechanism was made for the magnet and coil
assembly so that these adjustments could be made. The tuned
nature of the transducer ensures that the line is driven
with a reasonably pure tone (the transmitter output being
a square wave) and that noise and resonances at other
frequencies are filtered out. It has the disadvantage that
it is necessary to retune when looking at other modes of
the same resonator and that transients in the echo are not
reproduced due to the limited bandwidth.

4.1b The transmission line   .

Three diameters of transmission line were used - 0.5mm, 1.0mm
and 3mm. The thinner lines were used to drive the longitudinal
resonators according to the tightness of coupling (Q_c)
required. The thin lines were generally made of a 50/50
iron-nickel alloy (telcoseal). This alloy is magnetostrictive
so that the transmission line can be part of the transducer.
The attenuation is higher than for steel but as only short lines
up to 4m length were used this was not a disadvantage. The
wire had to be stretched before use to harden it. The 3mm
lines were of mild steel and used for driving the tuning
fork resonators. A piece of 3mm permendure about 80mm long
was silver soldered to the end to use as a magnetostrictive
transducer. The line must be free of kinks and mechanical
damage otherwise spurious echoes will be caused. Considerable
care has to be taken when supporting thin lines to prevent

unwanted echoes. Outside the furnace the line can be
supported on pieces of rubber foam. Inside the furnace
ceramic wool can be used. A vertical arrangement means that
a minimum of guides are required. When the line was lead
into a vacuum system it was fed through a short length of
rubber bung, and the line was greased to prevent adhesion.
For the inert gas systems, which were slightly pressurised,
a hole packed with ceramic wool was used.

The line length must be sufficient to prevent overlap between
the transmitter signal and the return echo. The time delay
between transmitter pulse and return echo produced by the
line will be:

$$t = 2\frac{l}{c}$$
4.1

or in general terms were a composite line is used:

$$t = 2\sum\left(\frac{c_i}{l_i}\right)$$
4.2

Generally the number of oscillations in the transmitter burst
was made about twice the initial oscillations to crossover.

Thus the criterion:

$$\sum\left(\frac{l}{c}\right)_i \geqslant \frac{1.5n_o}{f}$$
4.3

can be drawn up for the line length required.

The 1.5 factor gives a safety margin between the end of the
transmitter burst and the start of the return echo.

A hazard that can occur with transmission lines is that the
line itself can generate a crossover signal due to resonances

in the line, probably caused by mode conversion. The
frequencies used in this work were usually over 50 kHz
and little trouble was experienced with this effect.

4.1c Acoustic joints

Normally joints have to be made in the acoustic system.
For high temperatures, joints between say a longitudinal
resonator and the line, which are an acoustic mismatch,
were made by flash butt welding. This technique could be
used for lines up to 1.5mm diameter with the 'STP' type W L4
welder which was used. To improve the mechanical strength
a 1mm deep clearance hole was drilled in the end of the
resonator to fit over the transmission line. Where temp-
erature permitted araldite or silver solder was used.
Ceramic cements e.g. autostick were found to be rather un-
reliable and their use was avoided in internal friction work
as a bad joint could affect Q_c and cause errors in the results.

Joints between different sections of transmission line were
made by silver soldering. The two ends were filed flat and
carefully tinned with a little silver solder. The rods
were then placed on guides, heated up and the ends pushed
together. After cooling any excess silver solder was
removed. Using this technique the residual echo was about
1% of the end echo at 100 kHz. To give a small junction echo
the silver solder thickness must be a very small fraction of
a wavelength (see Appendix A). When a joint is made of two
dissimilar materials then they must be acoustically matched
at the junction otherwise there will be an echo of amplitude
given by:

$$A = A_o \left(\frac{Z_1 - Z_2}{Z_1 + Z_2} \right) \qquad\qquad 4.4$$

Z = acoustic impedance   A = amplitude

To make $Z_1 = Z_2$ the cross sectional area must be adjusted so that:

$$\rho_1 c_1 A_1 = \rho_2 c_2 A_2 \qquad\qquad 4.5$$

A_1, A_2 = cross sectional areas.

A 5% error in diameter will give a 10% error in impedance giving a 5% echo.

For poorly characterised materials (e.g. ceramics of unknown porosity) ρ was first measured by measuring and weighing and c determined by setting up a sample as a longitudinal resonator.

A line of one acoustic impedance can be made to drive a line of another acoustic impedance if the cross sectional area is adjusted by tapering. One of the rods can be tapered down by up to 30% of its diameter over a distance of 50mm. More drastic tapering is likely to produce too great an unwanted echo and a smaller diameter rod should be used.

Although the two lines may be correctly matched and the soldered joint good, an echo can still arise if the two parts of the line have a very different shape - an example of this is the junction between a rod and a strip feeding a tuning fork resonator. 3mm diameter mild steel rod gives an acceptable performance when joined to mild steel strip 1.5mm x 4.7mm but performance is poor for 1mm x 7.1mm. If the strip had a higher specific acoustic impedance than the steel,

it would be narrower but in general it can be said that joints to strip thinner than 1mm are not very satisfactory. A solution to this problem was not found but it is suspected that if a 'matching section' of the shape shown in Figure A.3 were inserted then a good joint would result but fabrication is difficult.

A special technique had to be used to make ceramic to steel joints. At first araldite was used but this gave a very poor joint. The type of joint used is shown in Figure 4.4. This type of joint keeps the ceramic under compression. The ceramic is machined on a diamond wheel and the sockets in the steel adjusted to fit. There was some controversy over the cause of the large echoes obtained using araldite. Two suggestions were that the echo was due to imperfect mechanical fit in the joints or poor adhesion of the araldite. The authors view was that practical improvements in the joint quality would not reduce the echo and that a jointing medium of higher impedance than araldite must be used. A few experiments were done to show the effects of different adhesives. The table in Figure 4.4. shows the great super-iority of silver solder over araldite and 'black vacuum wax' for the same joint. An attempt was made to increase the acoustic impedance of araldite by suspending copper powder in it but this gave no better result.

It was decided that a new approach must be tried of putting a metal coating on the surface which could then be soldered to the steel transmission line. After considering evaporation it was decided to try Johnson Matthey silver paint preparation.

This was extremely successful, giving an echo of 5% at 150 kHz.

The process takes some time and care, to be successful. It works with most ceramic materials. The ceramic is carefully cleaned after machining and degreasing. It is then painted with FSP/411 (see the Johnson Matthey Data Sheet for full details) and allowed to dry. It is then painted with FSP/412 allowed to dry, slowly heated and fired at 700°C in air. Careful use of a flame was found to be satisfactory for 3mm rod but the most reliable way is to use a furnace. Next the steel and the ceramic were tinned with silver-tin-lead ceramic solder (Johnson Matthey Ceramic Solder No.1) using a resin flux. Finally, the parts were put on guides, heated and pushed together. The maximum recommended soldering time is 10 seconds but it was found that this could be exceeded. Nevertheless, soldering time was kept to a minimum by rapidly cooling the parts after soldering.

This section may be summarised as follows:

1. For joints between a line and a resonator the joint quality is not particularly important provided it stays constant. Suitable processes are araldite, silver soldering and welding.

2. Joints in the transmission line must be very high quality and soldering is the best process. Welding is not so satisfactory because the material becomes coarse grained.

3. Slight 'keying' of the joint improves mechanical strength and acoustic performance due to the larger contact area.

4. All joints give progressively larger echoes as the frequency increases (i.e. act as low pass filters).

4.1d Resonators

The useful types of resonant systems that can be attached to the transmission line will now be discussed and are shown in Figure 4.2.

The Longitudinal resonator:

This type of resonator usually consists of a round or square section bar but a rectangular plate can also be used.

The formula for the resonant frequency is:

$$f_{(m)} = \frac{m}{2l} \sqrt{\frac{E}{\rho}} \qquad 4.6$$

for the case when $\lambda \gg d$ where d is the diameter or width of the resonator. For a rod the Rayleigh correction can be made when this condition is not fulfilled. In all resonant modes the ends are antinodes and there are one or more nodes in the resonator.

The coupling Q_c is given by:

$$Q_c^{-1} = \frac{\pi}{2m} \frac{Z_l}{Z_r} \qquad 4.7$$

$$\text{where } Z = \rho c A \qquad 4.8$$

This resonator type was much used for the metal specimens - the specimen usually being flash butt welded to the line but sometimes silver soldering was used. This is not a suitable resonator for non metal specimens except near room temperature when various adhesives can be used. The advantages of this type of resonator are that frequency dependence of internal friction can be measured by use of the harmonic modes and also the higher modes giving a lower

$Q_c{}^{-1}$ can be used to give improved sensitivity when the damping is low.

The integral line tuning fork resonator

This type of resonator was developed for the ultrasonic thermometer (Seth 1974; Bell, Seth, Fathimami 1975). It overcomes the problem of making a high temperature joint between the line and resonator by forming the resonator on the end of the transmission line.

The general design of this resonator is shown in Figure 4.2. It involves making three slots in a round rod or a strip transmission line, and this design is very suitable for ceramics as a diamond wheel can be used to cut the slots. The tuning fork lines vibrate in a flexural mode and are coupled to the main part of the transmission line by the neck.

The mathematical theory of such a resonator is obviously complicated and has not been explicitly solved. An experimental approach has been used to discover the properties of this resonator.

For the rod resonator:

$$f = \frac{C}{D} \, f_1(\frac{a}{D},\frac{b}{D},\frac{c}{D},\frac{d}{D},\frac{e}{D}) \qquad\qquad 4.9$$

$$n_o = f_2(\frac{a}{D},\frac{b}{D},\frac{c}{D},\frac{d}{D},\frac{e}{D}) \qquad\qquad 4.10$$

where D is the diameter and a-e are dimensions as shown in Figure A.1.

For the strip resonator analogous formulae apply where
D represents the strip width. The thickness has little
effect provided it is much less than D. Seth (1974) gives
an empirical formula for calculating f, n_o which works over
a limited range of parameters. The resonator designs in
this thesis were first made in mild steel and then the
dimensions scaled to suit the particular specimen for the
values of C, D. Accurate machining (tolerances of the
order of 0.01mm) is required to achieve the calculated
performance. This tolerance is difficult to achieve in
hard metals or ceramics, so the resonators were machined
to 0.1mm limits and a final adjustment made if necessary
after an acoustic test. The frequency is mainly controlled
by the length d of the tines. Shortening the tines increases
the frequency and tightens the coupling. The coupling for
a given frequency is mainly controlled by the dimensions
a, c. In the rod resonators it is difficult to achieve a
tightly coupled low frequency resonator. For the strip
resonators it is much easier to adjust the coupling.

Seth (1974) observed the second overtone to be several times
the fundamental but the coupling is very strong so that
this type of resonator cannot be used for frequency depend-
ance work unless the tines are cut down to increase the
frequency on a subsequent furnace run.

Other types of resonator

The in plane modes of a disc have been used (Sharp (1974);
Bell, Sharp (1974)) to measure Young's modulus and Poisson's
ratio. These resonators would also be useful for measuring
internal friction.

Flexurally driven bars, with the transmission line coupled at the centre can be used. By using a thin bar the length for a low frequency can be less than for a longitudinal resonator, but the coupling of the overtones does not vary in such a regular manner as the longitudinal resonator.

An integral line longitudinal resonator can be made by machining down the line to a small diameter at the end. A diameter ratio of 1/3 gives $n_o(m=1)=6.2$. This design is rather fragile but combines the advantages of the long- itudinal resonator with the integral line principle.

4.2 Electronics

The function of the electronic system is to generate bursts of oscillations at a measured frequency and having a pre- determined number of oscillations in the transmitted pulse. This is similar to the type of signal generated in radar and sonar systems. Circuits are also provided to facilitate the analysis of the return echo. The block diagram is shown in Figure 4.5. The circuit diagram and some notes on the electronics are given in Appendix B. Where possible TTL digital integrated circuits were used.

The transmitter consists of a variable frequency voltage controlled oscillator covering 10-300 kHz in four ranges. It consists of a pair of cross coupled monstables and has a short term stability for a few Hz per minute and a voltage sensitivity $(\frac{1}{f} \frac{df}{dV})$ of 0.01% per mV. The advantage of this type of oscillator is that it can be started and stopped at will without transients. This is useful when measurements on the echo are being made using a reference signal and

also when using an automatic tracking mode. A digital
frequency meter reads the oscillator frequency. This
signal is fed into a gate which is open for a variable
duration to control the number of oscillations in the burst.
A second oscillator of similar design controls the repetition
rate. This is normally set to about 50 Hz but a lower rate
has to be used if very long bursts are used. The output
circuit is a push pull transistor arrangement giving an
output of 30V peak to peak, at a maximum peak current of
0.5A. The square wave output is converted to an approximately
sinusoidal waveform by the electrical and mechanical
resonance of the transducer.

The second electronic unit is used for counting oscillations
in the echo and the decrement for measuring internal friction.
The 'front end' opens the gate at the start of the echo. A
level control adjusts the amplitude at which the gate triggers
and a time delay control holds off the gate until shortly
before the echo starts, thus preventing stray noise from
triggering it. The gate is shut off after a number of
oscillations set by a thumbwheel switch 0-999 on the front
panel. The oscillator signal feeds into the gate and the
output drives the second beam of the oscilloscope. This
allows easy counting of the oscillations to crossover or
counting of oscillations in the decrement.

The third unit was built into the same box as the trans-
mitter and can be used to measure phase in different parts
of the echo. A sample of two oscillations is taken at the
beginning and end of the echo signal and compared with a
reference signal of the same frequency. When the oscillator

is on tune the late part of the echo signal is in antiphase
with the early part of the echo. Thus the phase detector
output can be used to control the voltage controlled oscill-
ator, which will track resonances of the resonator. The
principle is shown in the block diagram. The echo is
identified as in the second unit and this restarts the
oscillator (which has to be stopped in this mode to allow
generation of a reference signal of the correct phase). This
starts a counter which opens a gate for the second and third
count and also two late oscillations (adjustable by patching
- typically oscillations 20 and 21). These signals are fed
into an integrator together with the reference signal giving
an analogue output which is a measure of the phase (see
Pelmore 1971 for a full description).

This phase detector system is not fully satisfactory. During
a temperature run the echo will go 'off crossover' - typically
the frequency error is 0.1% for a 5% change in frequency.
This is due to the fact that the phase detector is frequency
sensitive due to the finite switching delay of the gates
(10ns) compared with the period of the oscillations (typically
$10\mu s$).

The phase detector system was little used for the measurements
in this thesis for a number of reasons. If several modes
were to be measured it required resetting up for each mode
and it could not make measurements when there was no cross-
over. Further development work on this system was discontinued
because Seth (1974) started work on a tracking oscillator
system which sampled the echo decrement and this seemed more
promising. This work was further developed by Fathimani (see

Bell, Fathimani and Seth 1974). This system has very good performance, is flexible and could now be applied to the automatic measurement of Young's modulus up to high temperatures and at the same time to facilitate the internal friction measurements.

4.3 Acoustic experiments

Before making use of the apparatus to measure internal friction at very high temperatures a number of preliminary experiments were carried out. At this time the mathematical analysis of Sharp (1974) had not been completed.

Firstly, a series of amplitudes in the echo signal and the echo decrement were measured to check that the signals were truly exponential. Using a mild steel specimen at room temperature this was found to be so to within the limits of experimental error. A deviation could have indicated amplitude dependent internal friction but Q_m^{-1}/Q_c^{-1} would have to be appreciable for this effect to show up.

A second experiment was the result of an accidental observation while observing the phase of the early and late parts of the echo signal, using the automatic system. It was noticed that if the resonator was damped, then the phase seemed to change more rapidly with detuning than for the undamped case. A brief experiment was performed to investigate this effect. A mild steel resonator was used with a frequency of 120 kHz and $n_x = 20$ ($Q_c^{-1} = 11 \times 10^{-3}$). Oscillations 3, 4, 51, 52 were observed in the echo signal. Experimental observations using a two beam oscilloscope showed that the discriminator output varied between $\pm 3V$ corresponding to phase differences of 90°

and 270° giving a sensitivity of 33mV per degree. Phase
measurements were first made for a lossless resonator.
Then a thin film of grease was applied to the resonator to
increase n_x to 30 ($Q_m^{-1} = 6.6 \times 10^{-3}$) and another set of
readings taken. The results are shown in Figure 4.7. The
results were surprising and at first difficult to understand
from general principles. The theory of Sharp (1974)
formulated after this experiment also showed this effect,
which thus gave very satisfactory verification of the exact-
ness of the Sharp model.

The effect can also be understood in a qualitative way,
referring to Figure 4.8, when tuned to crossover the late
part of the signal must always be 180° out of phase because
the signal B is dominant and is at the same frequency as
signal A. However, off tune the signal B is not at the
same frequency as signal A and therefore the late part of
the signal consisting of a composite signal (A+B) will not
have the same phase as previously. The smaller signal B,
the closer (A+B) will be to 360° for $f_s > f_r$, i.e. the
greater $\Delta\phi$. The causes of the small signal B on detuning
are either a high Q or high Q_m^{-1}/Q_c^{-1} and in both cases there
will be a large change of phase on detuning. It is worth
mentioning at this point a weakness of the simple explanation.
This theory would predict a continuous beating of (A+B)
whereas in practice the amplitude modulation effect decays.
The Sharp theory, however, gives the correct result.

Another experiment was performed to determine the approximate
strain amplitude of vibration in the resonator. This was done
using a Bruel and Kjar condenser microphone. A measurement
of the 40 kHz fundamental mode of a typical longitudinal

resonator gave a strain amplitude of $\sim 3 \times 10^{-5}$ at the ends.
Another experiment by JCK Sharp on the in plane modes of a
disc using a speckle interferometer at NPL yielded a similar
result. From these results it can be assumed that the internal
friction measurements were made at a 'medium' amplitude i.e.
in the range $10^{-5} - 10^{-4}$.

4.4 Methods of determining Young's modulus and internal friction from the echo

In the following sections the various possible methods of
determining Young's modulus and internal friction from the
echo will be discussed together with some experimental tests
to compare their advantages.

4.4a Young's modulus

To determine Young's modulus of the specimen the resonant
frequency must be determined. For a longitudinal resonator:

$$f(m) = \frac{m}{2l} \sqrt{\frac{E}{\rho}} \qquad\qquad 4.11$$

where $\lambda \gg d$ otherwise the Rayleigh correction must be
applied:

m = mode number

$$E \propto f^2 \rho l^2 \qquad\qquad 4.12$$

Equation 4.12 also holds true for flexure and torsion.
When determining the change in Young's modulus with temperature
a small correction must be made for the change in specimen
length and density.

$$\frac{E(\theta)}{E(\theta_o)} = \frac{f^2(\theta)}{f^2(\theta_o)} \left[1 - \alpha_{le}(\theta - \theta_o) \right] \qquad\qquad 4.13$$

α_{le} = coefficient of linear expansion. θ = temperature.

Typically for mild steel the coefficient of linear expansion is 5% of the temperature coefficient of Young's modulus.

There are five ways of determining the frequency from the echo:

1. Tune for a crossover.
2. Tune for a 180° phase difference between the early and late parts of the echo signal.
3. Tune for minimum E_∞
4. Tune for maximum decrement amplitude.
5. Measure the frequency of the echo decrement directly.

Method 1. is very simple and very accurate, giving a resetting accuracy of about 0.01%. The sensitivity of this method increases with the Q of the resonator. It could be analysed using the method of Sharp (1974).

Method 2. does not give a useful visual signal but has been used as the principle in several automatic instruments. The most recent one was built by Pelmore (1971). The disadvantage of this method is that phase detectors tend to be frequency sensitive giving an error of say 0.1% for a 10% change in frequency.

Method 3. is used when the internal friction is too high to see a crossover but is not as sensitive as method 1.

Method 4. is always applicable and the tuning characteristic is given by (for small frequency deviations):

$$A = \frac{A_r}{\sqrt{1 + 4Q_T^2 (\frac{\delta f}{f_r})^2}}$$

4.14

at the half power points $\quad Q_T = f_r/2\delta f$ 4.15

and $\quad \dfrac{\delta f}{f} = \dfrac{1}{Q_T} \sqrt{\dfrac{A_r}{2A_r}}$

Thus if $Q_T = 50$, the preciseness of tuning would be expected to be 0.2% for a 2% drop in amplitude.

Method 5. is intellectually the most satisfactory but requires complex instrumentation. The usefulness of this method was recognised by Johnson (1971) who also did some pilot work on it. Instruments have been built by Seth (1974) and Fathimani (1974).

In this work method 1. was used when there was a crossover. Failing this methods 3. and 4. were used. Automation was considered not worthwhile, method 5. being unavailable at the time. Another consideration was that in some experiments several modes of resonance needed to be measured making complete automation very difficult.

Absolute values of Young's modulus can be obtained for the longitudinal resonators but are very difficult to obtain for the tuning fork resonators due to the accuracy of dimensional measurement required. The measurements of frequency during the experimental runs were used to monitor changes in Young's modulus as an addition to the internal friction measurements.

One source of inaccuracy in measurements of frequency is the transducer. Although the Q of the transducer is small

relative to the Q of the resonator, and can be further reduced by use of a damping resistor, the effect is not entirely negligible and can give errors of 0.01% and more. This problem has been briefly discussed by Pelmore (1971) and Sharp (1974). The best policy during an experiment is to keep the transducer tuning fixed and tuned to a frequency midway between the highest and lowest. This is particularly true of the ultrasonic thermometer application were frequency reproducibility is all important.

A more important source of error is the presence of noise – particularly obvious in method 1. This will be discussed in 4.4b.

4.4b Internal friction

There are four possible methods of measuring internal friction:

1. Measuring the number of oscillations to crossover n_x.
2. Measuring E_∞/E_o for the echo signal.
3. Measuring the logarithmic decrement, i.e. measuring Q_T of the echo decrement.
4. Measuring the sharpness of tuning of the echo decrement.

Method 1

Equation 3.12, 3.13 will be repeated here for convenience:

$$\frac{n_x}{n_o} = \frac{\ln 2 - \ln(1 - Q_m^{-1}/Q_c^{-1})}{(\ln 2)\,(1 + Q_m^{-1}/Q_c^{-1})} \qquad 4.16$$

$$n_o = Q_c/4.55 \qquad 4.17$$

The accurate determination of n_o will be dealt with in 4.4c. In many cases at the start of a temperature run $Q_m^{-1} \ll Q_c^{-1}$

and therefore the initial value of n_x is in fact n_o.

Using 4.16 a graph can be drawn of Q_m^{-1}/Q_c^{-1} against n_x/n_o. This is shown in Figure 4.9. It is obvious that the method can be used over the range of values Q_m^{-1} lying between about 0.1 Q_c^{-1} and 0.9 Q_c^{-1}. A feature of the method is that to observe an initial friction peak of a certain magnitude the value of Q_c^{-1} must be chosen correctly. To observe small peaks the value of Q_c must be high. The lower limit of sensitivity can be calculated:

For small n_x/n_o

$$(\frac{n_x}{n_o} - 1) \simeq \frac{Q_m^{-1}}{Q_c^{-1}} \times 0.6$$

$\qquad\qquad\qquad\qquad\qquad\qquad\qquad\qquad$ 4.18

The smallest observable change in n_x for n_o = 50 was found to be about 0.5. Taking $\frac{\delta nx}{n_o}$ = 0.01 and the lowest Q_c^{-1} as 4.4 x 10^{-3}

$$Q_m^{-1} = 7 \times 10^{-5}$$

This is the lowest value of internal friction that can be reasonably expected to observe using visual methods, and quite probably electronic ones as well, due to acoustic noise on the transmission line and the inherently high background damping (Q_c^{-1}).

The relative sensitivity $\delta Q_m^{-1}/Q_m^{-1}$ varies with Q_m^{-1}. As Q_m^{-1}/Q_c^{-1} approaches 1 the sensitivity is potentially very high but it is realistic to take the value of $\delta Q_m^{-1} = 0.02 Q_c^{-1}$ as the detectable change over most of the range. For measuring Snoek peaks in iron n_o was set at 40 ($Q_c^{-1} = 5.5 \times 10^{-3}$) to measure a maximum internal friction of 2 x 10^{-3}. For the

high temperature grain boundary peaks of much larger amplit-
ude n_o was set at 8-15. When using the longitudinal resonators
Q_c^{-1} can be reduced to observe small values of Q_c^{-1} by using
higher modes but this is, of course, accompanied by a change
in frequency. This method is attractive because it is a null
method and only one observation i.e. n_x is required. Counting
the oscillations visually is laborious but use of a dual
beam oscilloscope and a reference signal makes the measurement
easy. For an unknown material it is worthwhile making a
preliminary experiment to determine approximate values for
velocity and damping. The specimen geometry can then be
optimised. While results are always obtainable by making
the coupling very loose it is more convenient to be able to
see a crossover over at least part of the temperature scan.

Method 2

The basis of this method is:

$$Q_m^{-1} = \frac{(1 - E_\infty/E_o)Q_c^{-1}}{(1 + E_\infty/E_o)}$$

4.19

This is shown graphically in Figure 4.10.

This method can be used over the whole range of values of
Q_m^{-1}. At first sight this method is attractive and has
been successfully used by Sadalat (1974) but it is often
difficult to make an accurate determination of E_∞, E_o in
practice. Firstly, the observed value of E_o will be less
than the true value due to the limited transient response
of the transducer. In fact, sometimes the observed value of
E_o is considerably less than E_∞ and the correction can vary
with frequency. Secondly, direct observation of E_∞ requires

a large number of oscillations. In this work short lines
were used and so this was not possible. An attempt was
made to overcome these disadvantages by measuring two
amplitudes as shown in Figure 4.11. This really amounts
to measuring the logarithmic decrement but an extra measure-
ment has to be made because the position of the asymptotic
line AB is unknown. A programme for a Hewlett Packard 2000
calculator was written to extract values of Q_m^{-1}/Q_c^{-1} from
the readings. The results were found to contain random
errors of up to 10%, due to accumulated errors in the readings.
This method was not pursued on grounds of inconvenience and
inaccuracy as compared with the crossover method.

Method 3

The principle of this method is that of free decay as
employed in many resonant methods e.g. the torsion pendulum.

$$A_2 = A_1 \exp\left(\frac{-\pi(n_2-n_1)}{Q_T}\right) \qquad 4.20$$

$$Q_T^{-1} = \frac{0.73}{n_2-n_1} \log_{10} A_1/A_2 \qquad 4.21$$

The amplitudes A_1, A_2 were measured on the oscilloscope
screen and n_2, n_1 determined with the electronic reference
signal already referred to (Method 1). Another method used
by KS Mahil (1974) is to use a logarithmic timebase and adjust
for a trapezoidal trace. The method frequently used for
which the number of oscillations taken to fall from one
amplitude to another cannot be used due to the low value of
Q_T.

Method 4

Measurement of the sharpness of tuning is a method which is
sometimes employed for methods where Q_m is high(> 1000). In
this work the measurements were of the low Q_m type and also
the Q of the transducer would affect the results so this
method was not employed.

4.4c   Determination of Q_c^{-1}

The absolute determination of internal friction by this
method requires accurate measurement of the coupling loss
Q_c^{-1} and measurement of this quantity will be discussed in
some detail.

Seven methods will be considered:

1. Arrange for Q_m^{-1} to be negligible and measure n_x and
    calculate Q_c^{-1}.

2. Calculate Q_c^{-1} from the dimensions of the resonator
    line, and relative specific acoustic impedance.

3. Measure n_x and Q_T^{-1}.

4. Measure Q_T^{-1} and E_∞/E_o.

5. Measure n_x, E_∞/E_o.

6. Measure n_x for various modes.

7. Measure Q_T^{-1} for various modes.

Method 1 - In a typical high temperature grain boundary
experiment Q_m^{-1} will be negligible at room temperature.
This can be checked by observing that $E_\infty/E_o \simeq 1$.   If this
is so then Q_c can be calculated as $Q_c^{-1} \simeq 4.55/n_x$.   This

method was used for the high temperature grain boundary peak
measurements where Q_m^{-1} was in the 10^{-2} to 10^{-1} range.

Method 2 - For a longitudinal resonator Q_c can be calculated
as follows:

$$Q_c = \frac{\pi m}{2} \frac{Zr}{Z_1}$$ 4.22

The disadvantage of this method is that the line diameter
may be   larger near the joint in the case of soldering
and smaller when welding so that calculation cannot be
relied on.   In the case of the tuning fork resonator
calculation is impossible as no theory is available.
Therefore, this method was not used at all.

Methods 3; 4 - These methods rely   on the fact that n_x, Q_T,
$E\omega/E_o$ are different mathematical functions of Q_c^{-1}, Q_m^{-1} so
that solution of two simultaneous equations will allow
extraction of Q_c^{-1}, Q_m^{-1} from the measurements.

$$n_x = \frac{Q_c Q_m}{\pi(Q_c + Q_m)} \ln(2Q_m/[Q_m - Q_c])$$ 4.23

$$Q_T^{-1} = Q_m^{-1} + Q_c^{-1}$$ 4.24

$$\frac{1 - E_\infty/E_o}{1 + E_\omega/E_o} = Q_m^{-1}/Q_c^{-1}$$ 4.25

From equations 4.23, 4.24 it can be shown for $Q_m^{-1} \ll Q_c^{-1}$ that

$$Q_m^{-1} \doteq 0.62(Q_T^{-1} - 1/4.55\ n_x)$$ 4.26

This method was used a great deal as a check for small Q_m^{-1}.
At the start of most experiments both n_x and Q_T^{-1} were measured.

Method 4 is similar to 3. but a measurement of E_∞/E_o is substituted for Q_T^{-1}.

From 4.23, 4.24 it can be shown for $Q_m \ll Q_T^{-1}$

$$Q_m^{-1} \simeq \left(\frac{1 - E_\infty/E_o}{1 + E_\infty/E_o}\right) \frac{0.22}{n_x - 0.7} \qquad 4.27$$

Method 5 uses measurements of E_∞/E_o, Q_T^{-1}.

From equations 4.24, 4.25 it can be shown that:

$$Q_c^{-1} = \frac{Q_T^{-1}}{1 + \dfrac{1 - E_\infty/E_o}{1 + E_\infty/E_o}} \qquad 4.28$$

$$Q_m^{-1} \simeq \frac{Q_T^{-1}}{1 + \dfrac{1 + E_\infty/E_o}{1 - E_\infty/E_o}} = \frac{Q_T^{-1}}{2}(1 - E_\infty/E_o) \qquad 4.29$$

Methods 4, 5 were not used because of the difficulty of determining E_∞/E_o in this work.

Methods 6; 7 - These methods are readily applicable to longitudinal resonators where measurements can be made on several modes and for obvious reasons are referred to as multimode methods. The measurement of Q_c^{-1} in this case relies on the fact that Q_c is proportional to the mode number. An assumption has to be made that Q_m^{-1} only changes slowly with frequency i.e. this method can be used when the damping is hysteretic or nearly so but not when there is a relaxation.

From equation 3.14:

$$n_x(m) = n_o(m)(1 + K Q_m^{-1}(m)/Q_c^{-1}(m)) \qquad 4.30$$

K is a variable but when $Q_m^{-1} \ll Q_c^{-1}$, $K \simeq 0.7$.

For a longitudinal resonator $Q_c^{-1}(m) = \dfrac{Q_c^{-1}(1)}{m}$ 4.31

Let us represent the change of internal friction with frequency by:

$$Q_m^{-1}(m) = m^a \, Q_m^{-1}(1) \qquad 4.32$$

For many materials $-\tfrac{1}{2} < a < +\tfrac{1}{2}$ and often a is nearly zero (Wegel and Walther 1935; Pines and Karmazin 1966).

Hence from 4.31, 4.32:

$$\frac{n_x}{m} = n_o + \frac{m^a K}{Q_c^{-1}(1)} \, n_o \qquad 4.33$$

Thus if the results are plotted as shown in Figure 4.13, the value of n_o can be found by extrapolation to $m = o$. The graph curves for high values of m and also if a differs much from zero. Computer fitting (Sharp 1974) can be applied in these cases. For many purposes a straight line fit will give a reasonable value for Q_m^{-1}. This method is open to the objection that an assumption has been made about the frequency dependence of internal friction, but in practice it has proved to be very useful.

An analogous method can be employed for readings of the decrement.

$$Q_T^{-1}(m) = Q_c^{-1}(m) + Q_m^{-1}(m) \qquad 4.34$$

making use of equations 4.32, 4.34, it can be shown that:

$$m Q_T^{-1}(m) = Q_c^{-1}(1) + m^{1+a} Q_m^{-1}(1) \qquad 4.35$$

Extrapolation as shown in 4.14b can be used to find $Q_c^{-1}(1)$.
An advantage of this method over the previous one is that
the graph is linear for a = 0, but from the experimental
standpoint it is less attractive because the decrement is
more difficult to measure and more error prone.

4.4d Validation

In this section the validation of the methods will be
discussed and a comparison of the different methods made.

There are three approaches to validation. Firstly, the
different methods can be compared to test for self con-
sistency. Secondly, the method can be tested on a
phenomenological basis, e.g. it should show Snoek peaks
of the correct shape at the right temperature (see Chapter
5). Thirdly, it would be desirable to make measurements on
a specimen by these methods and an accepted method. These
approaches will be discussed in order.

Self consistency

For this experiment (done in collaboration with JCK Sharp)
the choice of specimen material was spec pure polycrystalline
copper. The reasons were that a lot of work has been done
with copper (e.g. Lücke and Roth 1971), and it is known to
show only a small frequency dependence of internal friction
near room temperature. Secondly, it is readily available
and does not dissolve gases. Thirdly, the grain boundary
peak is at 450°C at 100 kHz so that mild heating will raise
the internal friction considerably.

A rod specimen 7.0 mm in diameter and 63 mm long was heated
in argon using the 1000°C furnace (see next section). The
fundamental frequency was 30 kHz and modes up to the fifth were
measured. The results of the second run are shown tabulated
in Figure 4.13. Readings of frequency, n_x and logarithmic
decrement, for several modes were taken as a function of
temperature. Three methods were used to obtain Q_c^{-1}.
Firstly, the crossover multimode method (6) is shown in
Figure 4.14a and recorded in column 11. The decrement
multimode method (7) is shown in Figure 4.14b and column 12.
Finally, the results of n_x, Q_T^{-1} calculations (Method 3) are
shown in column 16. The results show at 236°C good agreement
between methods 3,6 but not for method 7. The preferred
method is 3, but 6 can give very good results in practice.
Having determined Q_c^{-1}, Q_m^{-1} was calculated by different
methods from n_x (column 13) and Q_T^{-1} (column 14). While
agreement between the two methods is not perfect the self
consistency of each method is reasonable. An important test
is the frequency dependence of internal friction and this
is shown in Figure 4.12. At 205°C the internal friction is
independent of frequency, while at higher temperatures the
internal friction falls with frequency. This frequency
test was the most important part of the experiment, and
wrong answers would have made the method very suspect.

Though this section is primarily about the method it is
convenient at this point to discuss the metallurgical
aspect of the results. The internal friction and frequency
as a function of temperature are shown in Figure 4.16. On
the first run there is a marked dip in the frequency
temperature curve at 250°C without an accompanying increase

in internal friction. This is due to a type of recovery
process involving slip which does not result in dissipation
of energy (De Batist 1972 p.260). The broad peak at 420°C
(27 kHz) is a grain boundary peak. Using the Wert Marx
plot this gives a value of 1.35 eV activation energy and a
peak temperature of 480K at 1 Hz corresponding to the work
of Cordea and Spretnak (1966) on 99.999% pure copper but
rather lower than that of other work. The half width gives
a value of 0.7 eV for ΔE. This peak has the breadth and
temperature of a PM type peak (see 2.5).

An Arrhenius plot (Figure 4.17) gives a value of 0.38 eV
for ΔE in the range 250-350°C. However, the frequency
dependence is given by n $\curvearrowright$ -0.4 (230-270°C) and a much
larger value at 300°C, giving ΔE_o = 0.95 eV which is well
below the self diffusion value of 2.0 eV. The value of ΔE
agrees with Pines Karmazin's value but their value for n
was 0.25. The determination of background damping here was
below the grain boundary peak whereas Pines and Karmazin's
measurements were above it, but their work gives the
impression that the Schoek (1964) formula always gives
the right answers above and below the peak. The results
reported here show that this is not always so.

Phenomenological

The phenomenological validation is shown by the results in
Chapter 5. The Snoek peaks for iron, vanadium and tantalum
occurred at the correct temperature and the shape is correct.
The peak heights cannot be checked because the concentration
of the interstitial solutes were not measured by independent
means. Additionally, the less well characterised grain

boundary peaks were in general accord with published
information.

External validation

It would be very desirable to check the method by repeating
measurements on a given specimen by another method and com-
paring results. However, other types of apparatus were not
available and in any case frequently require a different
specimen shape. Because the self consistency and phenomen-
ological tests had proved satisfactory it was felt that this
type of test was not really essential. However, a possible
method would be to use a long 3mm copper rod as an ultrasonic
attenuation specimen in the first furnace run up to say 300°C
and then to use a portion of it as a resonator in a second
run.

4.5 Specimen heating

A comprehensive review of high temperature technology is
given by Campbell (1967). Apparatus was specially designed
and constructed for specimen heating between -190°C and
2000°C there being no suitable ready made apparatus in the
laboratory. The general requirement was that the specimen
temperature could be controlled to within a few degrees C.
As the maximum specimen length was about 50mm and usually
made of metal the problems of temperature uniformity were
not particularly onerous. For temperatures above 200°C the
specimens generally had to be heated in an oxygen free
atmosphere. Below room temperature they had to be in a
dry atmosphere to prevent condensation. Generally a vertical
arrangement was used making support of the transmission line
much easier.

Chromel/alumel thermocouples were used for the -190°C to
1000°C range. Platinum/platinum - 13% rhodium thermocouples
were used up to 1600°C. Above this temperature either
tungsten - 3% rhenium/tungsten - 26% rhenium thermocouples
or an optical pyrometer were used. The thermocouple emf's
were measured with 10 μV digital voltmeter using the
appropriate compensating cable and the cold junction
temperature measured with a mercury thermometer.

Attention will now be turned to the obtaining of an inert
atmosphere for high temperature experiments. At high
temperatures most metals react very rapidly with oxygen and
many with nitrogen. The rapidity of the reaction is a
consequence of the high temperature though the reaction
is usually thermodynamically possible at room temperature.
The oxygen pressure for stability can be calculated from
the free energy of formation of the oxide. Swalin (1962)
gives this information of high temperatures for some of the
metals.

$$M + O_2 \longrightarrow MO_2 \qquad -\Delta G°$$

$$\Delta G° = - RT \ln p_{O_2} \qquad\qquad 4.36$$

where,

$\Delta G°$ = standard free energy of oxidation

p_{O_2} = oxygen pressure in atmospheres.

For a certain oxygen pressure (the equilibrium pressure) ΔG
becomes zero and the system is in equilibrium. If the oxygen
pressure is greater than the equilibrium pressure the metal
will oxidise, while below the equilibrium pressure any oxide

present will dissociate. Many metals will reduce water
vapour and to a lesser extent carbon dioxide, so the partial
pressure of these gases must also be at a very low level.

$$H_2 + \tfrac{1}{2}O_2 \longrightarrow H_2O(g) \qquad \Delta G^\circ = -1228 \text{ kJ}$$
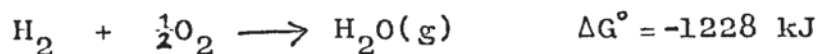
The equivalent oxygen pressure depends on the H_2O/H_2 ratio.
Some metals e.g. molybdenum, tungsten can be easily protected
from oxidation by the presence of hydrogen. Other metals
such as titanium, tantalum and vanadium are such good
'getters' that protection in this way requires the H_2O
pressure to be very low indeed.

The low oxygen pressure required for specimen heating can
be achieved either by the use of a vacuum or by the use of
an inert or reducing gas system. The author considers the
use of a gas system to be preferable. This method gives a
lower oxygen pressure, is less susceptible to leaks and
there is no possibility of failure due to breakdown of the
pump or power cuts. Furthermore, evaporation of the specimen
is reduced by the blanketing effect of the gas, the acoustic
signals are easier to lead in when there is no pressure
differential and there is no pressure on the outside of the
work tube - this can be a problem with silica which softens
at high temperatures. The best inert gas to use is argon.
For low oxygen pressure it must be purified of water by
passing over phosphorous pentoxide and of oxygen by passing
over heated titanium. The use of nitrogen is cheaper but
some metals e.g. vanadium, tantalum very easily form nitrides.
When a vacuum system is used the vacuum has to be good to
achieve a low oxygen pressure. For example a vacuum of 10^{-4}

torr - a realistic pressure at a high temperature - gives an oxygen pressure of 2.6 x 10^{-8} atmosphere assuming the gas composition to be the same as air. The advantage of a vacuum is that the system remains clean as volatile contaminants are pumped away. This is an important advantage at temperatures of 1500°C+ because most refractories are damaged by impurities. A second advantage is that the lack of convection currents gives a more uniform temperature distribution.

The refractory materials used were transparent silica up to 1200°C and 99.7% pure recrystallised alumina up to 1900°C. Transparent silica is insensitive to thermal shock and allows the specimen to be seen after the work tube has been put on. The grade of alumina used is quite sensitive to thermal shock. With both materials, as with all refractories, care has to be taken to prevent contamination, which will degrade them.

4.5a Aluminium block (-190°C →300°C)

This is shown in Figure 4.18. Aluminium was used because of its high thermal conductivity and resistance to oxidation. For work below room temperature it was cooled in liquid nitrogen and then jacketed in an expanded polystyrene sleeve. The temperature then slowly rises at a few deg. C per minute enabling measurements to be made as a function of temperature. A slow flow of dry argon through the specimen chamber prevents icing up of the specimen. For work above room temperature, the block can be heated on an electric hot plate.

4.5b 1000°C Furnace

A Wild Barfield nichrome wound furnace was used up to 1000°C. The length was 60 cm and the internal diameter of the furnace tube was 50 mm. The whole apparatus is shown in Figures 4.19, 4.20. The furnace is suspended from stranded cables using pulleys and counterweights. It can thus be easily moved up over the work tube. The work tube was made of transparent silica with an internal diameter of 40 mm. This is a very convenient arrangement because the experiment can be set up and visually inspected through the walls of the work tube before the furnace is slid over. Should anything go wrong during the course of an experiment the furnace can be moved away for inspection. This arrangement also allows rapid heating of the specimen by use of a preheated furnace and rapid cooling. A brass work tube head was designed with several ports to allow flexibility of operation. The temperature profile of the furnace had to be determined before use. As an additional test three thermocouples were attached to a steel specimen and the temperature was found to change by less than 3°C over a length of 5 cm.

The specimen was welded to the transmission line outside the furnace and then passed through the 25mm port. This furnace was always used with inert gas, usually high purity argon, sometimes nitrogen. It was found unnecessary to use purification for the experiments performed in this furnace but the copper tube and copper turnings at the bottom of the work tube kept the oxygen pressure low. As the system operated under slight positive pressure the acoustic line could be lead through a plug of ceramic wool. This caused

no visible echo. As 0.5 mm lines were normally used stray echoes could easily be caused at this point.

An 'Advance' proportional controller was used to control the temperature. For some experiments a Variac transformer allowed the heating rate to be set at a few deg. C per minute.

4.5c 1800°C Furnace

A Metals Research PCA10 furnace was kindly lent by UKAEA, Harwell – shown in Figures 4.21, 4.22. This consists of a pure alumina 25mm internal diameter furnace tube wound with molybdenum. A 25% hydrogen-nitrogen mixture was used to protect the winding. This mixture was used, rather than pure hydrogen for safety reasons. The outside of the furnace is water cooled.

A special brass head was designed to allow convenient operation. Because of the small bore, no work tube was used so care has to be taken to avoid damage to the furnace tube. The top of the alumina specimen tube gets hot due to thermal conduction and has to be cooled. A beaker of water, a wick and a fan were used to cool it.

A Eurotherm three term controller was used to give very good control of the temperature. As the controller used was for use with platinum thermocouples an external 15 mV source was put in series with the tungsten/tungsten rhenium thermocouple so that temperatures up to 1800°C could be controlled.

A two stage AEI rotary pump was used to evacuate the furnace tube and the pressure was measured with a pirani gauge. A

pressure of about 10^{-2} torr was generally achieved when hot.
It would have been desirable to use a diffusion pump to give
pressures in the 10^{-4} range but this was not readily available.
Because the furnace tube is slightly porous the residual gas
will be mainly nitrogen and hydrogen giving an improvement in
oxygen pressure. Normally a 30 cm long rod specimen was used
with a tuning fork cut into one end. This was then joined to
a 3mm diameter steel transmission line. Because of the height
of the ceiling the maximum convenient total length was 1.5m.

4.5d Flame 800-2000°C

Temperatures in excess of 1900°C generally require the use of
a vacuum furnace because this is the highest usable temperature
of alumina refractories. As no such furnace was available an
oxygen-coal gas Flamemaster torch was used to heat non-
oxidisable specimens up to 2050°C. Figure 4.23 shows a
photograph of an iridium specimen heated in this way.
Temperature control is not very good but the hot zone is
very small and experimental work is very rapid, because of
the fast heating and cooling rates.

Temperatures were measured using a Pyrowerk optical pyrometer
(disappearing filament type). The temperature reading has to
be corrected for the emissivity of the specimen and herein
lies a source of error. The sapphire specimens were heated
inside an alumina tube to prevent the formation of hot spots
with consequent melting. The outside temperature of the tube
was taken as the specimen temperature because it was assumed
that the radial heat flux would be small giving a small
temperature gradient.
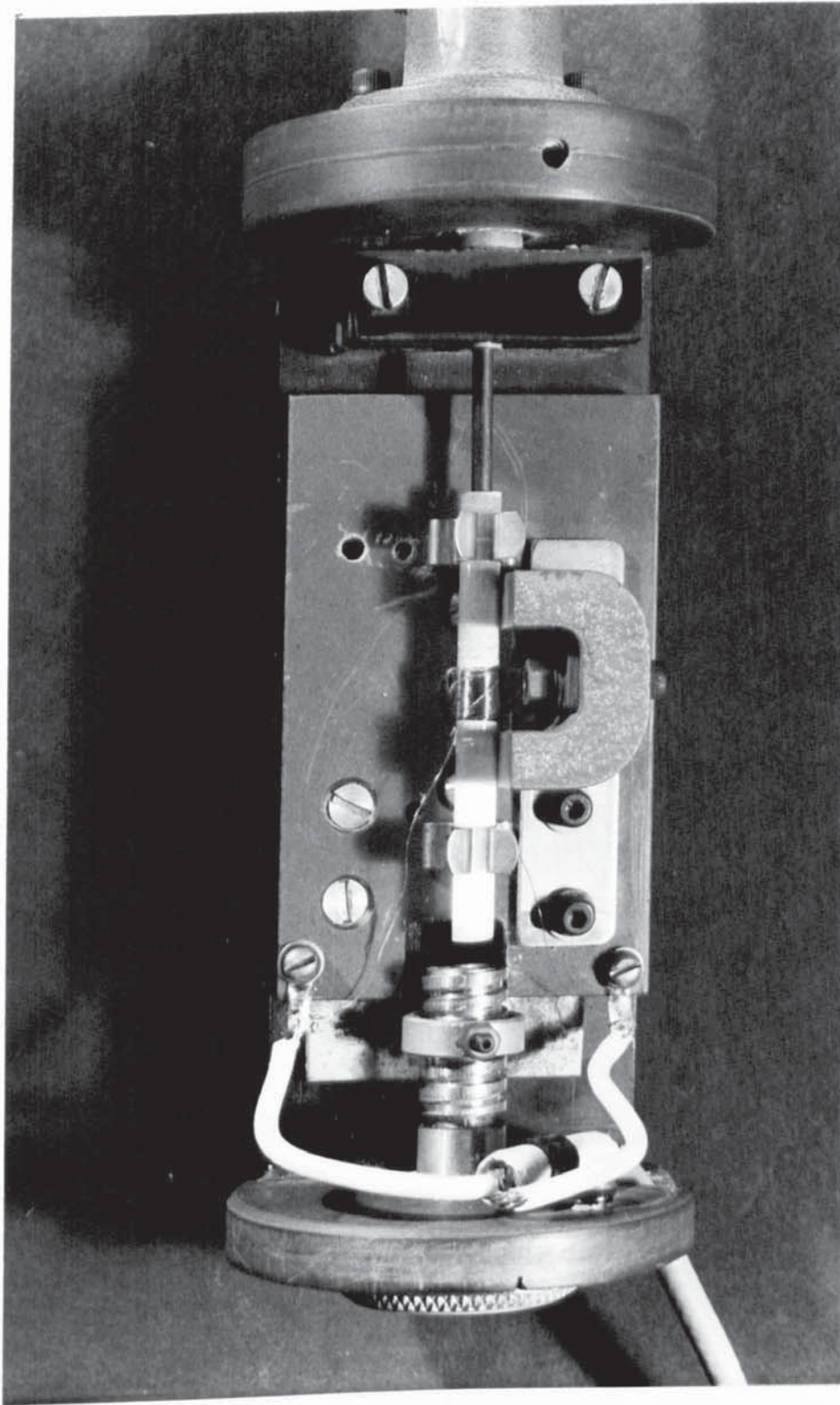
FIGURE 4.1 - A magnetostrictive transducer for a 3mm transmission line. This was the transducer used for the sapphire thermometer probe (figure 6.4). The screw on the left adjusts the mechanical tuning and the magnet provides the bias. Quite a large one is necessary for this diameter line. A short coil is required for the operating frequency of 150 kHz.
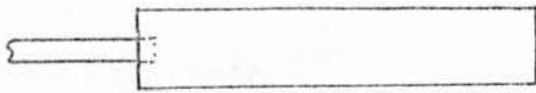
A Longitudinal Rod Resonator
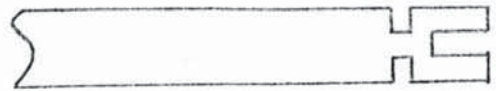
C Seth Tuning Fork Resonator
(Rod or Strip)

B Longitudinal Plate Resonator
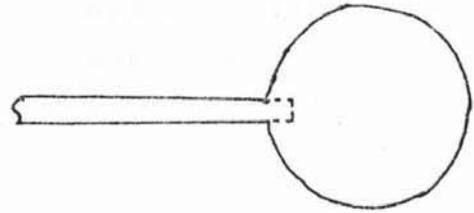
D disc resonator
(for Poisson's ratio)

3mm
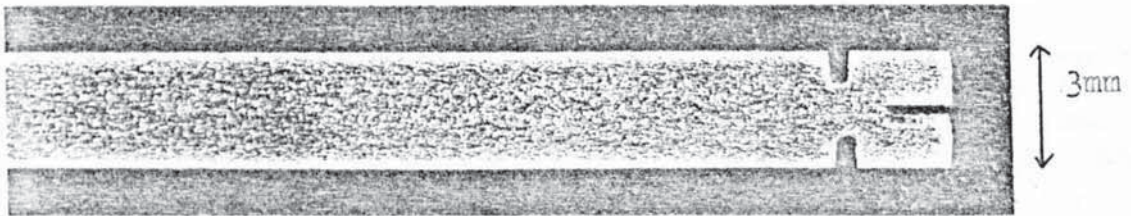
E Sapphire rod resonator(Seth Tuning fork)

←——— 5mm ——→
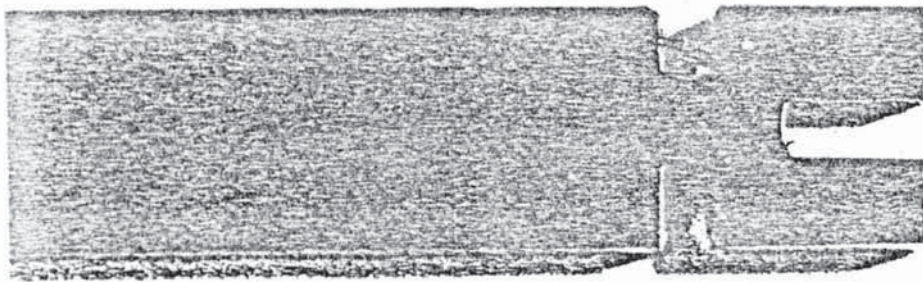
F Silicon nitride strip resonator (Seth Tuning Fork)

FIGURE 4.2 - The resonators mentioned in this report
are shown. There are various other possibilities.

Materials	Method
Most metal rod - metal wire <2mm dia.	Flash butt welding
Metal plate - metal wire <2mm dia.	Spot welding
Steel - steel rod ⎫ Copper " ⎪ Permendure " ⎬ Tungsten¹ " ⎪ Rhenium " ⎪ Iridium " ⎭	Silver solder, easy flo No. 2 flux
Molybdenum - steel	Diffuse nickel into Mo. Then silver solder Easy flo No. 2
Alumina, Sapphire - steel and many non metals	Coat with Johnson Matthey silver paint FSP411/412, use ceramic solder and resin flux (up to 150° only)

NOTES: Special fluxes for the silver soldering of titanium
and molybdenum exist but are not readily available.
There are various special processes for the jointing
of ceramics reviewed by van Houten (1959).

1 Not a very good joint

FIGURE 4.3. - ACOUSTIC JOINTING METHODS
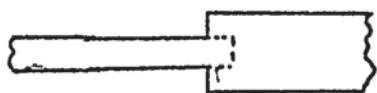
WIRE-ROD RESONATOR
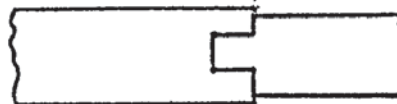
ROD-CERAMIC ROD
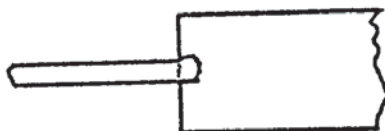
WIRE-STRIP RESONATOR
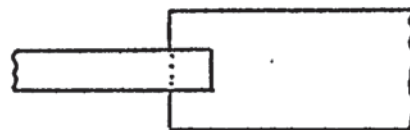
ROD-STRIP(TOP VIEW)

ROD-STRIP (SIDE VIEW)

% Junction echo in a 3mm transmission line joint

Frequency kHz	Araldite (tongued)	Silver paint process (butt)	Silver paint process (tongued)	Silver solder (butt)
60		7.5		
100	15-25	8		1-5
150		9.5		
165			10	
200		14		

FIGURE 4.4 - Jointing methods: for the line to resonator joints an acoustic mismatch is required but in the transmission line joints on exact match is required. The bonding material should have a similar impedance to the materials to be joined otherwise a large junction echo will result. This is illustrated by the results in the lower half of the diagram.
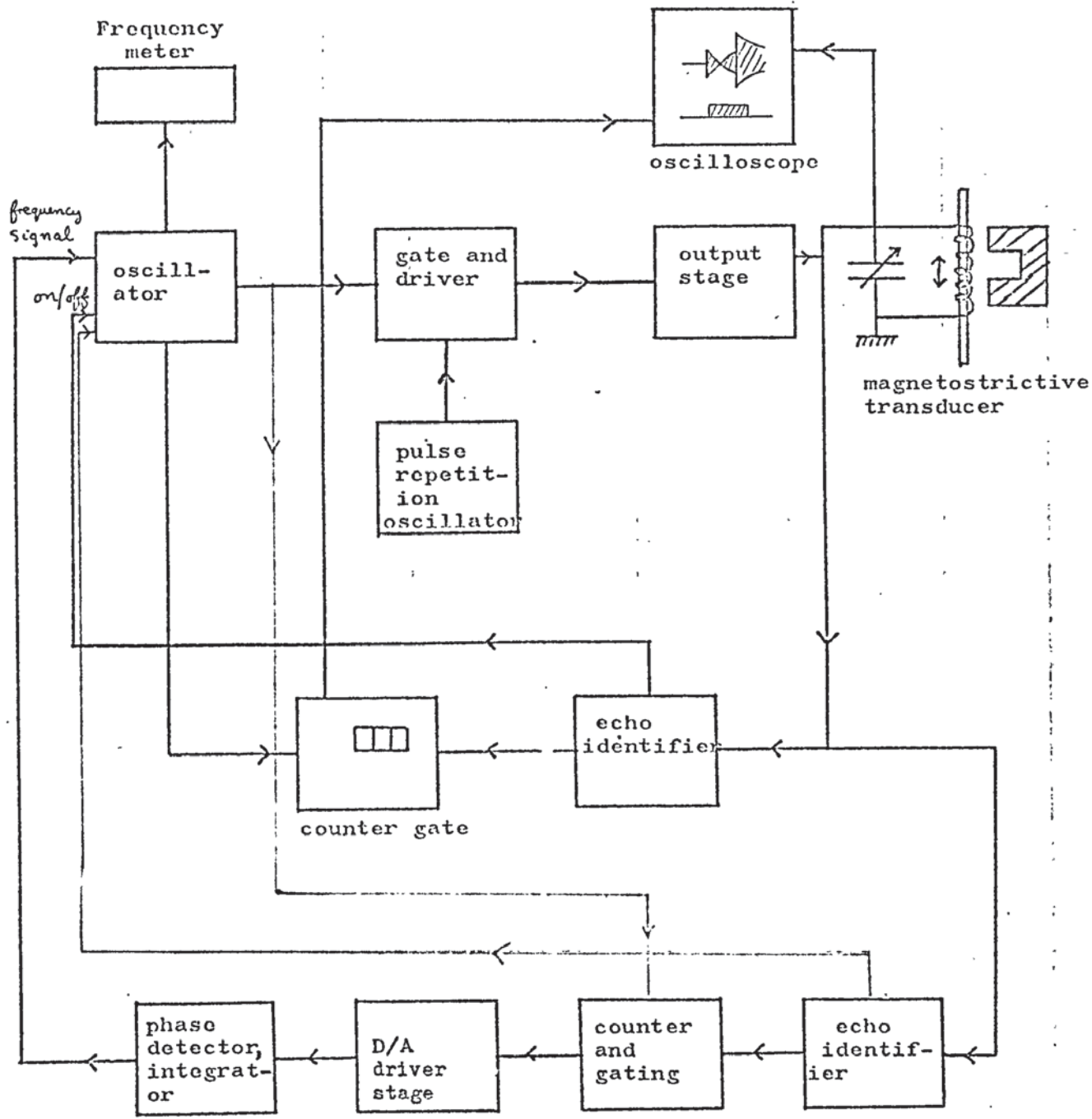
FIGURE 4.5 - Block diagram of the electronic systems. The upper section is the transmitter, the middle section the reference counter signal generator, and the lower the phase detecting system. This can be used for measuring phase in the echo and to provide a control signal for automatic operation.

'early signals'   'late signals'

echo

reference
signal

gate
output

detector output

phase
degrees

90   270
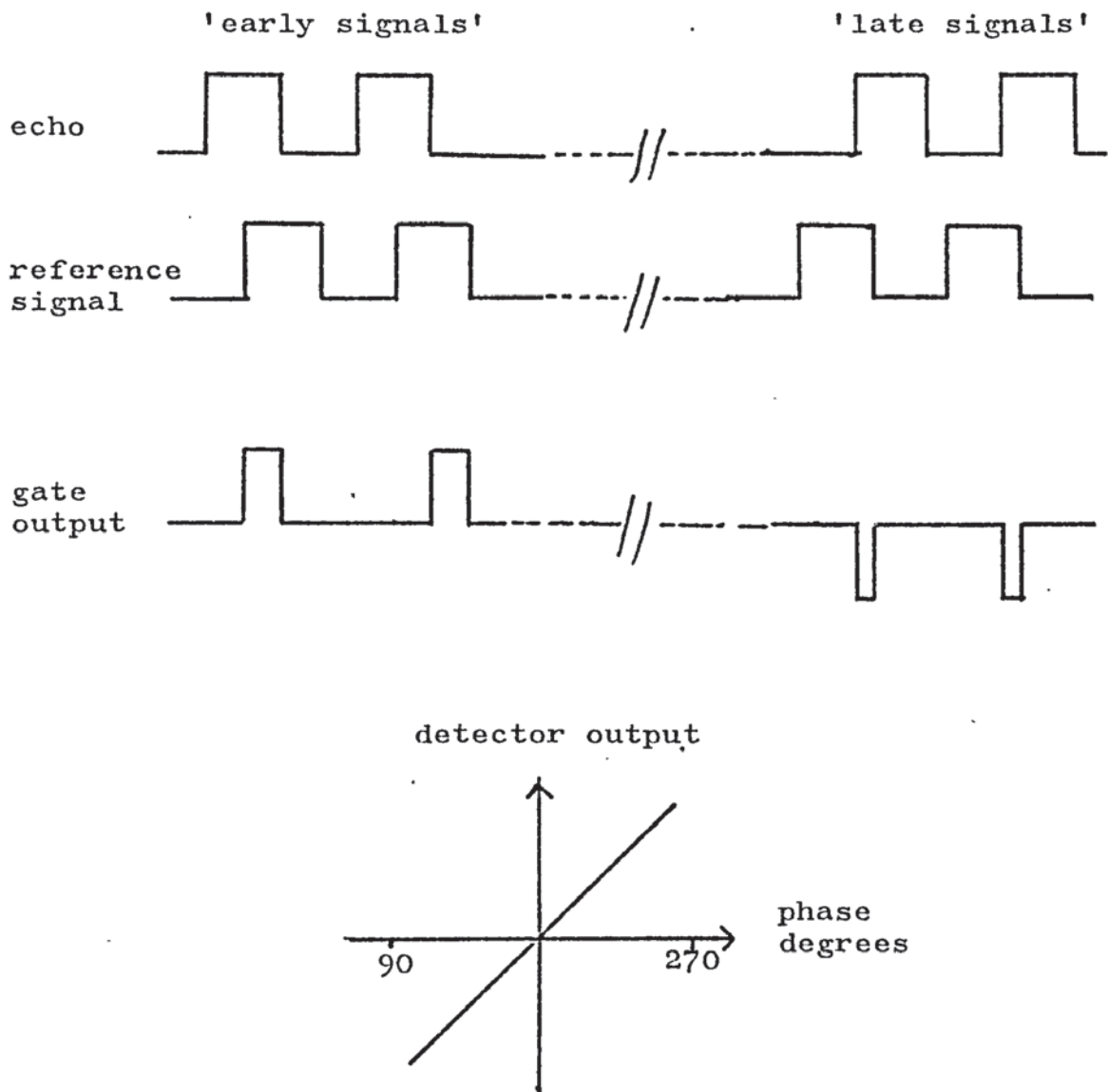
FIGURE 4.6 - Principles of phase measurement. 'Early' and 'late'
parts of the echo signal are sampled and compared
with a reference oscillation at the transmitter
frequency. The gate outputs are fed into an
integrator which gives a phase dependent analogue
signal (The early part of the echo is at the trans-
mitter frequency and the late part of the echo is
nearer the resonance frequency.) In the illustration
the late signal lags the early signal by 235°.
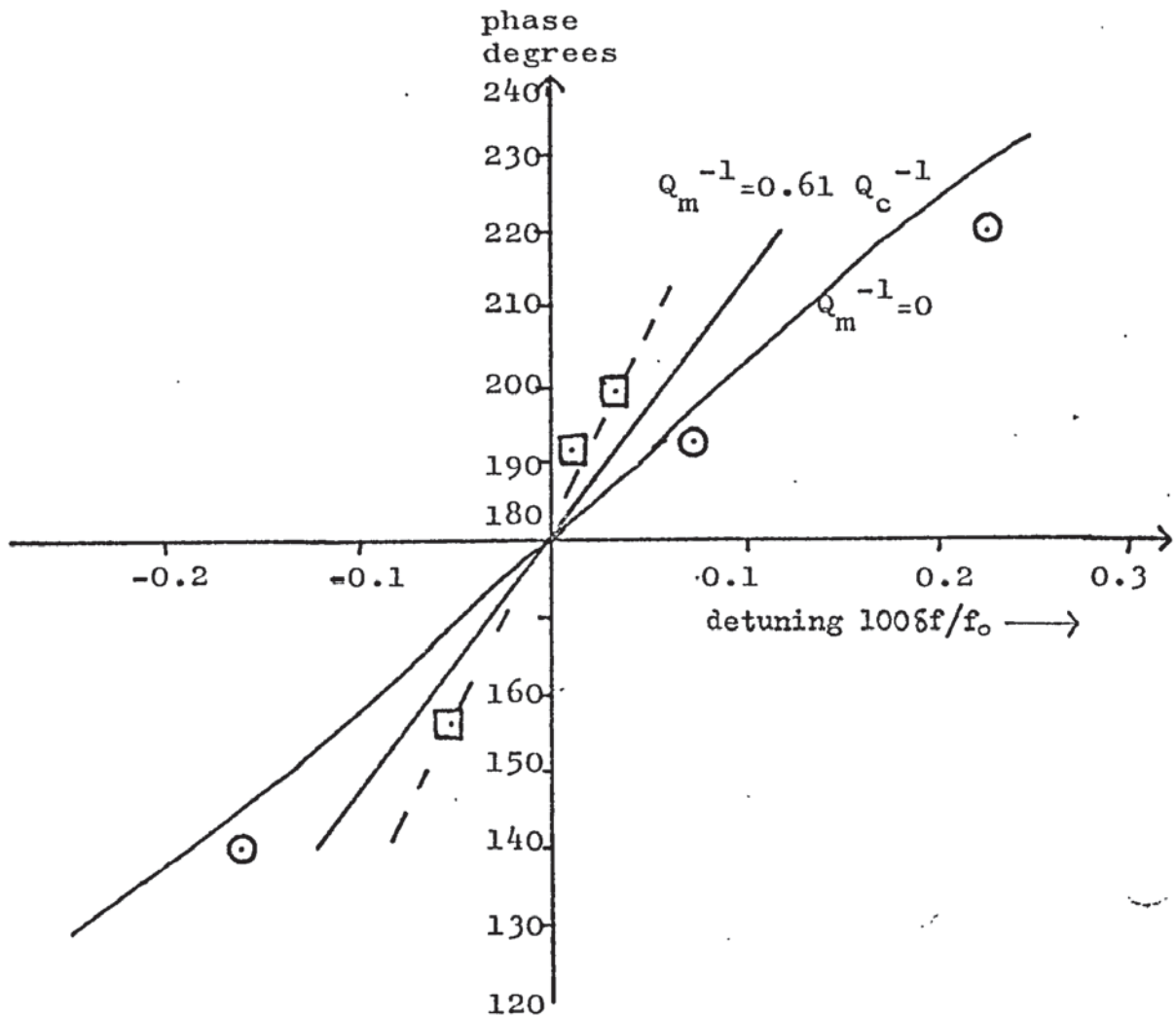
FIGURE 4.7 - Relative phase of the early and late parts of
the echo signal as a function of detuning for
negligible internal friction and $Q_m^{-1} = 0.61 \, Q_c^{-1}$.
The lines are theoretical curves (Sharp 1974) and
the points experimental values.

$(f = 120 \text{ kHz} \quad Q_c = 95)$

	High Q_c $Q_m = \infty$	Low Q_c $Q_m = \infty$	Low Q_c $Q_m = 2Q_c$
A Reflection of transmitter burst f_s			
B Resonator signal f_r			
A + B Sum Echo signal	large $\frac{\delta\phi}{\delta\omega}$	small $\frac{\delta\phi}{\delta\omega}$	large $\frac{\delta\phi}{\delta\omega}$
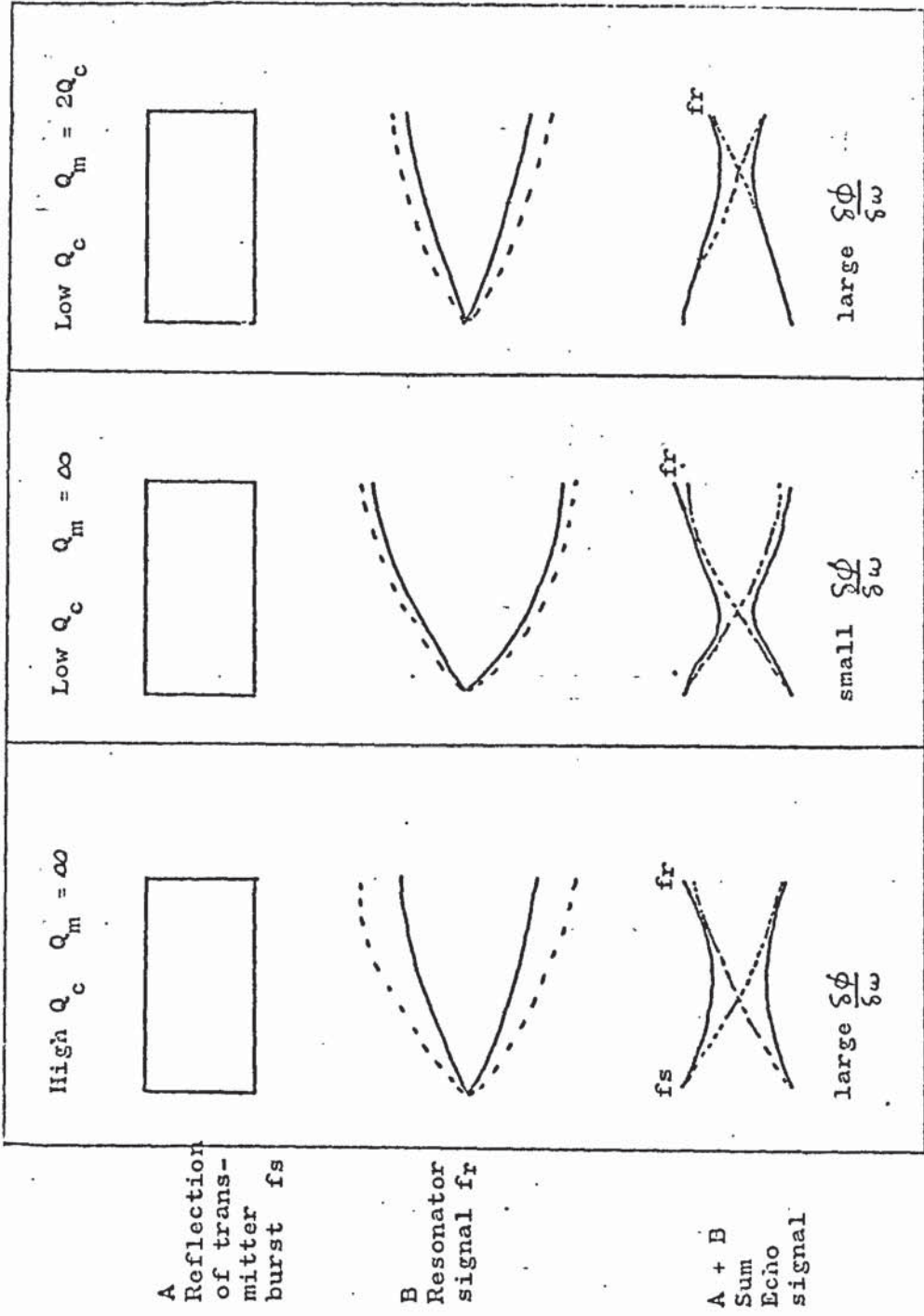
FIGURE 4.8 - Qualitative explanation of phase effects in the echo. The phase difference between signal A and signal B is 180°, so that 'on tune' the phase difference must be 180° between the early and late parts of the echo. 'off tune' the phase difference approaches zero when signal B becomes small. This occurs most readily when Q_c is large or Q_m-1 is large. Both these cases give large phase sensitivity to detuning.
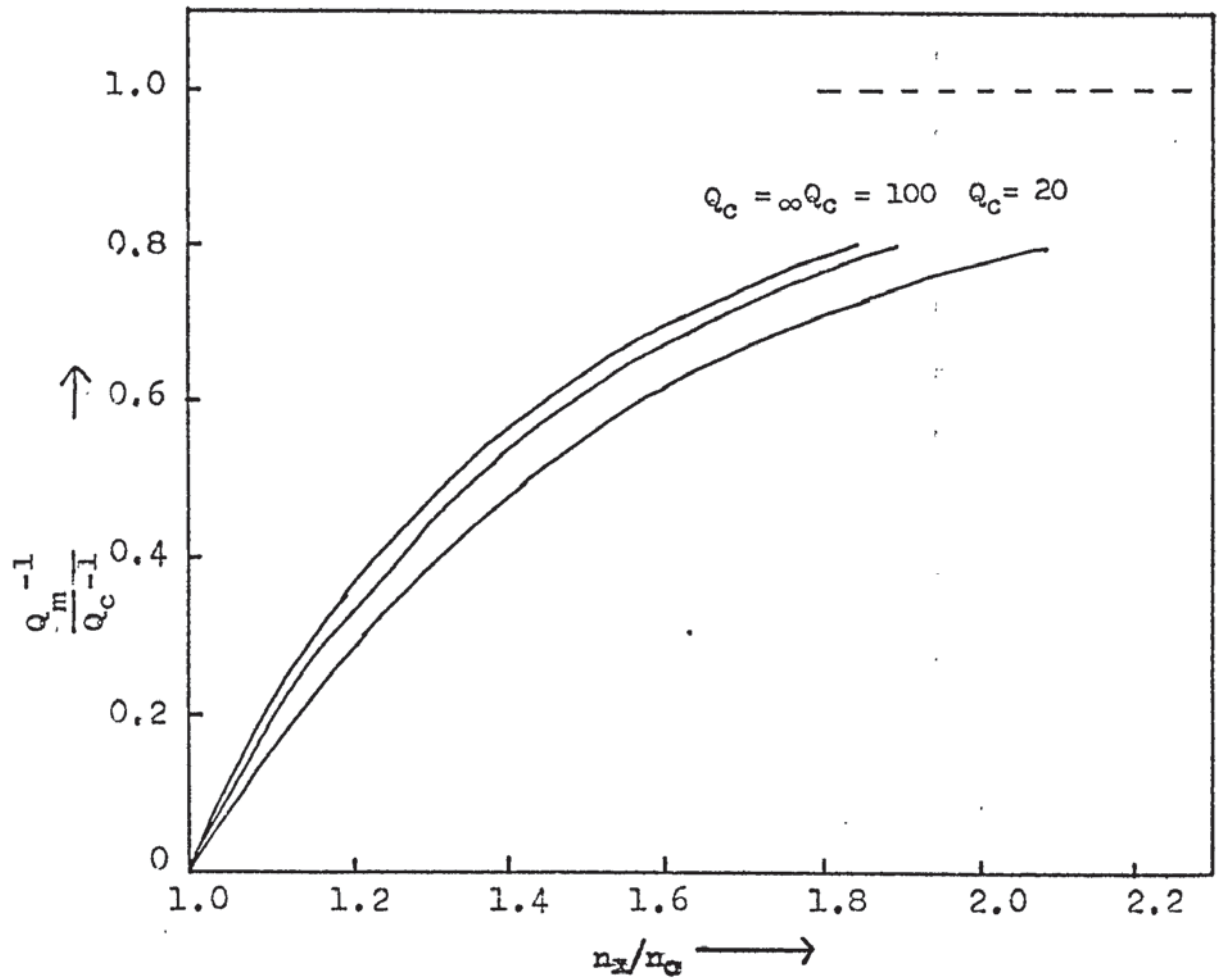
FIGURE 4.9 - Calibration curve of oscillations to crossover against Q_m^{-1}/Q_c^{-1}. This is the basis of a most convenient method of measuring internal friction.
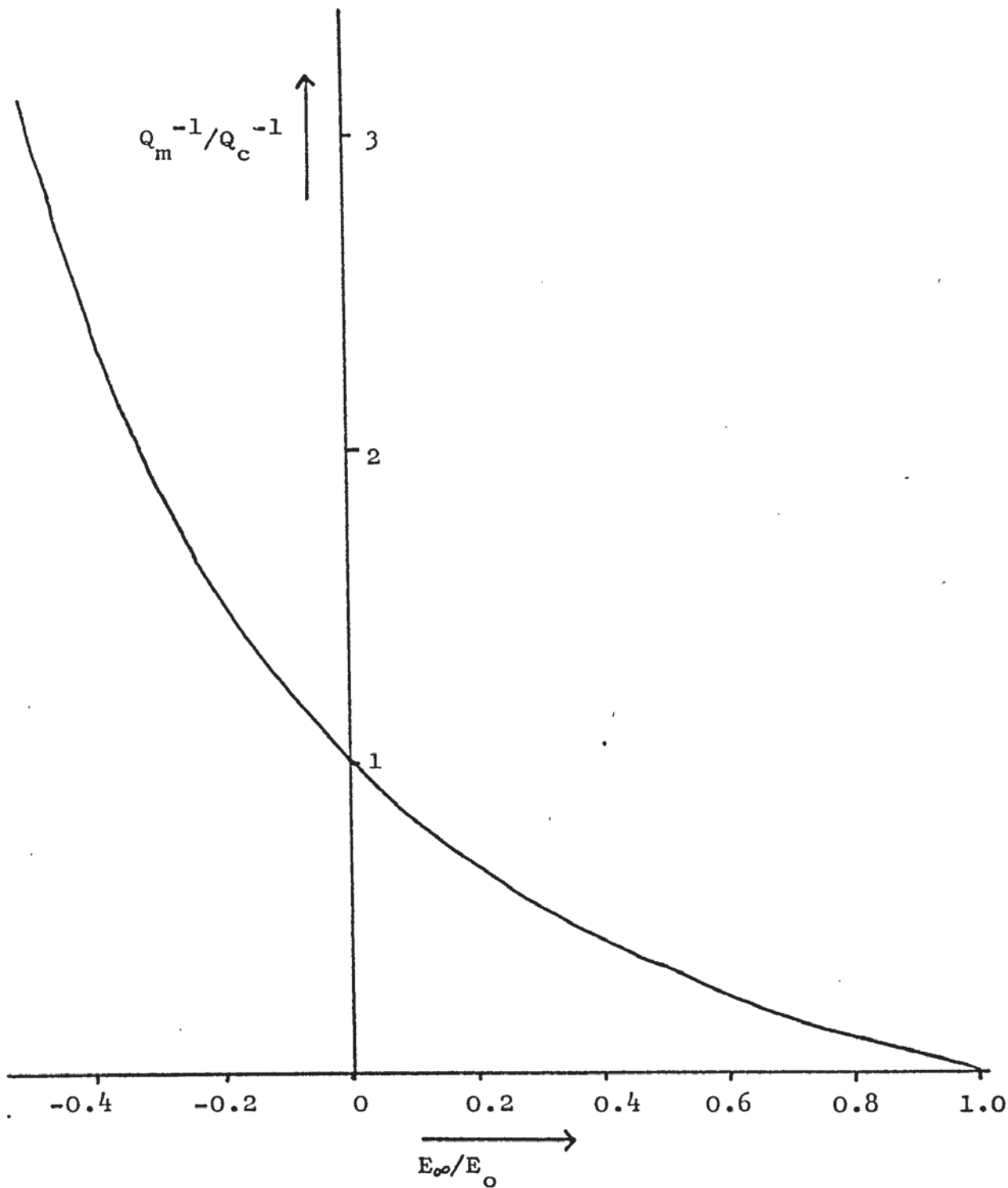
FIGURE 4.10 - Calibration curve for the E_∞/E_o method. This method was not applicable to this experimental work because it requires a long burst length so that E_∞ is reached and a wideband transducer is required to reproduce the correct value of E_o.
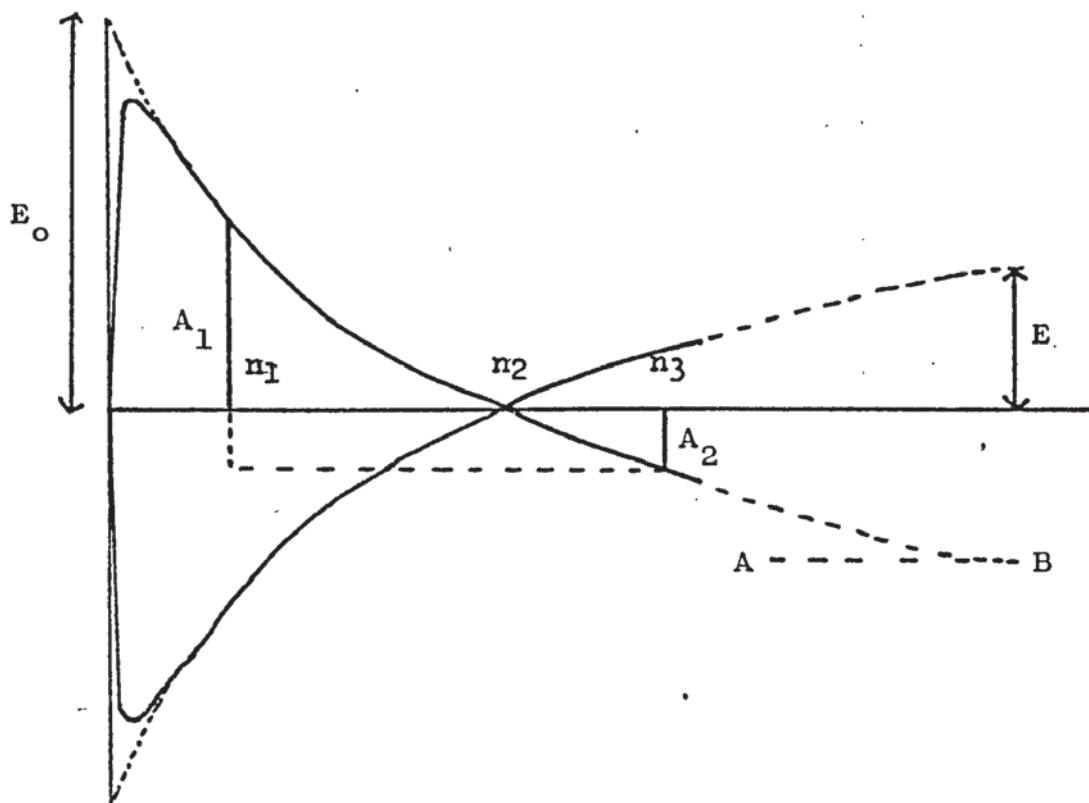
FIGURE 4.11 - In practice the E_∞/E_o method may not be applicable. If the burst length is not ·long enough E_∞ cannot be measured directly and there may be an error in E_o. Measurement of the quantities n_1, n_2, n_3, A_1, A_2 allows calculation of E_∞/E_o and Q_T thus giving both Q_c^{-1}, Q_m^{-1}. The method is laborious and requires a photographic record to ensure sufficient accuracy.
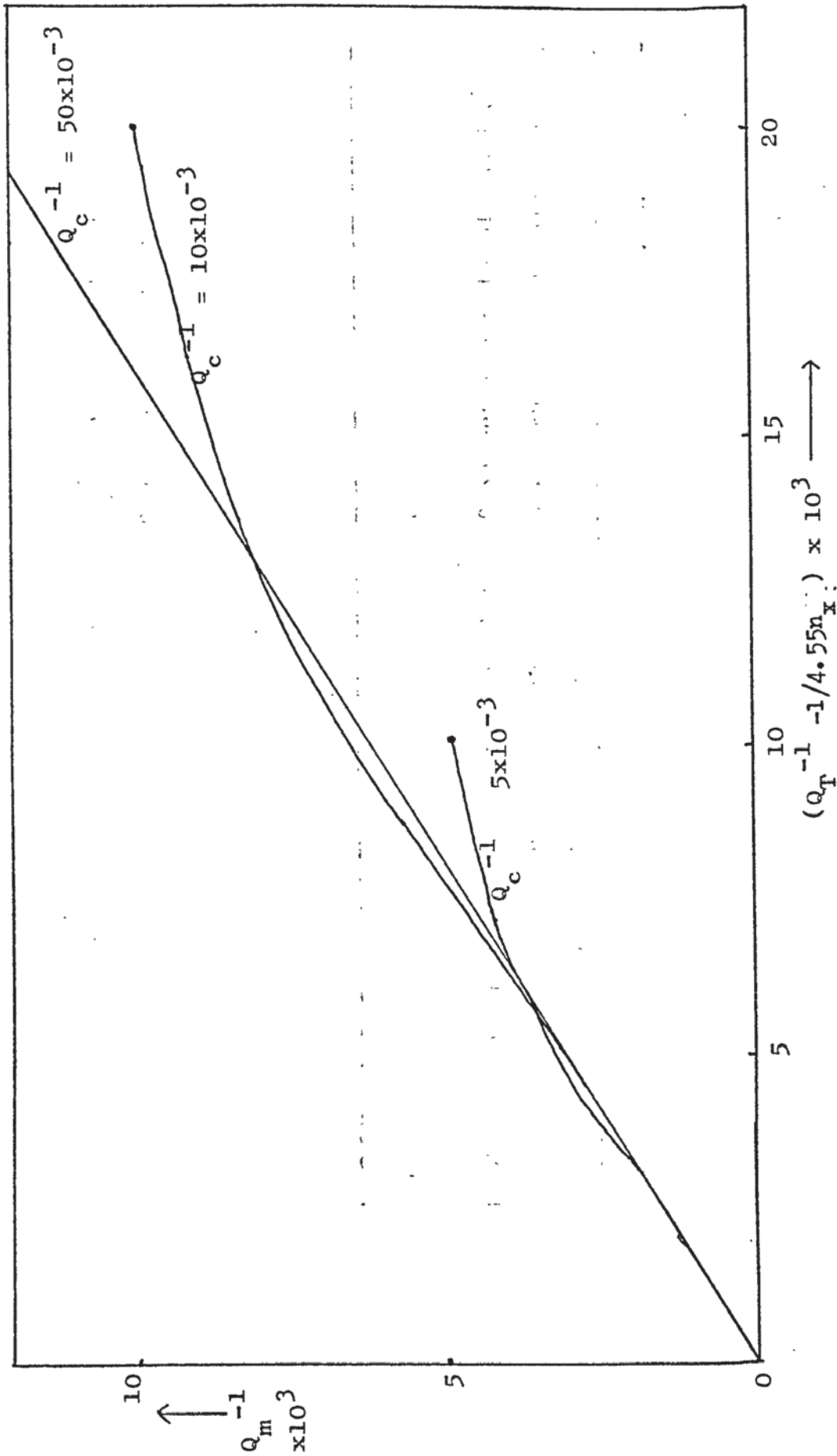
FIGURE 4.12 - Curves for the determination of Q_m^{-1} from measurements of nx, Q_T^{-1}. This is used when Q_c^{-1} is unknown. The method of calculating these curves is explained in Appendix C.

| 1 m	2 Cr/Al thermo mV	3 θ °C	4 f kHz	5 n_x	6 h_1 mm	7 h_2 mm	8 n_1	9 n_2	10 Q_T^{-1} ×10⁻³	11 Q_c^{-1}	12 Q_c^{-1} ×10⁻³	13 Q_m^{-1} ×10⁻³	14 Q_m^{-1} ×10⁻³	15 Q_m^{-1} ×10⁻³	16 Q_c^{-1} ×10⁻³
1	0	20	30.20	17	43	20	46	63	14.1	13.1 (n_o=16.8)	13.2	0	0.6	0.7	13.5
2	0	20	60.20	32.5	35	19	86	109	8.4			0	0.6	1.0	15.0
3	0	20	89.91	50.5	68	36	126	170	4.55			0.2	0.1	0.05	13.5
4	0	20	119.12	65.0	53	30	170	216	3.9			0	0.4	0.35	14.2
5	0	20	147.56	81.5	37	20	207	266	3.25			0	0.4	0.5	13.7
6	0	20	174.96	102.5	27	12	242	334	2.8			0.1	0.4	0.4	14.4
															14.1
1	7.50	205	29.18	17.5	44	20	43	59	15.3			0.6	1.9	1.9	13.6
2	7.50	205	58.25	35.0	33	21	80	101	6.8			1.0	0.2	0.35	12.9
3	7.50	205	86.40	55.0	36	18	120	160	5.5			0.74	1.1	1.0	13.5
4	7.50	205	115.78	71.0	59	25	166	217	5.35			0.57	2.0	1.5	15.8
5	7.33	201	142.83	89.5	35	17	197	262	3.52			0.50	0.9	0.7	14.0
6	7.46	204	169.27	103.5	22	13	230	287	2.92			0.04	0.7	0.6	12.9
															13.6
1	8.90	236	28.98	18.0	45	23	40.5	53	16.9	12.8 (n_o=17.2)	15.5	1.4	1.7	3.4	13.5
2	8.90	236	57.87	34.5	36	14	66	92	8.3			0.75	2.7	1.4	12.8
3	8.90	236	86.40	57.5	39	25	76	100	5.9			0.4	1.5	1.4	13.5
4	8.96	240	114.18	77.0	37	22	130	163	5.0			1.0	1.7	1.4	14.4
5	8.96	240	141.77	103.0	30	15.5	158	210	4.0			1.1	1.4	1.2	14.0
6	8.96	240	168.08	126.0	19	15	190	213	3.2			0.8	1.0	1.1	12.6
															13.5
1	10.50	268	28.70	21.0	36	15	56.5	65	19.1			4.9	5.9		
2	10.50	268	57.34	46.5	27	12	107	131	10.7			4.0	4.1		
3	10.50	268	85.64	83.0	42	20	150	177	8.7			3.16	4.3		
4	10.50	268	113.47		29	10	192	242	6.7			–	3.3		
5	10.50	268	140.57		18	9	197	239	5.2			–	2.6		
6	10.50	268	166.55		17	10	465	495	5.6				3.4		
1	12.76	313	28.23	62.0	68	26	81	91	30.6				17.4		
2	12.76	313	56.48		31	10	116	134	20.0				14.6		
3	12.76	313	84.33		24	8	171	196	14.0				9.6		
4	12.76	313	119.93		12	7	234	253	9.1				5.8		
2	0	20	60.23	32.5								0			
5	0	20	147.63	83.0								0.1			

FIGURE 4.13 – Table of readings for spec. pure polycrystalline copper (2nd run) showing different methods of obtaining values of Q_m^{-1}, Q_c^{-1}. The results for six modes are shown. Columns 1–9 show the readings. Columns 11, 12 show the n_x and Q_T^{-1} multimode methods of calculating Q_c^{-1} plotted in figure 4.14. columns 13, 14 show the values of Q_m^{-1} obtained from the n_x, Q_T^{-1} methods respectively. Columns 15, 16 have been calculated from the n_x, Q_T^{-1} readings for each separate mode.
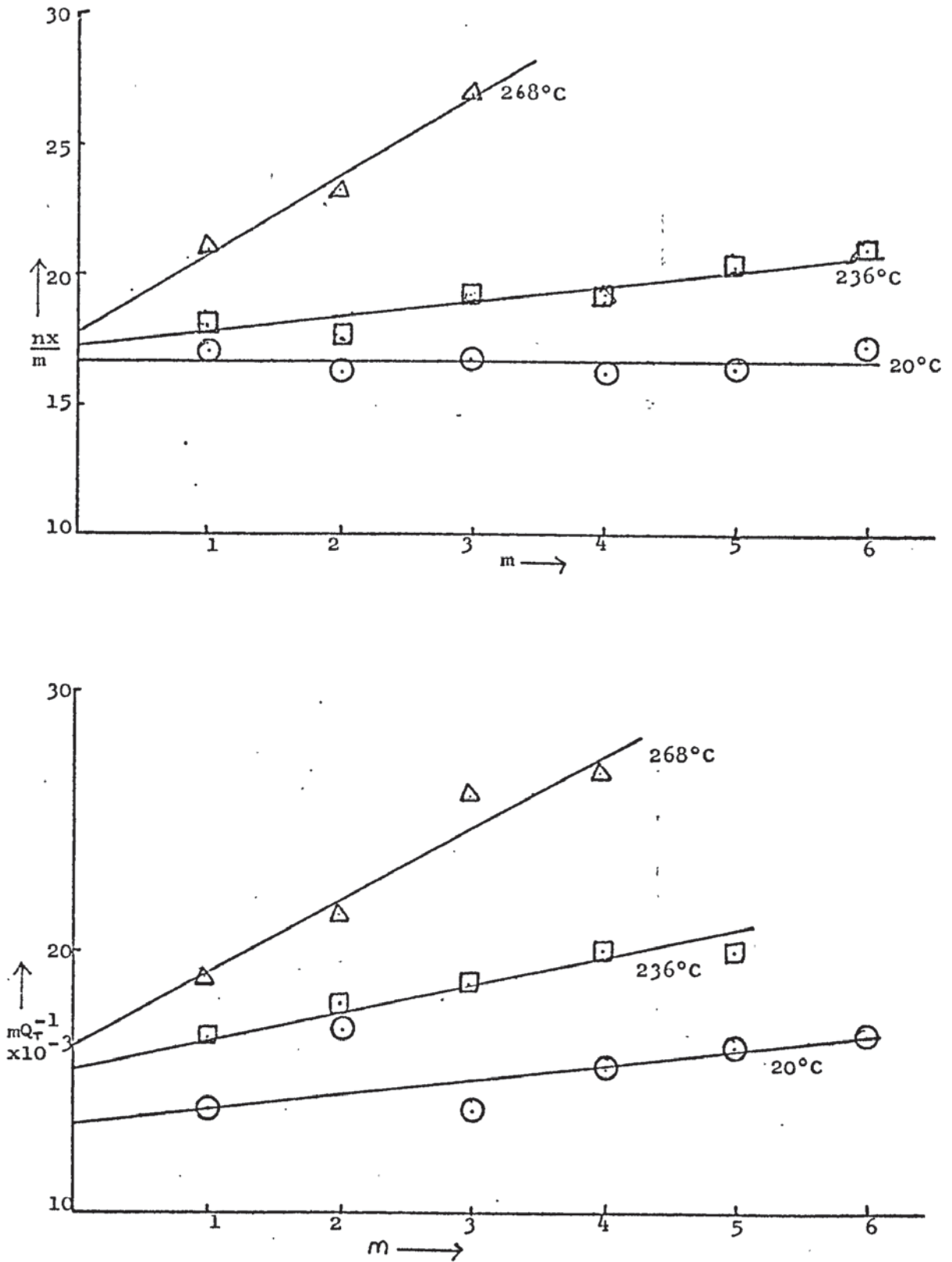
FIGURE 4.14 A/B - 'Multimode' plots for copper. This is one type of method for determining the coupling loss Q_c^{-1}. The results for several modes m are plotted as shown and extrapolation back to m = 0 gives a value for Q_c^{-1}. This is only applicable when Q_m^{-1} is small and the frequency dependence is small.
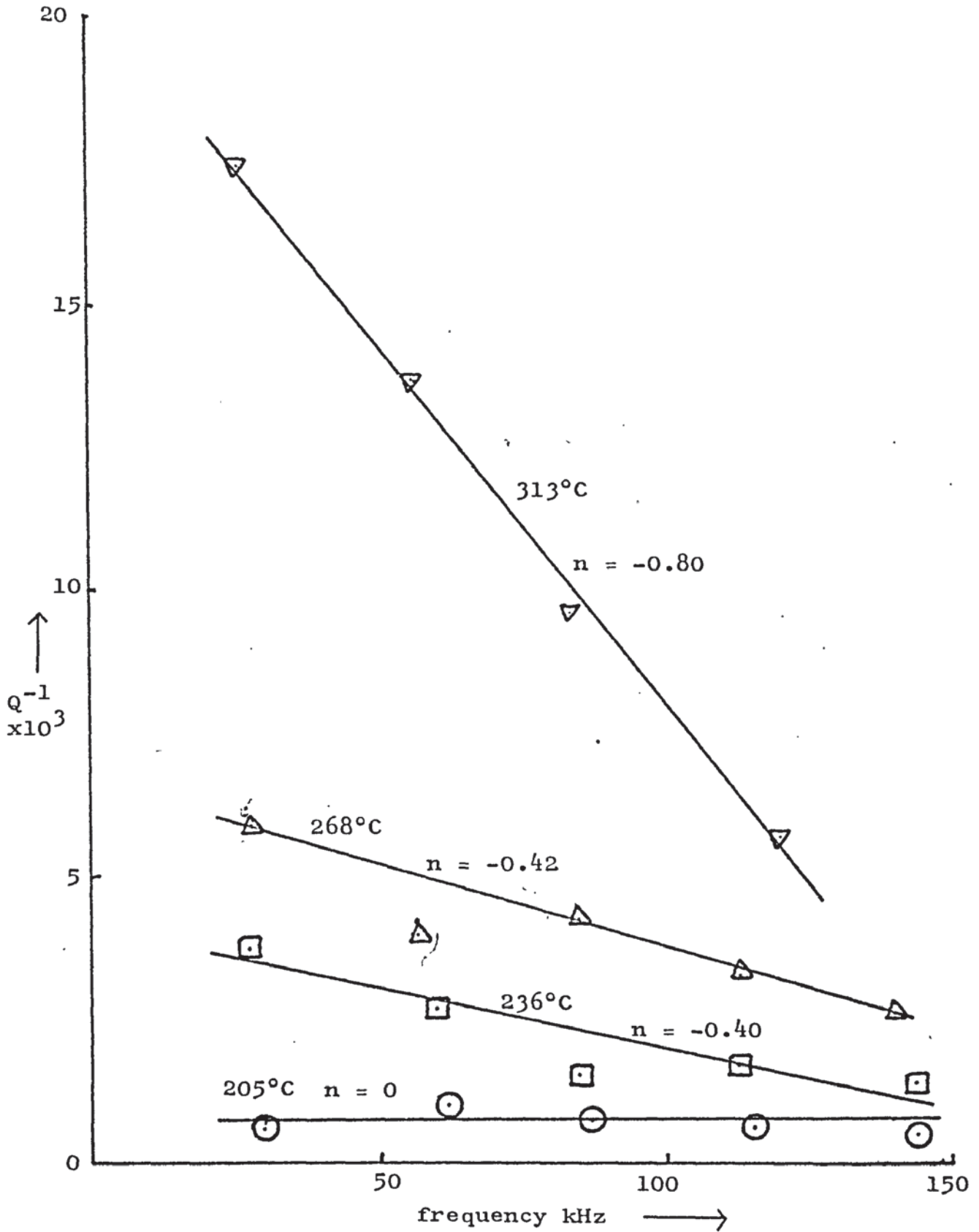
FIGURE 4.15 - Internal friction vs frequency for pure copper
at various temperatures. Up to 200°C the frequency
dependence is very small.
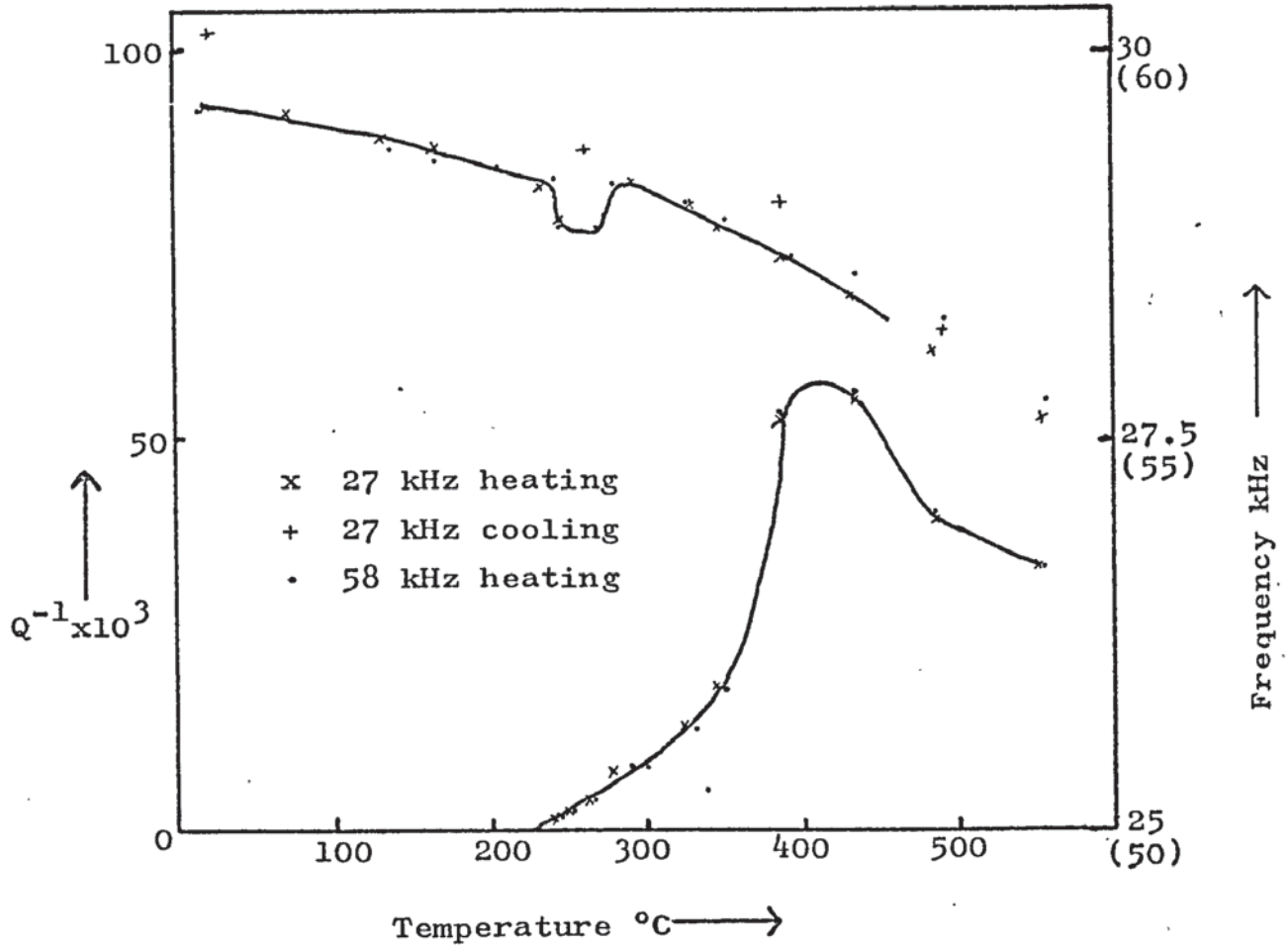
FIGURE 4.16 - Internal friction vs temperature for
polycrystalline copper. The dip in
in the Young's modulus curve only
occurs on the first run. The internal
friction peak is a grain boundary
relaxation.
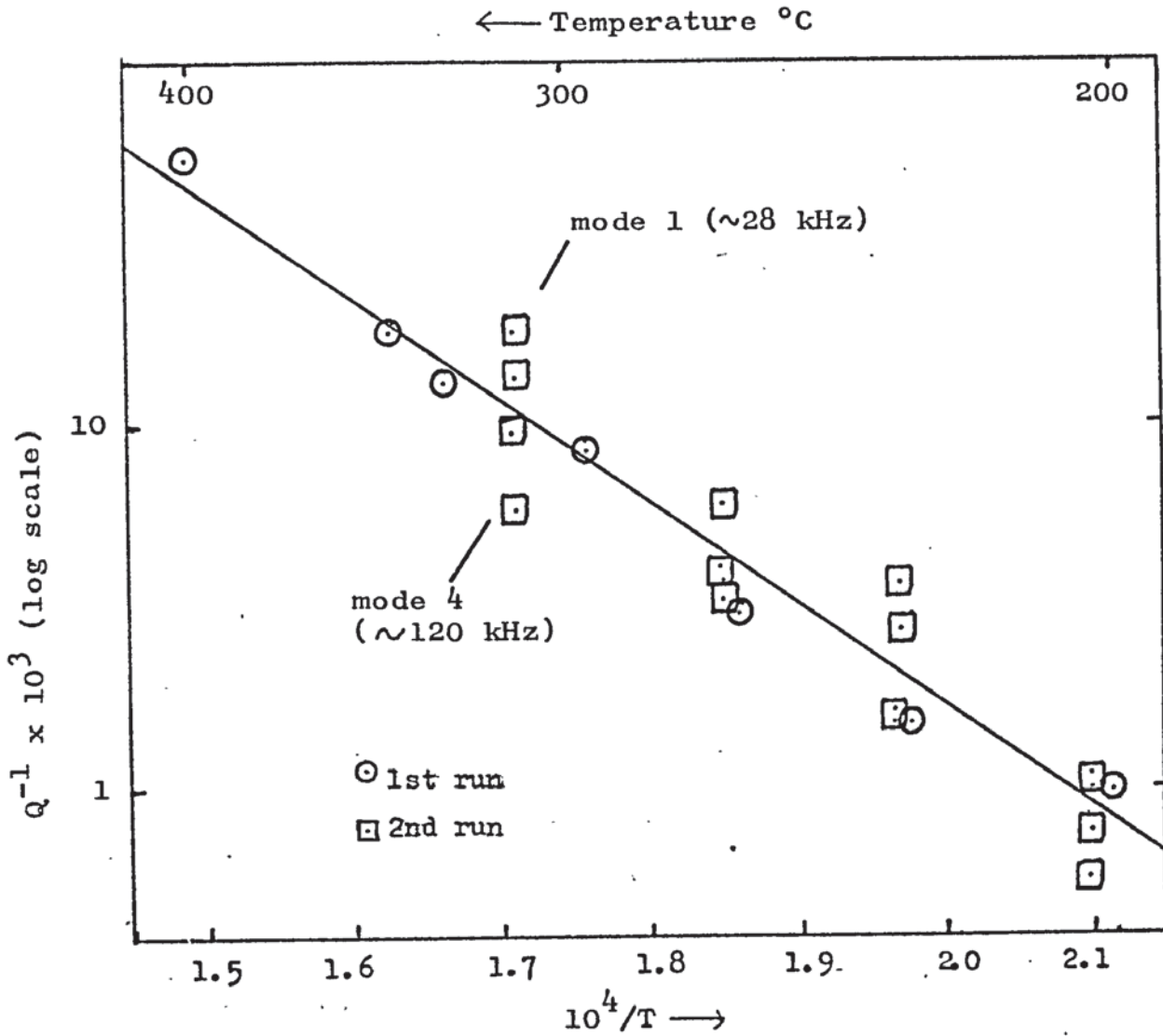
FIGURE 4.17 - Arrhenius plot of internal friction in poly-
crystalline copper. The frequency shift can
clearly be seen for the results of the
second run.

nitrogen in⟶ ⟶ nitrogen out

pyrex tube

bracket

thermocouple

specimen

thermocouple
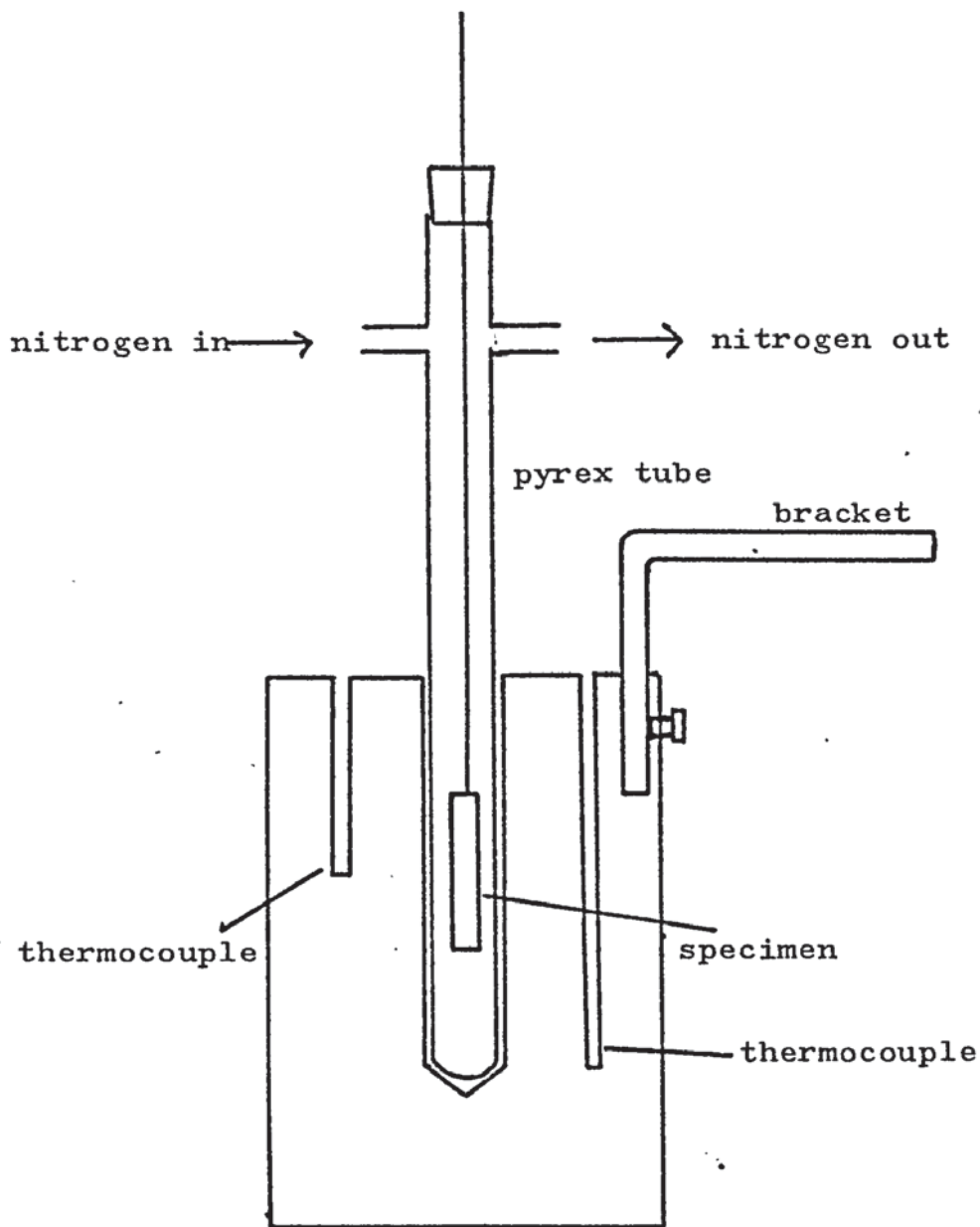
FIGURE 4.18 – Aluminium block for specimen temperatures in the range -190°C - 300°C. The block can be cooled in liquid nitrogen and the use of an expanded polystyrene jacket will give low rate of temperature rise. Above room temperature it can be heated on a hotplate.
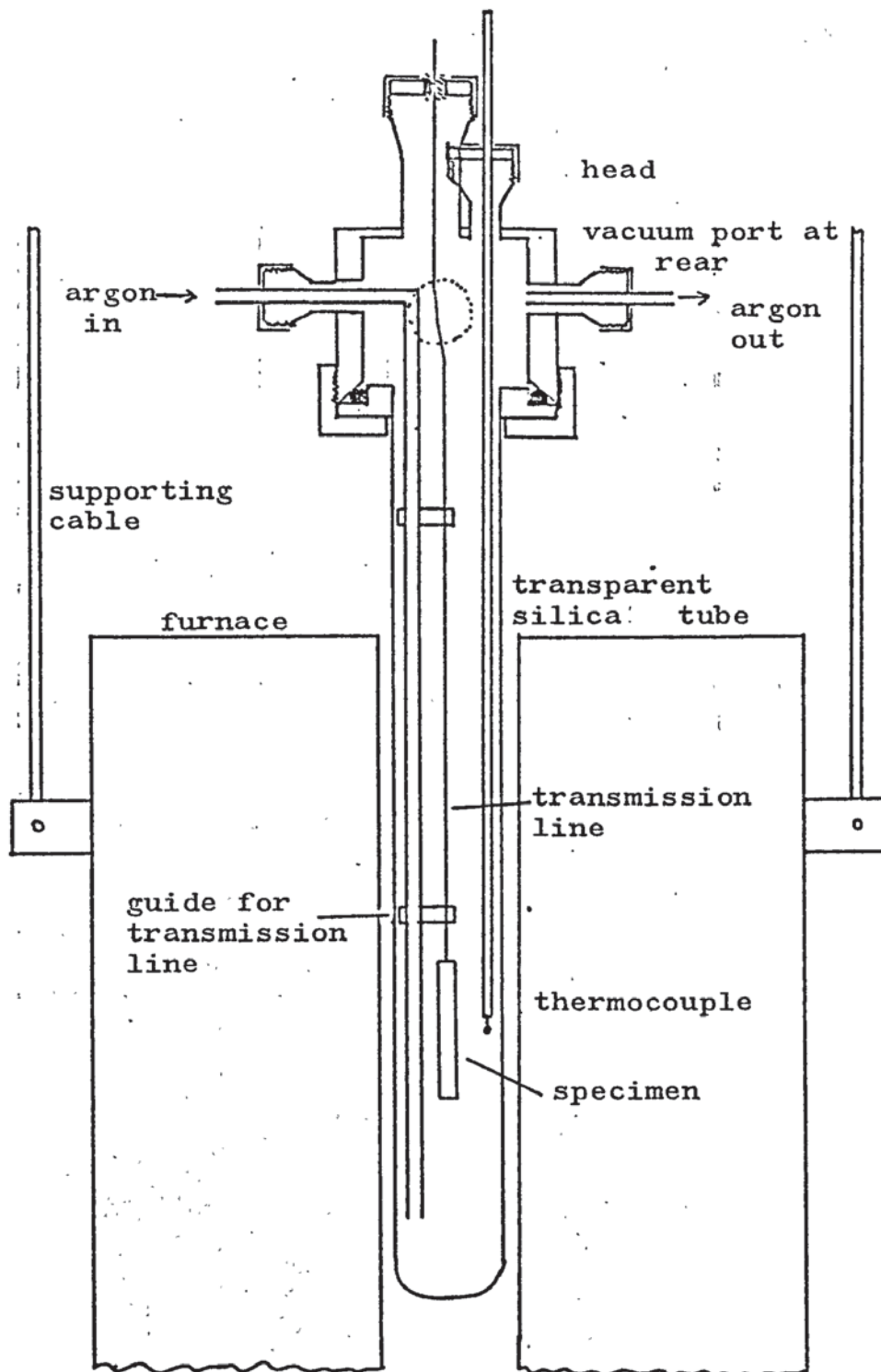
FIGURE 4.19 - The 1000°C furnace. The system was
designed to allow easy specimen
changing and rapid cooling.
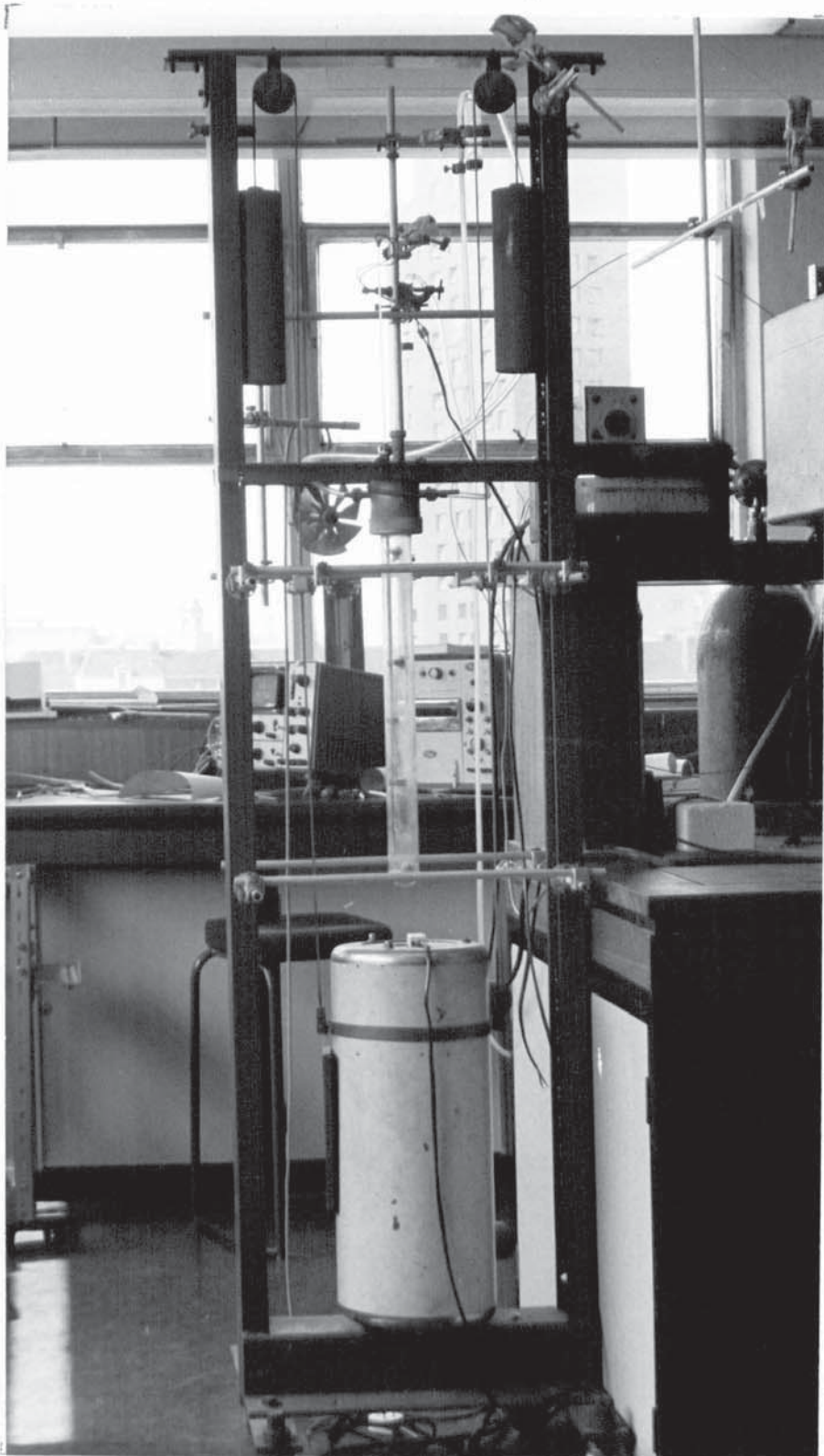
FIGURE 4.20 - The 1000°C furnace. The counter-
weights can be seen at the top then
the brass head cooled by a fan, and
below this the transparent silica
specimen chamber.

Enlarged diagram of furnace

FIGURE 4.21 – The measurement system for operation up to 1800°C. The enlarged diagram shows the mounting of the specimen – in this case a ceramic rod which is joined to the standard 3mm transmission line via a matching section.
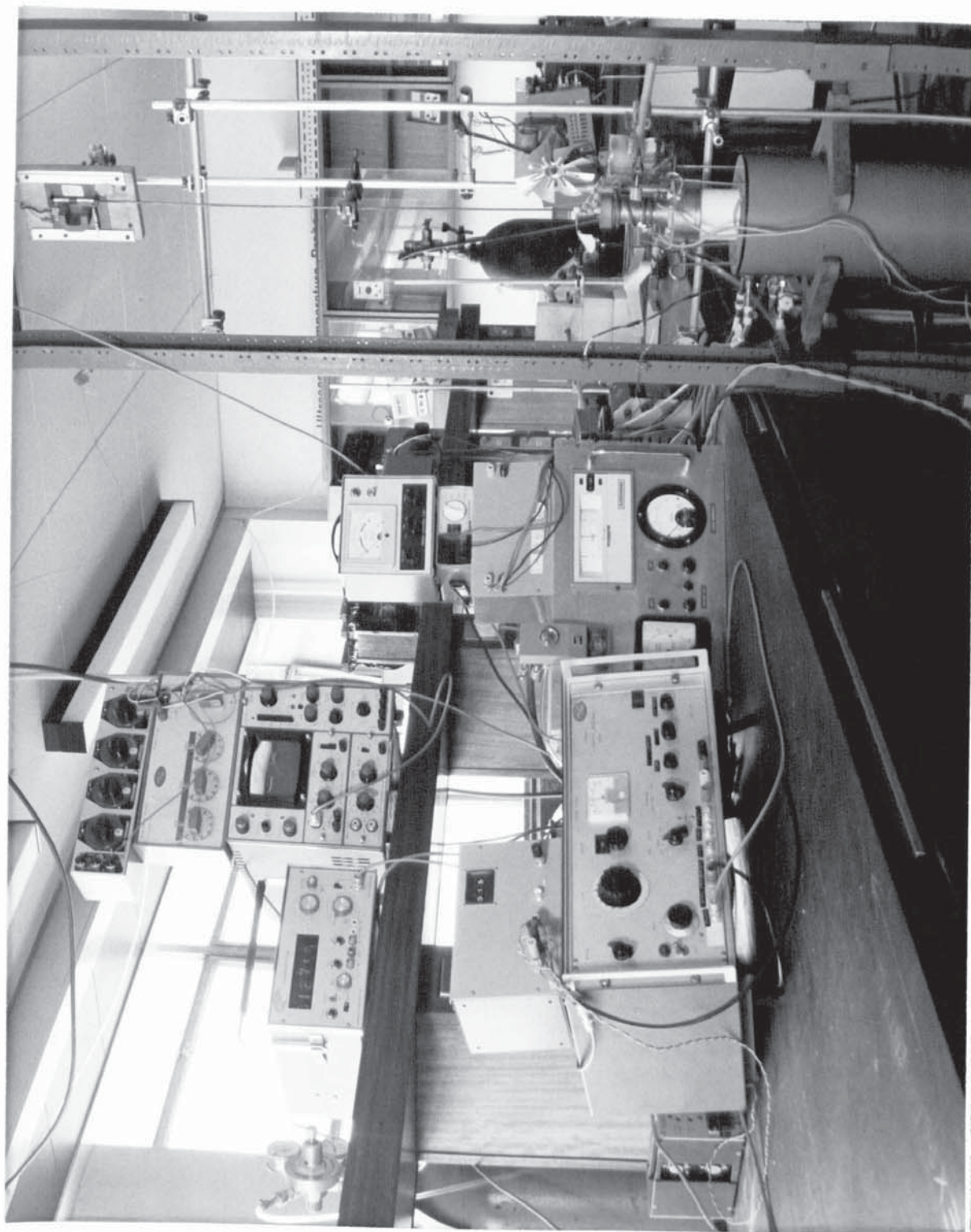
FIGURE 4.22 - The complete 1800°C system. On the bench is the transmitter and counter unit, above these the frequency meter and oscilloscope. In the centre is the temperature control equipment. On the right is the transmission line leading into the 1800°C furnace. At the top is the magnetostrictive transducer tuned by the capacitor box on top of the oscilloscope.
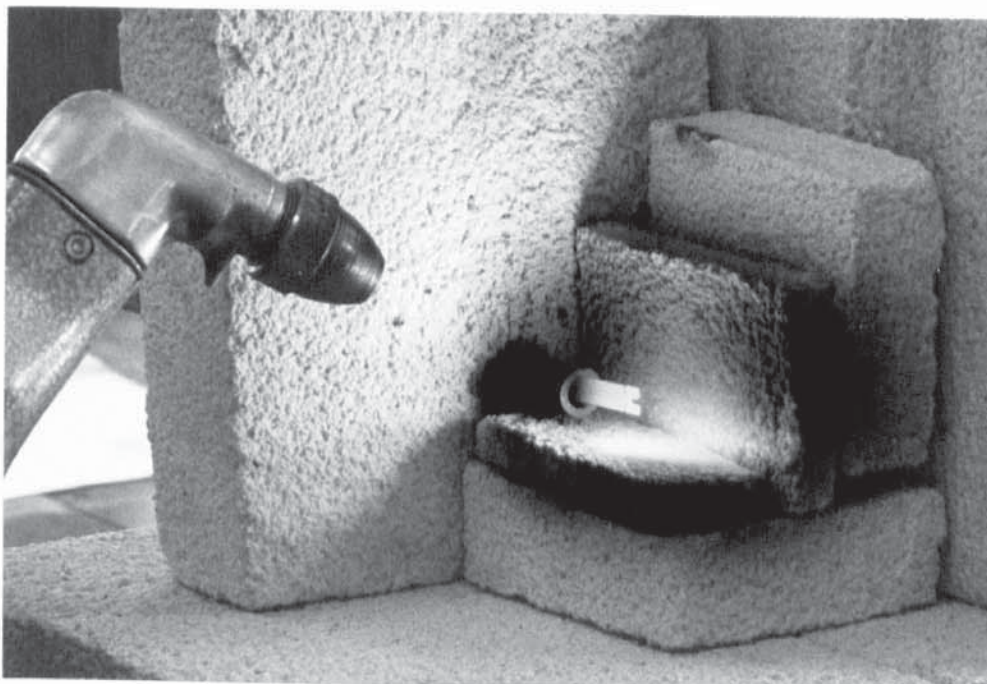
FIGURE 4.23 - An oxygen-coal gas flame was used
to heat some of the specimens up
to 2000°C. This was useful in
attaining higher temperatures than
the furnace and also for heating
short specimens. The temperature
was measured with an optical pyrometer.
The specimen is an iridium strip with
a tuning fork cut into it.

CHAPTER 5: EXPERIMENTAL AND RESULTS

5.1 Introduction

This chapter describes internal friction results for a number
of materials, which fall into two groups. In 5.2-5.4 measure-
ments of Snoek peaks and moderate temperature grain boundary
and background damping are described. The object of this
work was mainly to establish further confidence in the method
but the vanadium results were required for the application
described in Chapter 7. The work on pure polycrystalline
copper has already been described and discussed in 4.4d.
All the specimens were heated in the 1000°C furnace.

Sections 5.5-5.12 are concerned with measurements on nominally
pure refractory materials. Metals are dealt with in 5.5-
5.10 and non metals in 5.10-5.13. Usually two furnace runs
per specimen were made. The first one was on the specimen
in the as received condition apart from necessary machining.
The 1800°C furnace was normally used but in some cases an
oxygen-coal gas flame was used to achieve a higher temperature.
The furnace was slowly heated at about 5°C minute^{-1} and
successive readings of temperature and frequency taken.
Internal friction measurements were made by the n_x method
for low damping and the decrement method for high damping.
Q_m^{-1} was always found to be negligible at room temperature.
In the case of the grain boundary peak determinations, the
approximate grain size was determined before and after heating
by standard metallographic techniques where this was possible
without cutting the specimen.

5.2 Aluminium

$$\text{fcc} \quad \text{mpt } 660°\text{C} \quad \Delta E_{sd} = 1.6 \text{ eV}$$

Early work on aluminium was due to Kê (1948). Since this time quite extensive work has been done on pure aluminium (see e.g. Peters (1964) Williams and Leak (1967)). At 1 Hz it shows a grain boundary peak at 390°C with an activation energy of 1.4 eV. Williams and Leak found a second peak in pure aluminium at 570°C with an activation energy of 3.0 eV. This only occurs when some grains extend right across the specimen to give a bamboo structure. The torsion pendulum will cause sliding in this case and they interpreted the lower temperature peak as a grain boundary migration peak and the higher one as a grain boundary sliding peak.

The work described here was on the commercial aluminium alloy Dural. A rod specimen 80 mm long and 6.3 mm diameter was welded to a 0.53 mm diameter, 3 m long telcoseal transmission line. The fundamental frequency was 31 kHz at room temperature and n_o (m=3) was 50 oscillations. The third and fifth harmonic modes were used for most of the measurements. The specimen was heated in the 1000°C furnace in an atmosphere of argon.

The results are shown in 5.1. This shows a small grain boundary type peak at 470°C (80 kHz). The Wert-Marx method gives an activation energy of 1.5 eV corresponding to the grain boundary migration peak. It is surprising that the peak temperature is not higher than this due to the alloying constituents. Because of the high value of the background damping the peak was not sufficiently well resolved to measure the half width, frequency dependance and relaxation

strength. This small peak shows that the sensitivity of the method is good.

The frequency dependence of the background damping was determined at 350°C and is shown in 5.2. As can be seen there is an effect due to the mode number. This effect did not occur with the copper experiment (4.4a) so cannot be an artefact of the method but must be due to some inhomogeneity of the specimen. This is a feature common to all resonator methods of this type. A possible explanation is shown in Figure 5.2. A peak occurs when there is stress at the centre so it could be that there was an inhomogeneity in this region. With these results only a rough estimate can be made of the frequency dependence. Taking $Q^{-1}(m=2)$: $Q^{-1}(m=6) = 2.2:1.6$, gives a value for n =-0.3 in the equation $Q^{-1} \propto f^{n}$. The activation energy (ΔE) for the background damping is 0.23 eV below the grain boundary peak and 0.43 eV above it. Putting in the value for n = 0.3 the Schoek equation (equation 2.41) gives values of ΔE_{o} of 0.76, 1.43 eV respectively. Schoek (1964), Pines and Karmazin (1966) have found the Schoek equation to apply well to pure and impure aluminium and found values of ΔE in the range 0.1-0.7 eV. When the values of n are put in the values of ΔE_{o} are in the range 1.4-1.65 eV. In this work if the rather dubious value for n is accepted the Schoek formula applies above the grain boundary peak but not below it.

5.3 Snoek peak in iron; carbon and nitrogen

bcc   mpt 1540°C

Snoek peaks have already been reviewed in 2.4. First the

Snoek peak of carbon in mild steel was measured using a longitudinal resonator. A rod 5.5 mm diameter, 25 m long was silver soldered to a 0.55 mm diameter telcoseal transmission line. At room temperature f(m=1) was 103 kHz and n_o (m=1) was 47 oscillations. This large value for n_o was necessary to give measureable changes in n_x for the rather small peak. The result is shown in Figure 5.3, together with an analysis of the measurements. The measurements of peak temperature and half width agree well with the accepted values. It is noteworthy that the calculated peak temperatures are correct despite extrapolation over five orders of magnitude of frequency. This peak is rather a small one for the method but again as in the case of the aluminium results it shows that the method works well.

Samples of pearlite and ferritic nodular iron were examined for Snoek peaks. Resonators similar to the mild steel one were cut from the 50 mm diameter bars supplied. The Snoek peaks similar in both cases were very small and not sufficiently resolved to measure a half width. The peak temperatures were 230°C approximately and the peak heights 0.5×10^{-3} giving a calculated 0.003 atom% of interstitial carbon.

An attempt was made to look for the nitrogen peak in nitrided steel. This was supplied by Newcastle University for investigation as it was too brittle for use in a torsion pendulum. A tuning fork was cut into the 4.8 x 0.35 mm strip before nitriding. Only a rough experiment could be performed due to the problem of matching the thin strip to a transmission

line. However, it was concluded that if there was a peak,
the height was below 5×10^{-3}. From the relaxation strength
data given in 2.4, and neglecting any other effects the
maximum interstitial nitrogen is < 0.03 atom %. A discussion
of internal friction effects due to nitriding is given by
Pope (1973).

5.4 Snoek peaks in vanadium: oxygen and nitrogen

        bcc   mpt 1920°C   purity 99.7% (Koch light)

At 1 Hz vanadium shows an oxygen Snoek peak at 180°C and
a nitrogen peak at 270°C (Powers and Doyle 1959). Interstitial
carbon (Powers and Doyle 1957, Klein 1967) also gives a Snoek
peak but precipitation in the form of a carbide is rapid so
this peak is unimportant.

The Snoek peak work described here was required to test the
feasibility of a proposed method of measuring trace levels
of oxygen in liquid sodium (see Chapter 7). A strip of
vanadium 45 mm x 10mm x 0.5mm was used as a longitudinal
resonator and spot welded to a 0.5mm diameter telcoseal
transmission line. The second harmonic at 100 kHz, $n_o(2) = 17$
was used for most of the measurements. Two experiments were
performed. In the first experiment the specimen was heated
in high purity nitrogen (argon being unavailable at the time).
Heating up to 800°C and cooling produced no peaks. The
specimen was then heated to 650°C, exposed to oxygen for
30 seconds and no peaks were seen though the surface had
visibly blackened. The specimen was then heated to 1000°C
for five minutes in nitrogen and a nitrogen peak was seen
on cooling, shown in Figure 5.4 Throughout the experiment

no more than a slight oxygen peak was seen. The mobile
furnace facility (4.5b) was essential for these experiments.

A second specimen was now heated, in high purity argon with-
out further purification, to 900°C for five minutes and
rapidly cooled. On reheating an oxygen peak and small
nitrogen peak were revealed as shown in Figure 5.5. The
data obtained is summarised in Figure 5.14, 7.1 The nitrogen
peak temperatures are as expected from calculation but the
oxygen peak was 30°C lower than expected. The half widths
were rather different. Oxygen gave a half width of 0.95 eV
(1.26 eV expected) and nitrogen 1.96 eV (1.48 eV). The
nitrogen peak is wider than the accepted value but this can
be accounted for by the relatively large concentration and
presence of other impurities. The oxygen result is rather
surprising and probably due to experimental error;precise
determination of the half width is difficult due to the
presence of the nitrogen peak.

An important feature of the results was that the background
damping level was below 6×10^{-3} at 600°C, thus making this
method of measuring oxygen/nitrogen levels quite feasible.

5.5 Molybdenum

bcc   mpt 2620°C ΔE_{sd} : 4.9 eV

Murray (1968), Belyakov et al. (1967) have found a grain
boundary peak at 1050°C at 1 Hz. Murray's results may be
summarised as follows. Only one grain boundary peak (not
two as reported by some authors) was found. The background
damping was always high compared with the peak but a strong
peak (~0.07) was seen in the as received condition but this
is reduced to ~0.03 on annealing. Raising the frequency to
4.8 Kz from 1.4 Hz gave a less well resolved peak with lower
background damping. Seth (1974) did some tests on pure
molybdenum as a thermometer probe as this material is of
interest in the nuclear field. He did not make any detailed
internal friction measurements but the background damping of
0.02 was reached at temperatures of 1350°C (120 kHz   3mm dia.
specimen) and 1550°C (70 kHz 4.5mm dia. specimen). In this
experiment the molybdenum alloy TZM (0.5% Ti, 0.08%Zr) was
studied. This has improved hot strength (Briggs and Beer
1971) over pure molybdenum and would be expected to have
a higher grain boundary peak temperature.

A Seth tuning fork resonator was cut into the end of a 3.2mm
dia. rod and the other end was matched and silver soldered to
a 3.2mm dia. mild steel transmission line. n_o was 22 oscill-
ations and the frequency 135 kHz. It was heated in the 1880°C
furnace in vacuum to 1420°C, this being the maximum furnace
temperature at the time. The results are shown in 5.6. The
frequency-temperature shows promising performance as a
thermometer. The internal friction curve shows the grain

boundary peak to be well above 1420°C - probably it lies in the range 1600-1700°C. From Murray's 1 Hz data of peak temperature and activation energy the grain boundary peak for pure molybdenum would be at 1900°C using the Wert Marx plot. Results for the refractory metals at 100 kHz described in later sections would lead one to expect a rather lower value. This is also indicated by Seth's work. The specimen appeared to be very fine grained (~0.03 mm) before and after heating .

5.6 Iridium

fcc　　mpt 2440°C　ΔE_{sd} = 3.5 eV? (from creep data)
sample purity 99.95%

Murray (1968) is the first person to report work on the high temperature internal friction of iridium. He found a grain boundary peak of height 0.075 at 1450°C measured at 2 Hz. The frequency shift was not measured but an estimate of 3.5 eV for the activation energy of the relaxation was obtained from creep measurements. The Wert-Marx method however, gives 4.8 eV which does give rather better agreement with the viscous grain boundary model of Kê and McClean (1957). Murray does not discuss the half width of the peak or the background damping but these quantities can be calculated from his results and are discussed below.

For this work a 4.75 x 0.5mm x 250mm strip 99.95% pure supplied by Johnson Matthey was used. A Seth tuning fork was cut in one end and a 3.2mm steel transmission line was matched and silver soldered to the other end. The sample was heated in a flame as illustrated in figure 4.23 so that temperatures of 2000°C+ could be reached. Temperatures were measured

with an optical pyrometer taking $\epsilon = 0.30$. Above 1800°C slight oxidation occurs as shown by a drop in frequency on prolonged heating but this is not troublesome. The as received grain size was about 0.3mm but it was not possible to determine it after heating without destroying the specimen. The results of two runs are shown in figure 5.7. The grain boundary peak on the second run occurred at 1900°C and had a height of 0.06 at 45 kHz (after subtraction of background damping). It was not possible to obtain a precise internal friction curve because fine temperature adjustment was not possible.

These results will now be compared with those of Murray but the discussion has to be somewhat speculative due to the limited accuracy of the data and differences in the specimen and mode of vibration. Murray's grain size was 0.14mm (in a 0.5x5mm cross section) whereas in this work it was rather larger. The very large frequency factor of 2×10^4 between the two experiments should, however, make the other differences relatively less important and some generalisations should be possible. The temperature shift of 1.21×10^{-4} K^{-1} gives an activation energy of 3.8 eV. Plotting the peak temperatures on a Wert-Marx diagram assuming $\tau_o = 10^{-15}S$ gives values of 4.0 eV (Pelmore) and 4.9 eV (Murray). From creep experiments Murray estimated ΔE_{sd} to be 3.5 eV. There are clearly some anomalies, but there is insufficient information to come to any definite conclusion. The peak was very narrow for a grain boundary peak giving a half width corresponding to an activation energy of 4.4eV (i.e. like a Debye peak) whereas Murray's had a half width of 1.4eV. The frequency curve gave a modulus defect corresponding to Q^{-1}_{max} of 0.11. Murray

similarly found a large modulus defect corresponding to
0.15.

The background damping will now be considered, and the
temperature shift between these and Murray's results can
be measured. The average shift over the internal friction
range $5-10 \times 10^{-3}$ is 1.7×10^{-4} and following the method of
De Batist (1972, p.392) this gives a value of ΔE_o of 5.0eV.
From Arrhenius plots of the background damping these results
give a value for ΔE of 1.3eV and Murray's results give 0.87eV.
Thus comparing results for ΔE_o, ΔE we find $n \simeq 0.2 - 0.25$
for the Schoek formula.

5.7 Tantalum

bcc   mpt 3000°C $\Delta E_{sd} = 4.7$ eV

sample purity 99.9%

Schnitzel (1959) found a grain boundary peak in tantalum at
1110°C (0.7Hz). Murray (1968) did more detailed experimental
work and found the peak to be at 1230°C (1 Hz) and from the
frequency shift determined $\Delta E = 4.2$ eV.

This work was done with a strip specimen 4.8 x 0.5mm cross
section and the acoustic design was similar to the iridium
(5.6). The silver paint method was used to join the tantalum
to the steel, silver soldering being difficult. The specimen
was heated up to 1800°C in a vacuum of 10^{-2} torr. The specimen
absorbed a large amount of oxygen and nitrogen at the high
temperature as shown by the large Snoek peaks on cooling.
The results are shown in figure 5.8. The average grain sizes
before and after heating were 0.03mm, 0.8mm.

As the furnace temperature was not high enough to see the grain boundary peak not much can be said about this aspect. From Murray's data on the peak temperature and activation energy, the peak temperature would be expected to be at 2030°C at 80kHz. From figure 5.8 the peak temperature can be estimated at 1900°C+ (if the height is assumed to be 0.08 and the half-width to be 4.2 eV) giving reasonable agreement.

The Snoek peak data available from figure 5.8 is summarised in figure 5.14. The oxygen peak occurred 30°C higher than the calculated value and was rather broader than calculated. The nitrogen peak occurred 80°C higher than calculated and again was broad. These differences are probably accounted for by the high interstitial concentrations.

5.8 Rhenium

fcc   mpt 3170°C ΔE_{sd} = 4.8 eV (Wert Marx method)
sample purity 99.9%

Schnitzel (1959) found a rather ill defined grain boundary peak at 1400°C (1.1 Hz). Use of the Wert-Marx plot gives an activation energy of 4.8 eV. There seems to be no more recent work.

In this experiment a strip of cross section 4.8 x 0.5 mm was used, set up as the iridium specimen and heated in the 1800°C furnace. The grain size was initially 0.1mm and 0.2mm after the second furnace run. On the first run a marked dip in the frequency curve was seen in the 500-1000°C temperature range. There was no associated internal friction change and the effect was not seen on cooling or in the second run. The

phenomenon is probably similar to that for copper (4.4d) i.e. a recovery process but is notable for the large temperature range. On the first run (heating) two peaks were seen at 1650°C (peak A) and 1780°C (peak B). The first peak reappeared on the second run at a higher temperature of 1710°C and always had a very narrow width corresponding to ~10eV.

If we take Schnitzel's peak temperature and calculate the value at 80 kHz using the Wert-Marx plot the answer is 3000°C. This seems unlikely but we might expect a similar peak temperature to iridium i.e. 1900°C+. Thus it seems likely that peak A is not a true boundary peak in view of the temperature calculation and the narrow width. It could simply be a result of insufficient annealing but it might be a PM/SS peak phenomenon. It would certainly be worth repeating this experiment with a higher temperature furnace.

5.9 Tungsten

bcc   mpt 3370°C $\Delta E_{sd} = 6.1$ eV

sample purity 99.9%

Schnitzel (1959) found a peak at 1250°C (1 Hz). Shestopal (1967) using zone refined unannealed tungsten found a peak at 1350°C (0.25 Hz) and determined the activation energy to be 5.7 eV using the frequency shift method. He also measured the background damping and found $\Delta E = 0.72$ eV, $n = 0.22$, giving $\Delta E_o = 3.3$ eV. A much higher value was found for coarse grained tungsten. Berlec (1970) found for annealed tungsten a broad grain boundary peak at 1730°C (0.5 Hz) superimposed on very high background damping, there being a Q^{-1}_{max} of 0.28.

A tungsten rod 3mm dia. and 900mm long was matched and silver soldered to a short length of 3mm permendure. The other. end had a Seth tuning fork cut into it. There were two furnace runs one up to 1600°C and the second to 1800°C. It was not possible to determine the grain size but the specimen had the appearance of being fine grained before and after heating. The results are shown in figure 5.10. The damping increases rapidly above 1600°C and there appears to be a peak at $\sim$1900°C.

The equivalent temperature of the 1900°C peak is 1300°C at 1 Hz assuming an activation energy of 5.7 eV. Thus this peak appears to correspond to Schnitzel's. Turning now to the background damping an Arrhenius plot gives a value of 1.5eV in the 1400-1750°C temperature range, as compared to Shestopal's value of 0.72eV. ΔE_o may be estimated from the temperature shift because once the tungsten is partially annealed the damping is 0.02 at 1000°C (1 Hz) whereas at 90 kHz it is 0.02 at 1750°C. This gives ΔE_o = 3.4eV - much lower than the energy of self diffusion, but in agreement with Shestopal's determination but not that of Pines and Karmazin (1966).

5.10 Carbon (graphite)

mpt 3500°C   sublimes 3300°C

Merlin (1969) and Firle (1969) have measured internal friction in graphite in the 50-300K range but high temperature data could not be found. A sample of 'nuclear' graphite 3.3mm dia. and 560 mm long was used. One end had a tuning fork cut into

it and the other end was flame sprayed with permendure
powder to make it magnetostrictive. Because the sound vel-
ocity in graphite is low ($\sim$ 2800 ms^{-1}), the use of a short
transmission line is possible. One furnace run up to 1800°C
was performed.

The results are shown in figure 5.11. The frequency-temperature
characteristic is unusual. The dip in the curve at 300°C is
thought to be due to the evolution of water. Young's modulus
then increases with temperature. Above 1400°C evaporation
of the graphite occurred due to oxidation and this accounts
for the drop in frequency. It was still possible to obtain
an approximate value for the internal friction despite the
evaporation and this is remarkably low at high temperatures.

5.11 Silicon nitride (hot pressed)

The properties of silicon nitride have been described by
Lloyd (1967) and Ashcroft (1973). Although there is copious
data on mechanical properties, internal friction data appears
to be lacking.

A sample of hot pressed silicon nitride 4mm x 0.8mm x 150mm
with a tuning fork cut into one end was kindly donated by
the Joseph Lucas Research Centre. A special method had to
be used to attach it to a steel transmission line because
a direct joint would have been difficult. A 5.5mm dia.
aluminium rod section was put between the 3.2mm steel
transmission line and the silicon nitride strip. One end
was aluminium soldered to the steel and the other was
fashioned to a screwdriver blade shape (see appendix A)

and araldited to the silicon nitride. The use of aluminium
with a low acoustic impedance allowed a large area of contact.
This joint gave remarkably satisfactory performance though
the use of the silver paint technique would probably have
been even better. The sample was heated in a flame and
the temperature measured using an optical pyrometer, ϵ being
taken as 0.60. The metal-ceramic joint was cooled with a
water wetted wick.

Two runs were made and the results are shown in figure 5.12.
In the first run only a small internal friction peak was seen.
In the second run there was a large sharp peak at 1160°C
appx. In the second run transparent glassy materials boiled
out of the edges of the specimen. The peak height is 0.070
appx. and the modulus defect gives a height of 0.05. The
activation energy from the Wert-Marx method assuming $\gamma_o = 10^{-15}s$
is 2.5eV and the half width gave a value of 2.45eV.

The sharp internal friction peak is clearly due to the soften-
ing of the magnesium silicate glass which is used as a
binding agent. The results show that this produces a Debye
type peak rather than a broad peak, and this effect should
occur in other materials containing a glass phase.

5.12 Stabilised Zirconia

Wachtman and Corwin (1965) measured the internal friction
in stabilised zirconia up to 800°C and found a peak in the
450-300°C range, depending on Ca concentration, of height 0.01,
thought to be due to oxygen vacancy motion.

A 5mm dia. rod was used with a tuning fork cut into one end and the other end matched to a 3.2mm dia. steel transmission line by a tapered matching section. The density of the sample was 5.28 g cm^{-3} and the rod velocity 5680m s^{-1}. Measurements were made up to 1500°C. Due to an acoustic design error internal friction measurements could not be made but the frequency curve showed a sharp knee at 1300°C (indicative of an internal friction peak). On cooling the frequency curve was very different. As the main interest of this experiment was to test its suitability for a thermometer probe no further work was done.

5.13 Sapphire

mpt 2050°C

Wachtman and Lam (1959) measured Young's modulus of sapphire up to 1200°C. Southgate (1966) measured the internal friction of single cyrstal magnesium oxide up to 1200°C and found the damping to be very low (10^{-5} at 1200°C). A 3mm dia. x 250mm sapphire rod had a Seth tuning fork cut into one end. The other end was joined to a 3.2mm steel transmission line using the 'silver paint' technique described in 4.1c. The specimen was heated in a flame and protected from uneven heating by a short length of 99.7% pure alumina tube. Measuring the specimen temperature by an optical pyrometer presented an emissivity correction problem as the inside of the protective tube was not a black body. It was decided to measure the outside temperature of the alumina tube taking ϵ = 0.3. This should closely correspond to the temperature of the sapphire, the radial temperature gradient being small.

The frequency temperature characteristic is shown in figure 5.13. The internal friction was too low to measure even at 1800°C being less than 2×10^{-3}. The frequency characteristic is notable for its near linearity and constancy. When the specimen was heated up and cooled the frequency returned to within 10 Hz at 120 kHz of the previous value. Prolonged exposure to temperatures in excess of 1800°C causes an increase in frequency caused by evaporation.

5.14 General Discussion

The main relevance of these results is to the technical applications to be described in chapters 6,7 but some metallurgical generalisations can be made.

Firstly, these results with a measuring frequency of approximately 100 kHz can be compared with the existing 1 Hz data. The Snoek peak experiments showed good agreement with the low frequency results with no serious discrepancies. Secondly background damping results were only sometimes in accord with the Schoek (1964) formula. Copper and aluminium below the grain boundary peak did not give agreement but aluminium above the grain boundary peak did. This area is one that clarifying and it would be useful to compile a review showing where the Schoek formula held and where it did not. Thirdly, the grain boundary results give indications that the temperature shift is less than calculated and that the peaks are sharper.

The method is a useful tool for the investigation of background damping and grain boundary relaxations at high temperatures. The experiments on iridium, rhenium and silicon nitride are certainly worth repeating in more detail. This

would require the use of a small vacuum furnace. More
generally a study of grain boundary peaks in all the
refractory metals could be made. It would be desirable
to use a resonator in which several modes can be used,
so that the frequency dependence can be measured during a run.
Perhaps the most interesting application is in the study of
ceramic materials. Internal friction could provide comple-
mentary information to that obtained by the more usual high
temperature techniques, and might be able to detect changes
in features such as cracks, voids and phase separation.
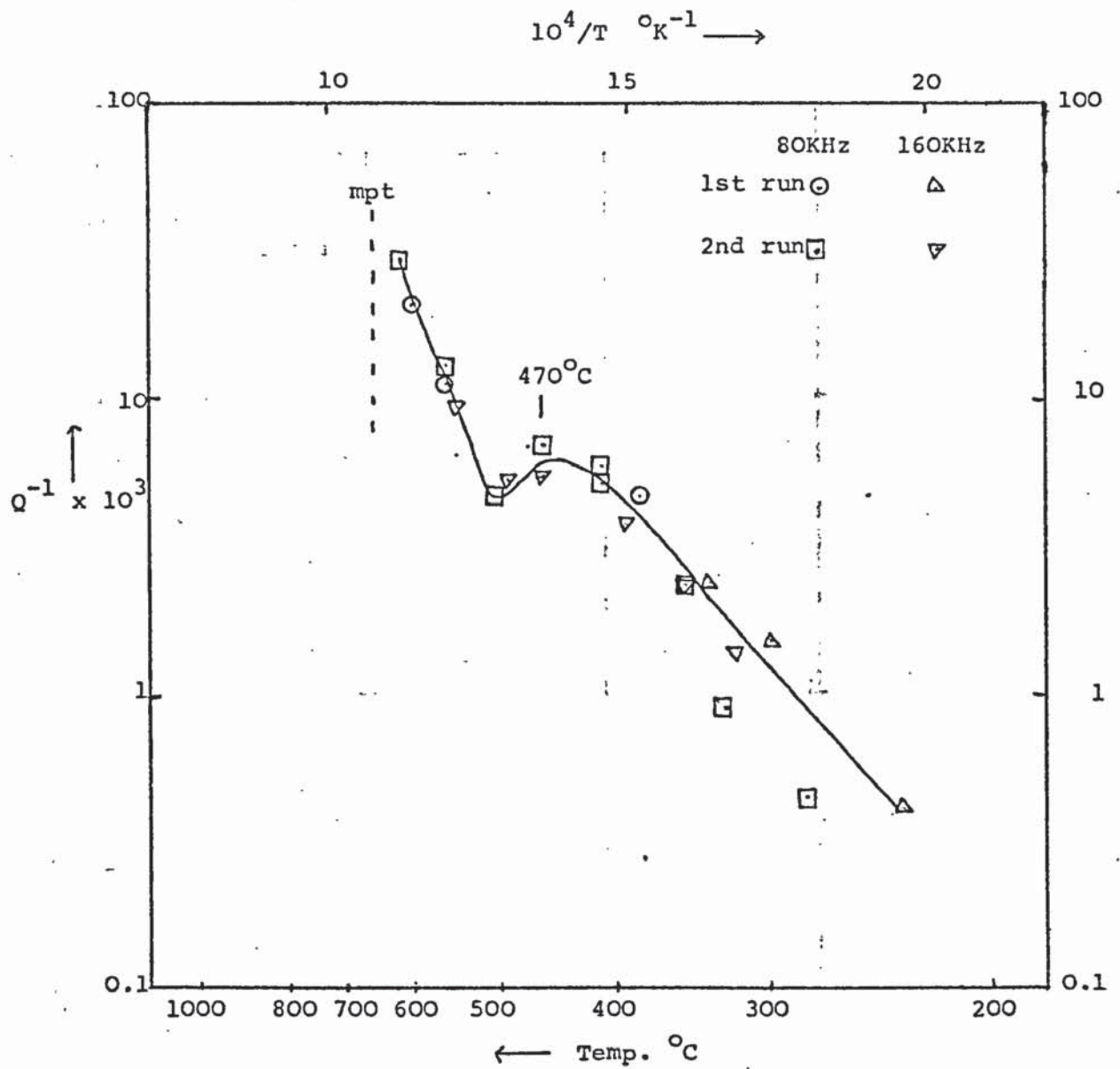
FIGURE 5.1 - Background damping in a polycrystalline
aluminium alloy (Dural) A small grain
boundary peak can be seen at 470°C.
The crossover was 'lost' at 400°C in
this run and the internal friction was
then measured from the decrement.
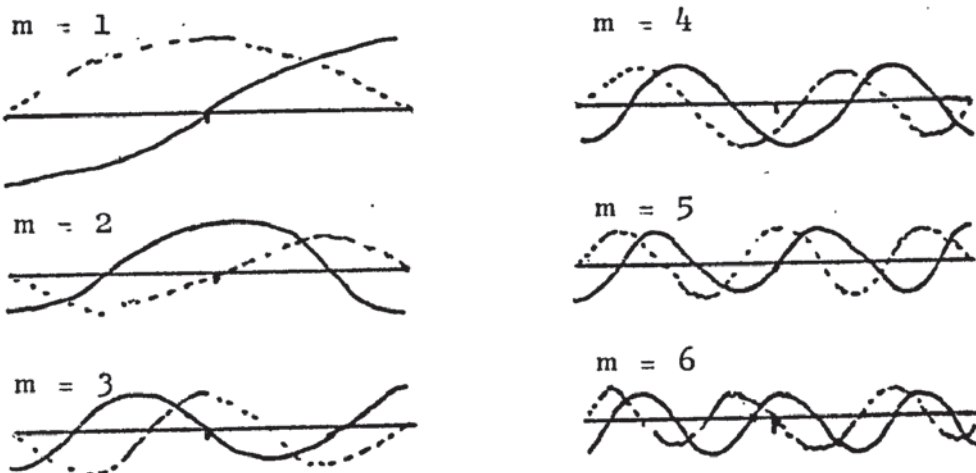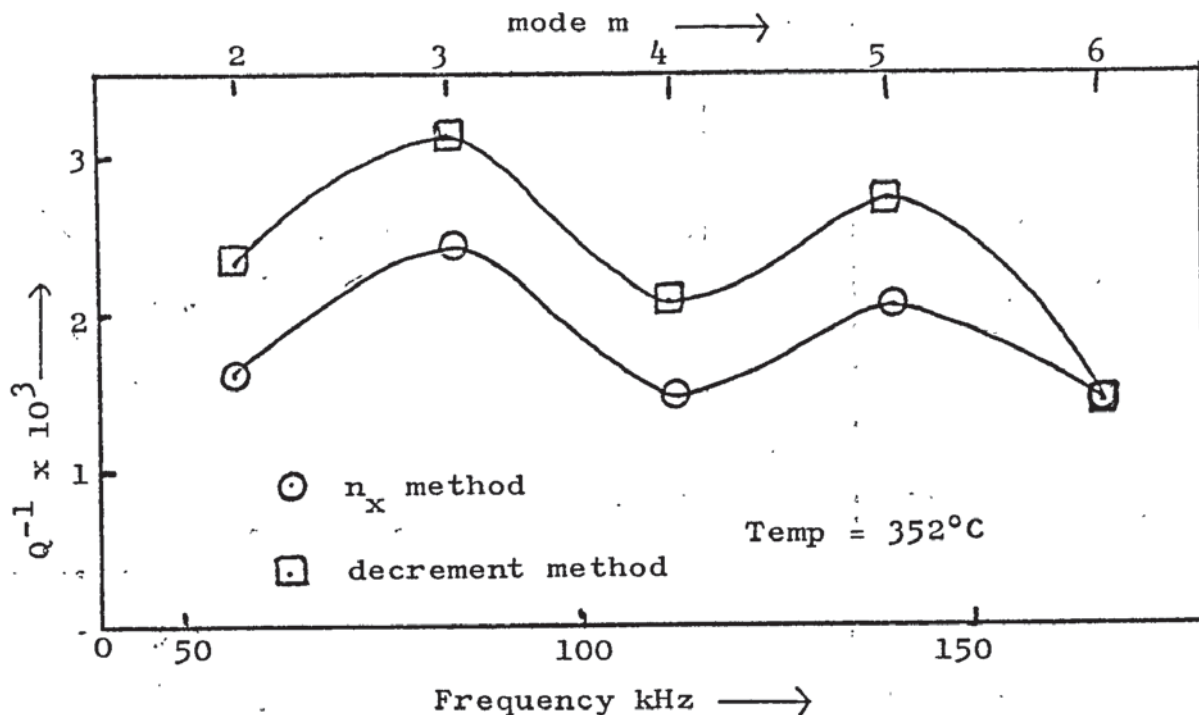
The lines indicate the strain and the dotted lines the stress in the specimen.

FIGURE 5.2 – Frequency dependence of internal friction in polycrystalline aluminium. A hazard of using different modes of a resonator to determine frequency dependence is that if the specimen is inhomogeneous, different modes of vibration may give different results. This effect is clearly shown here. As the peaks occurred when there was a stress maximum at the centre of the specimen the strong damping centre could have been located here.
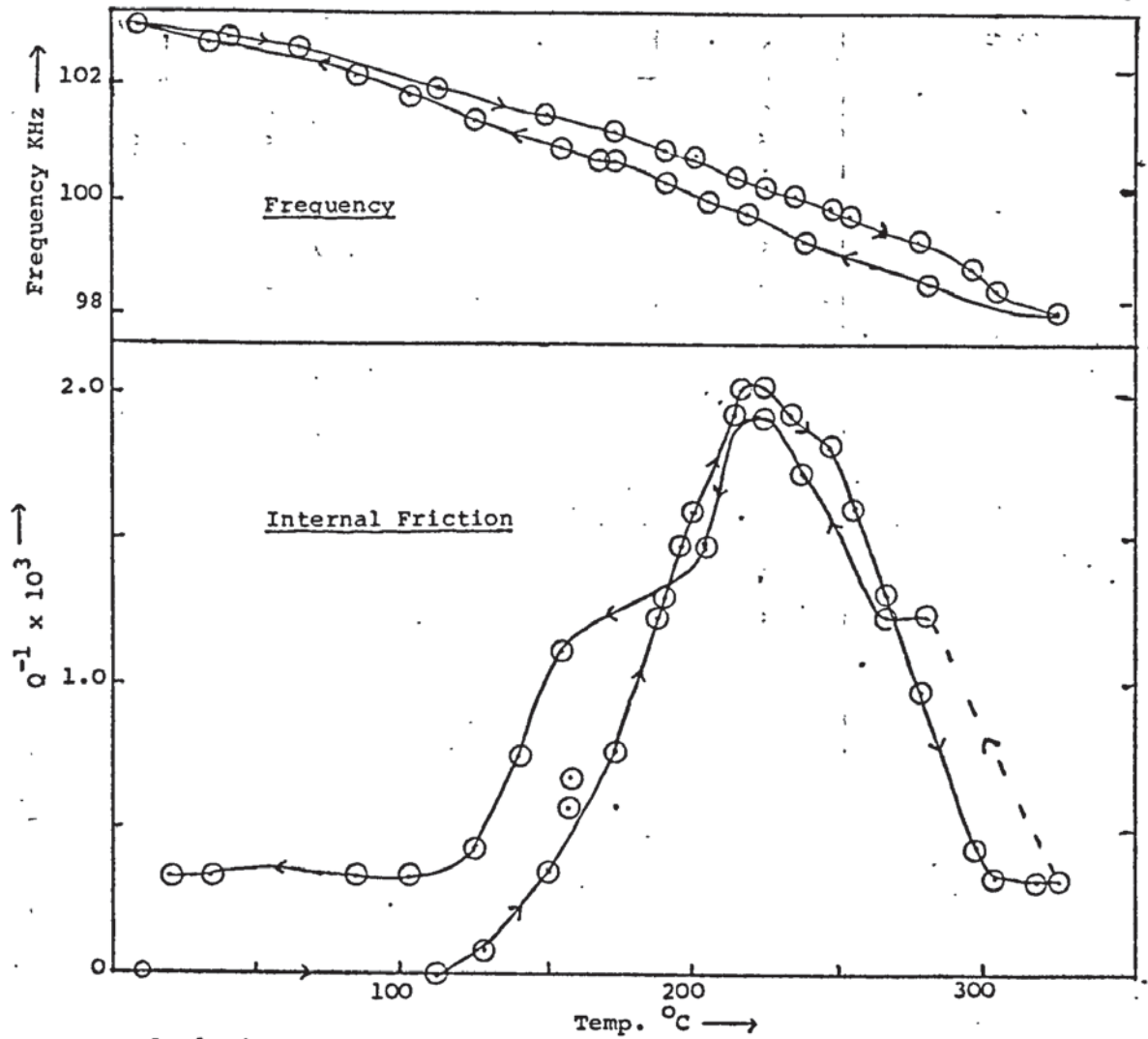
	Experimental	Calculated
peak temperature °C	210	195
$\triangle E$ from half width eV	0.78	0.78
$\triangle E$ from Wert-Marx method eV	0.85	

FIGURE 5.3 - Snoek peak of carbon in iron (mild steel). The concentration of interstitial carbon can be calculated from the peak height to be 0.010 atom %.
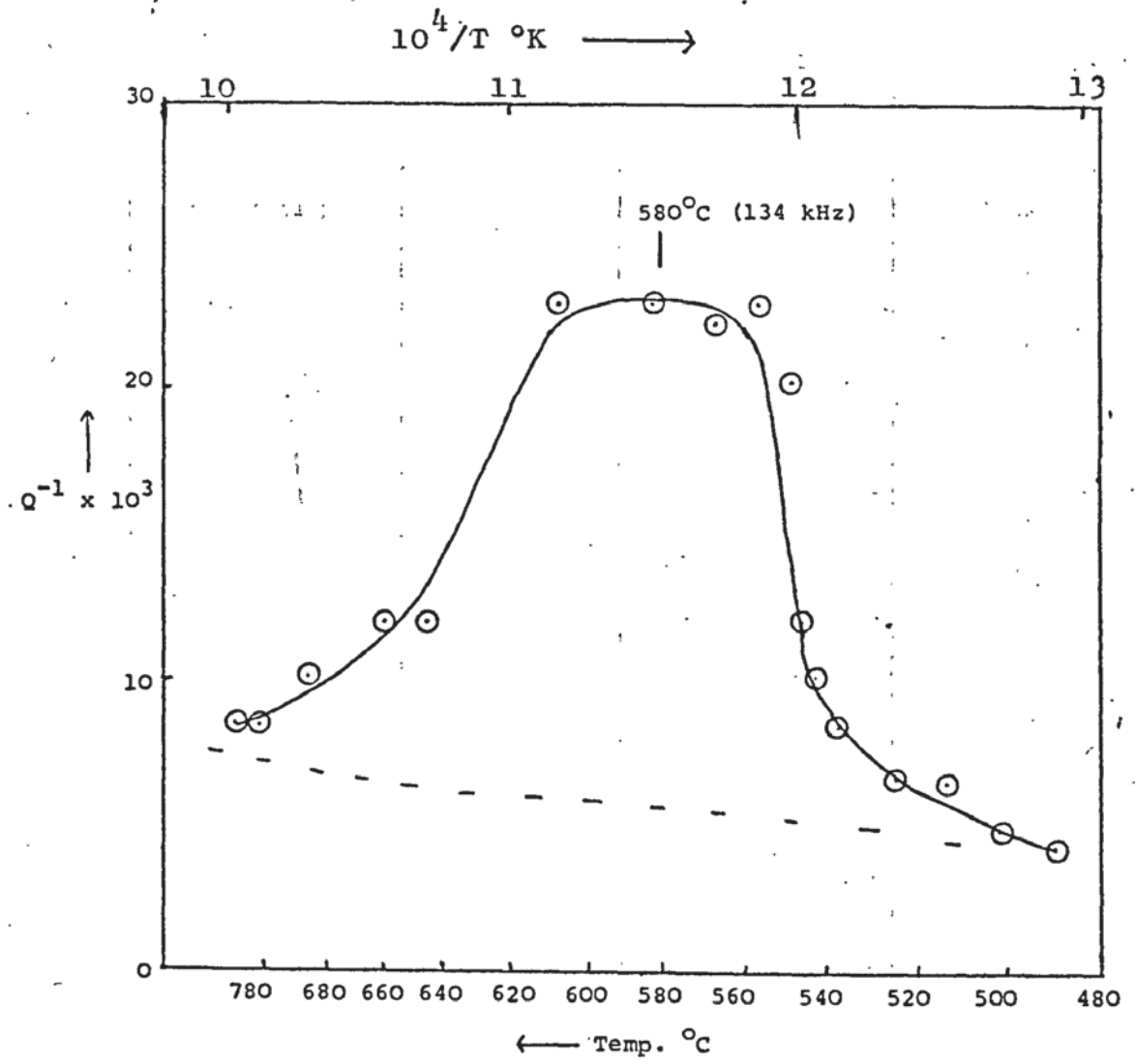
FIGURE 5.4 - Snoek peak of nitrogen in vanadium
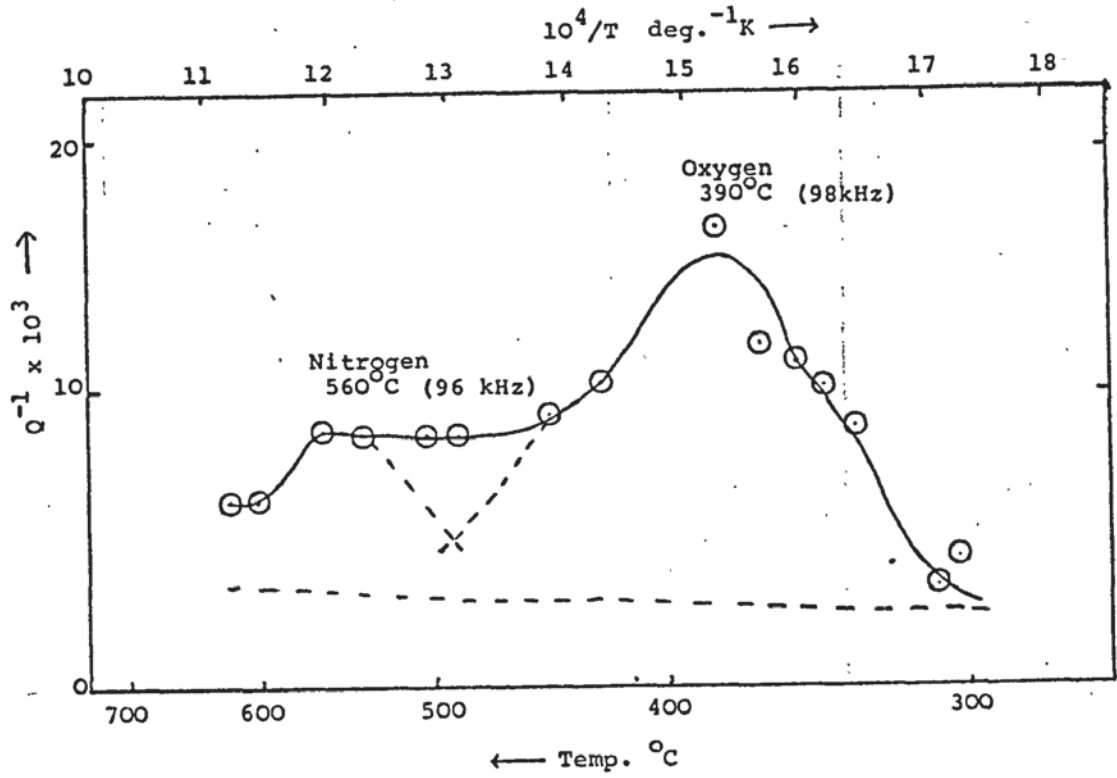
FIGURE 5.5 - Oxygen and nitrogen peaks in vanadium
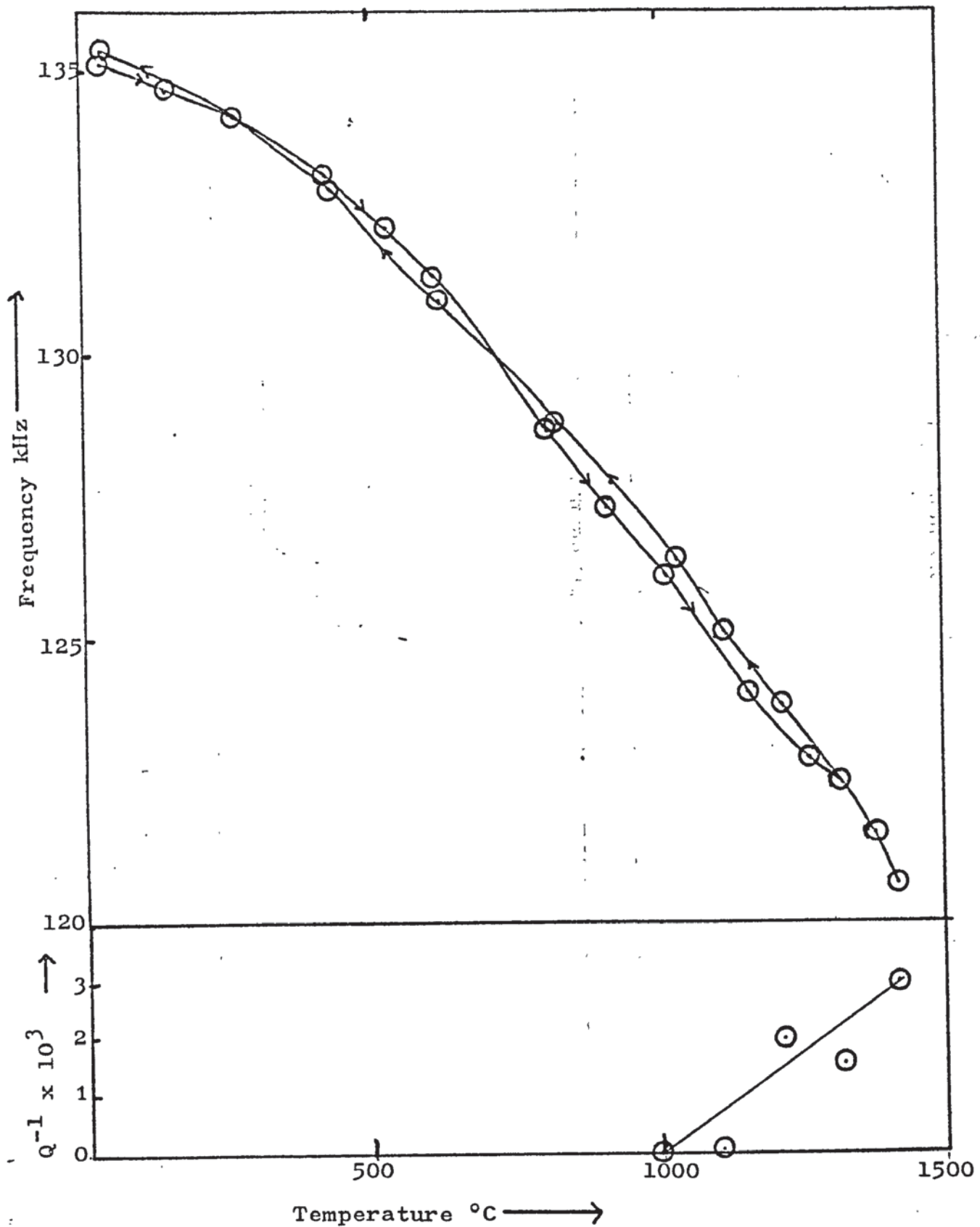
FIGURE 5.6 - Internal friction and frequency characteristics
for the molybdenum alloy TZM (1st run)
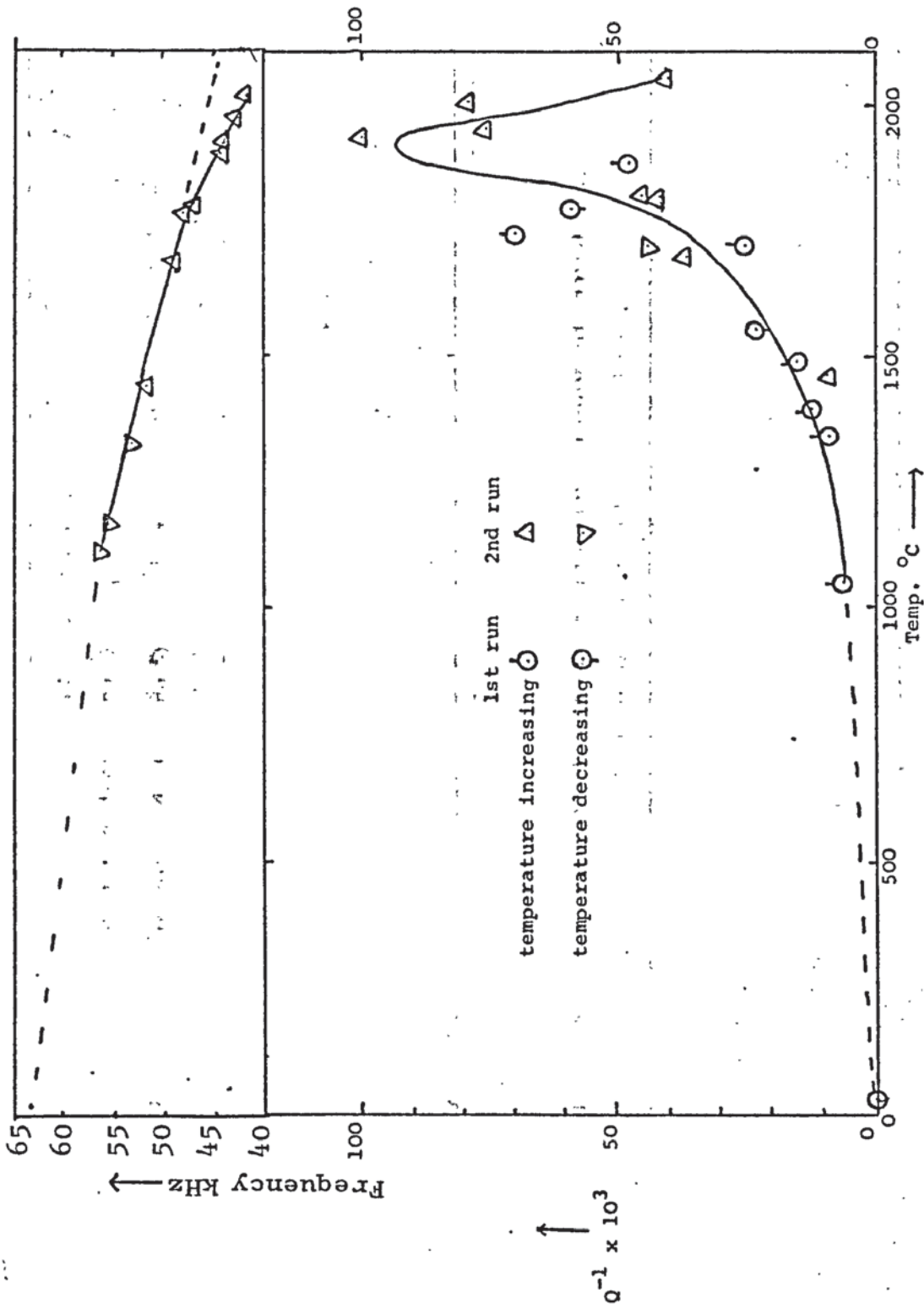
FIGURE 5.7 - Internal friction and frequency of iridium.
The specimen was heated in a flame.
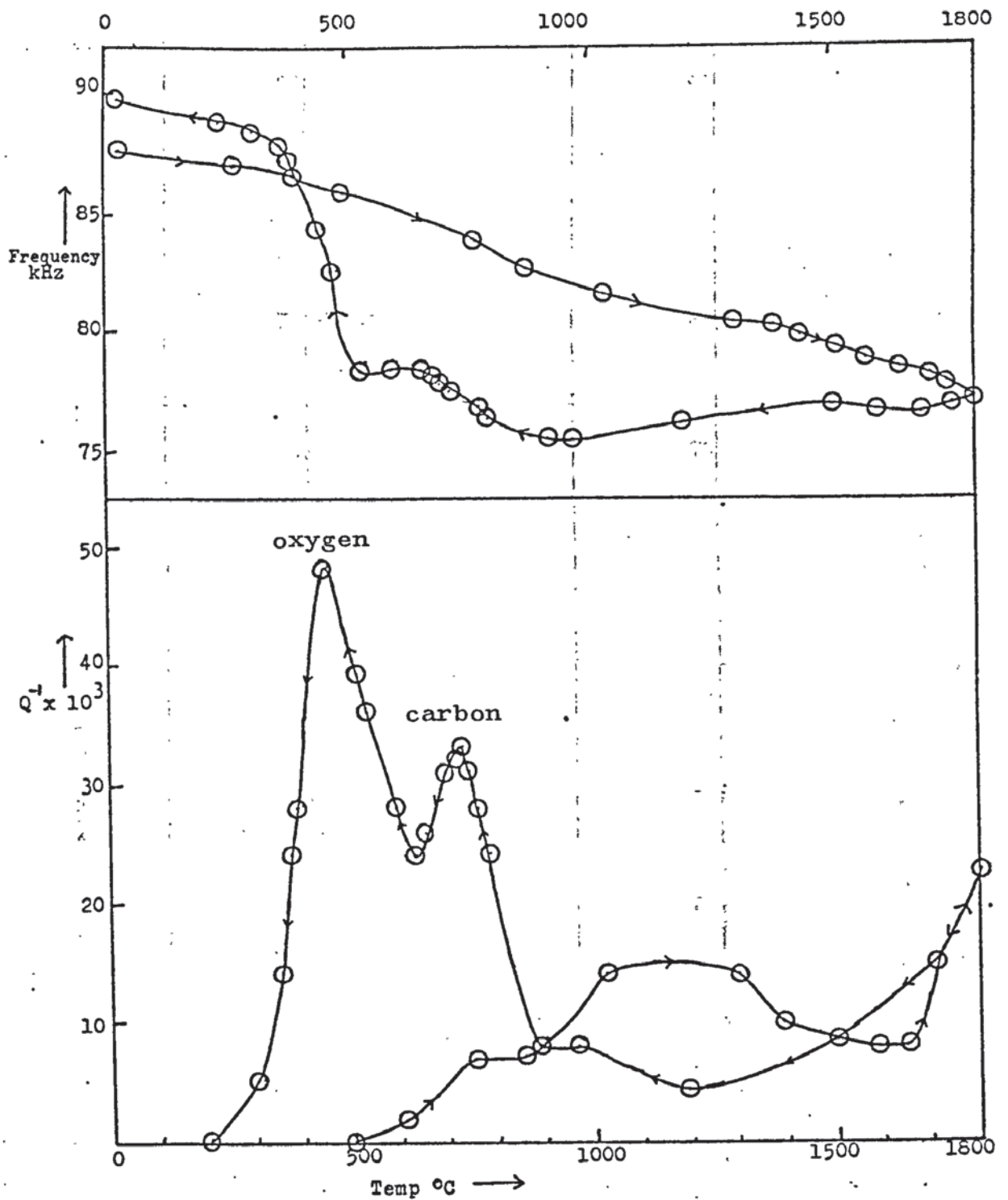
FIGURE 5.8 - Internal friction and frequency of tantalum 1st run. Snoek peaks were shown on cooling due to gas uptake at the high temperature.
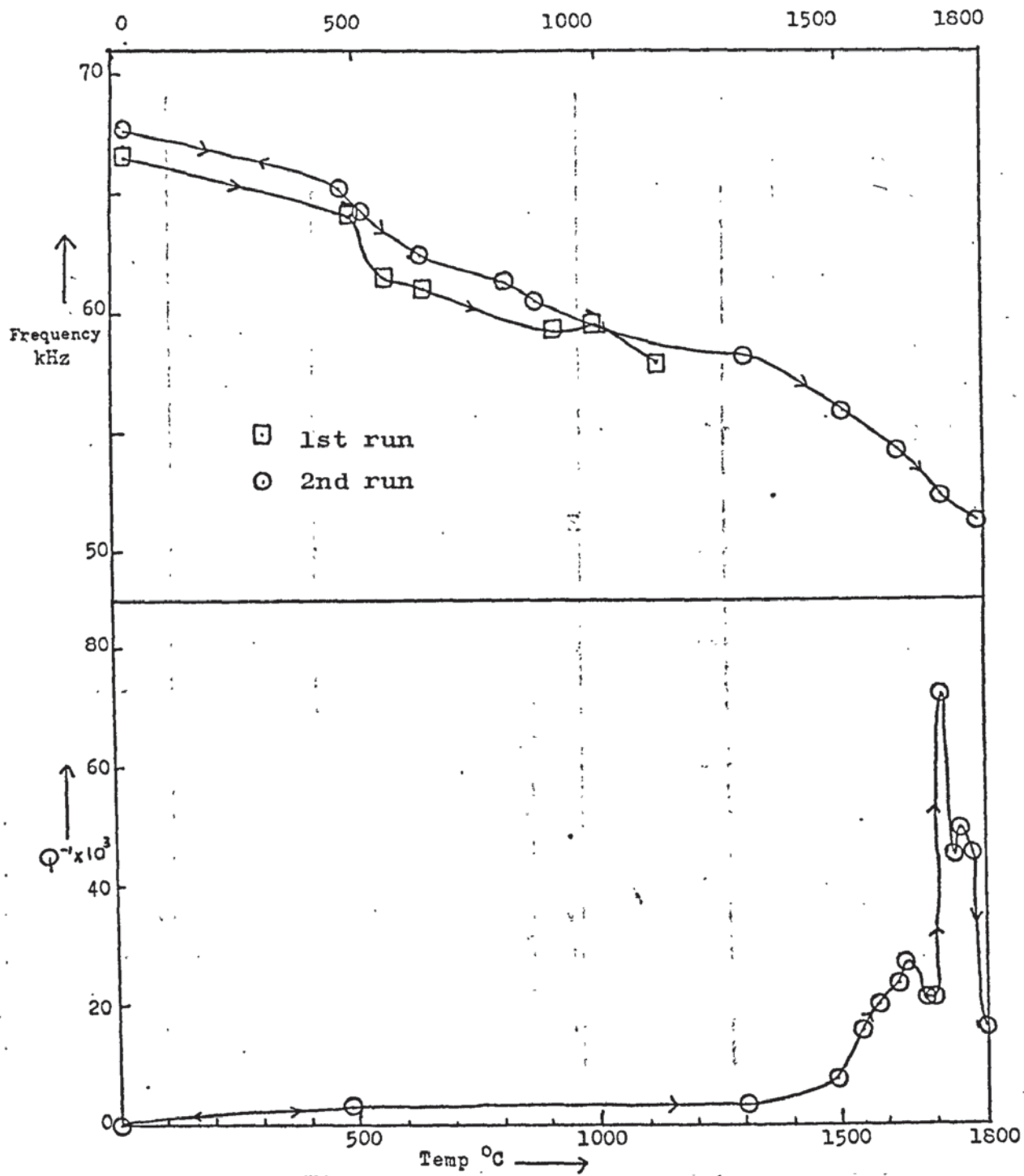
FIGURE 5.9 – Internal friction and frequency of
rhenium
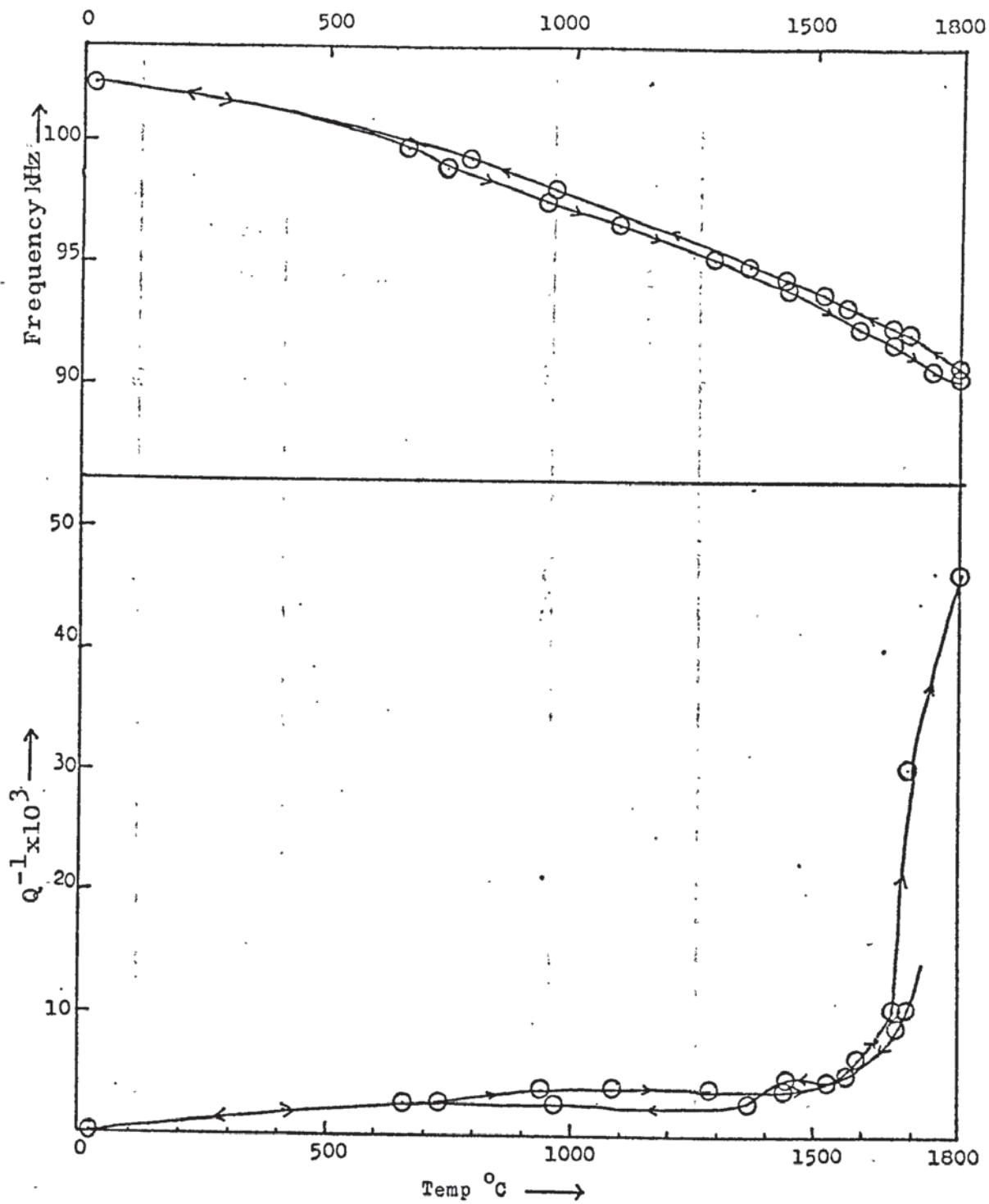
FIGURE 5.10 - Internal friction and frequency of
tungsten, 2nd run.
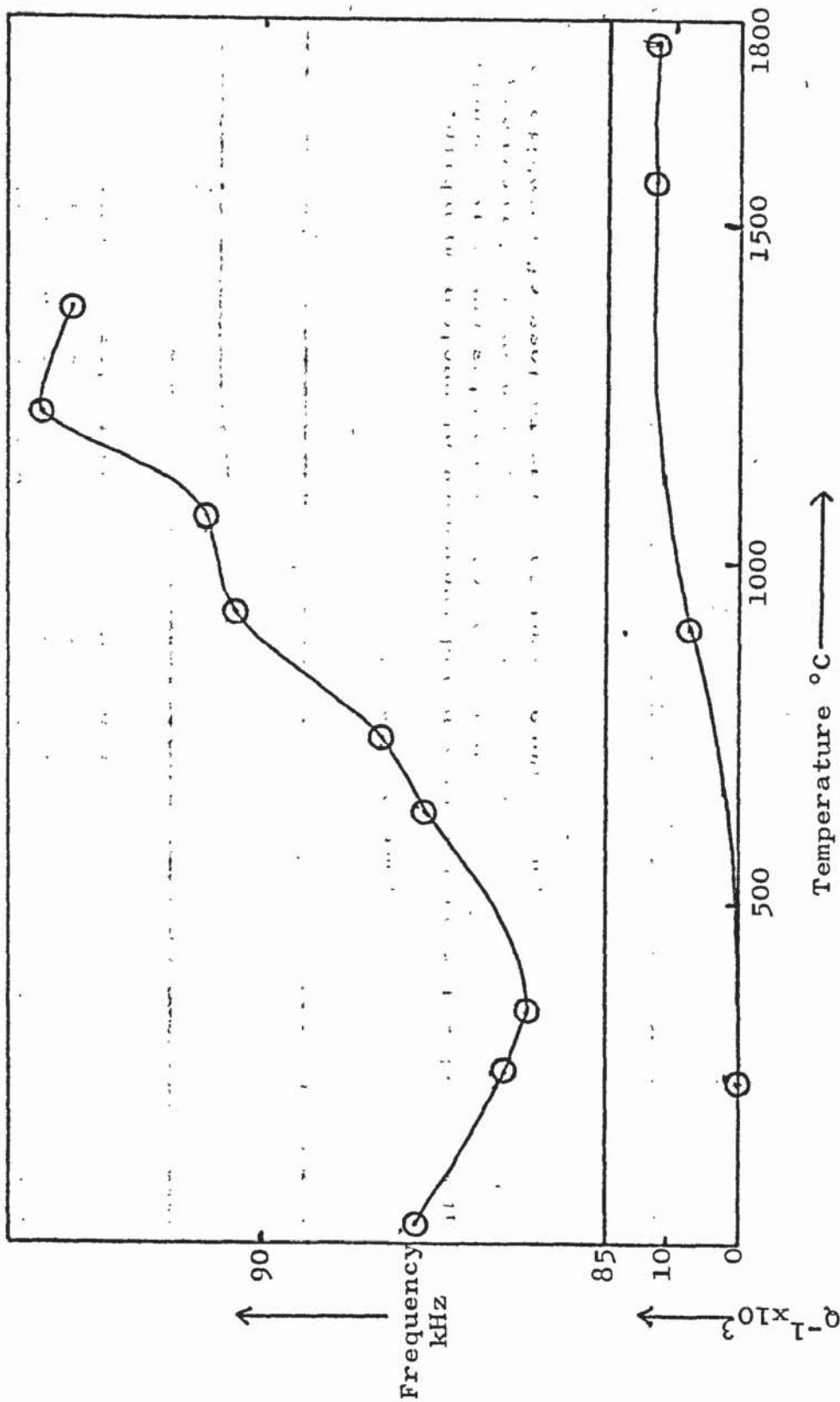
FIGURE 5.11 - Internal friction and frequency of nuclear graphite. The initial dip in the Young's modulus curve is thought to be due to the loss of water. Readings of frequency above 1500°C were unreliable due to loss of graphite by oxidation.
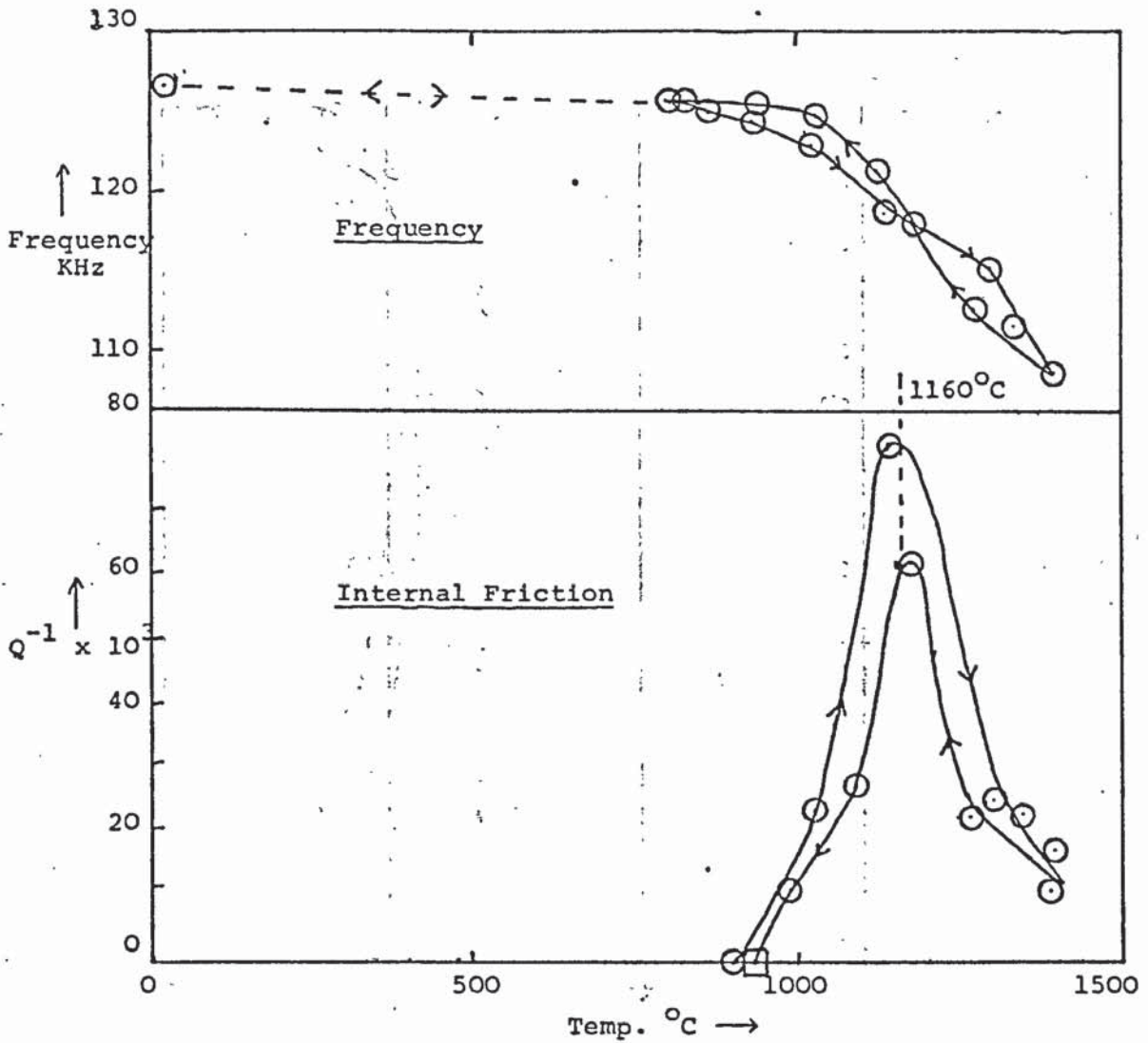
FIGURE 5.12 - Internal friction in hot pressed Silicon
Nitride, 2nd run (supplied by J. Lucas
Research Centre). The sharp internal
friction peak is due to softening of the
magnesium silicate binding agent and was
absent on the first run.
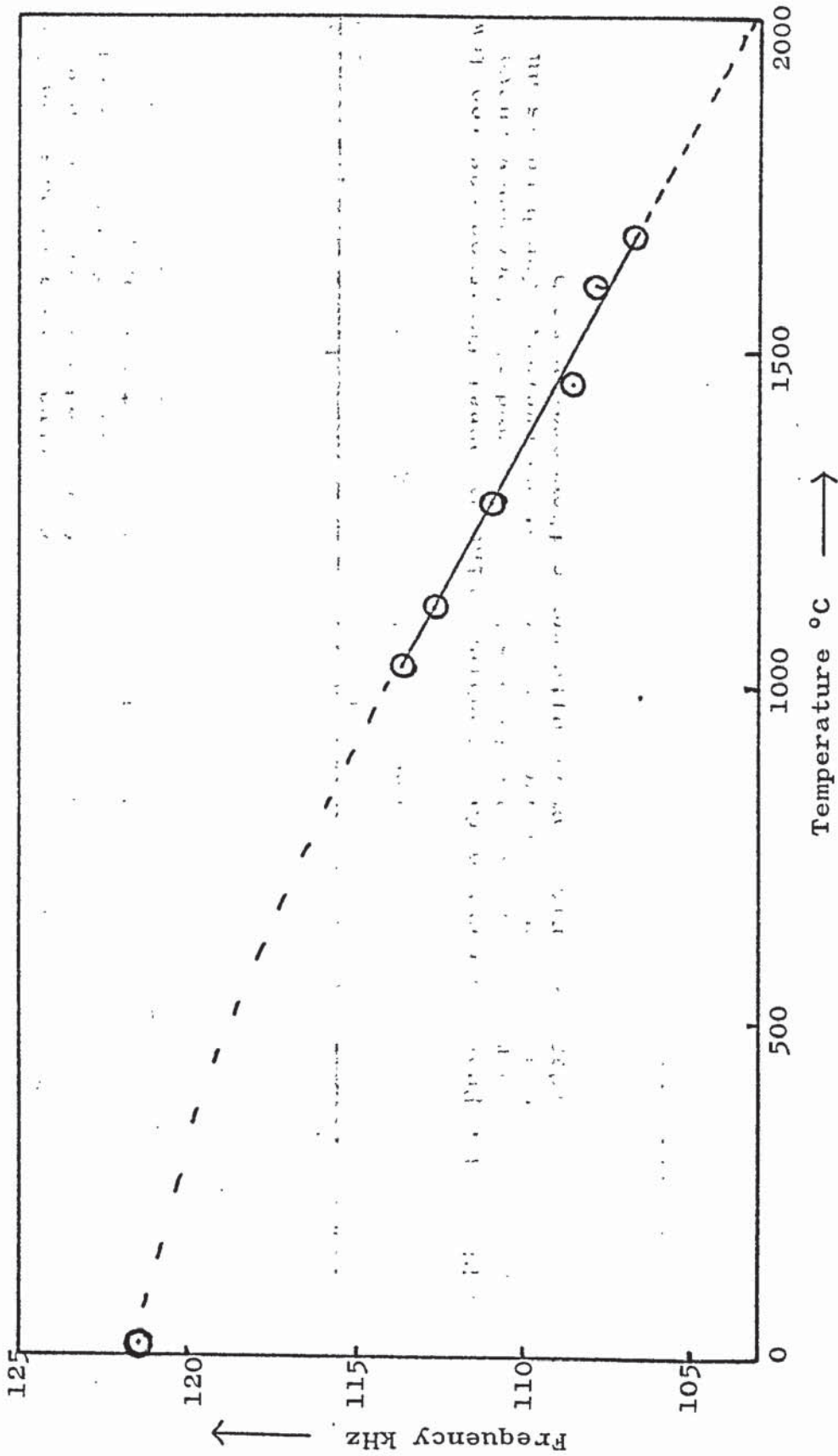
FIGURE 5.13 - Frequency curve for sapphire. The internal friction was too low to measure at 1800°C (i.e. $<2 \times 10^{-3}$), and the frequency curve was reproducible over many temperature cycles. Sapphire is an ideal material for an ultrasonic thermometer probe.

Solvent	Solute	Frequency kHz	Measured peak temp. °C	Calculated peak temp. °C	ΔE from $W_{\frac{1}{2}}$ eV	Q^{-1}_{max} x10⁻³	Calculated interstitial atom %	Peak temp. at 1 Hz °C	ΔE eV	Δm per atom % solute
Fe mild steel	C	100	220	195	0.73	2.0	0.010	35	0.84	1.5 at 200°C
Fe nodular iron ferritic	C	80	~230	195	-	0.5	0.003	35	0.84	1.5 at 200°C
Fe nodular iron pearlitic	C	80	~230	195	~	0.5	0.003	35	0.84	1.5 at 200°C
Tantalum	O	84	445	412	0.84	49	1.07	145	1.11	0.52 at 500°C
Tantalum	N	78	725	637	1.01	33	0.49	350	1.64	1.06 at 500°C
Vanadium 99.7% pure	O	98	390	420	0.96	11.8	0.059	175	0.87	4.4 at 500°C
	N	133	580	560	2.1	18	0.46	260	1.48	1.17 at 500°C

FIGURE 5.14 - Summary table of the Snoek peak measurements. The data in the right hand columns is taken from Nowick and Berry (1972).

Material	Melting Point θ_m °C	ΔE Self-diffusion eV	Frequency kHz	Peak Temp. θ_p °C	T_p/T_m	Q^{-1}_{max}	ΔE from Wert-Marx eV	ΔE from $W_{\frac{1}{2}}$ eV
Cu pure	1083	2.0	27	425	0.5	0.025	1.3	0.7
Al(Dural)	660	1.6	80	470	0.8	0.005	1.4	-
W	3300	6.1	90	1850 appx.	0.6	-	-	-
Re	3170	4.8	53	1700	0.57	0.05	3.7	-
Ta	3000	4.7	77	1900	0.66	-	-	-
Ir	2443	3.5-4.8	49	1900 appx.	0.8	0.09	4.0	4.8

FIGURE 5.15 - Summary table of the grain boundary peak measurements

CHAPTER 6: ULTRASONIC THERMOMETER PROBES

6.1 Introduction

The change in Young's modulus of a material can be used to measure temperature Bell (1966, 1968). Recent developments in ultrasonic thermometry have been fully described by Seth (1974), and only additional information will be recorded here, with reference to material properties. Furthermore, the discussion will be confined to the application of ultrasonic thermometry to the measurement of temperatures in excess of 1500°C.

The frequency variation of a resonator with temperature mainly depends on the change in Young's modulus, though thermal expansion does account for some of the change (typically 5% - see 4.4a). Reproducible readings of temperature, therefore, depends on reproducible changes in Young's modulus. The sensitivity of the thermometer depends on the temperature coefficient of Young's modulus. The precision to which the frequency can be measured in turn depends on the total Q of the resonator. This is a combination of the coupling loss and the internal friction. The theoretical background to material properties has already been given in Chapter 2. The features relevant to ultrasonic thermometry will now be discussed.

6.2 Young's Modulus

Figure 6.2 shows the variation of resonator frequency with temperature for some refractory materials. It can be seen that the change in frequency with temperature above 1000°C

varies between 50 ppm deg.$^{-1}$C for tantalum to 150 ppm deg.$^{-1}$C
for iridium. This gives a variation of the order of 10 Hz
deg.$^{-1}$C at 100 kHz, a change well within the capability of
an electronic measuring system, thus giving a sensitivity
of better than 1 deg. C in all cases. For a few materials
e.g. graphite and silicon nitride, the coefficient is very
small at low temperatures but adequate at high temperatures.
This would mean that the thermometer could not be nsed to
monitor low temperatures during the heating cycle of a
furnace for example.

Attention will now be turned to hysteresis of calibration.
Before the thermometer is first used it must be annealed to
remove the effects of cold work arising from the machining
of the resonator. In the case of a polycrystalline material
the probe should be heated to a temperature in excess of the
recrystallisation temperature to stabilise the grain size.
Unless these procedures are followed there will be a frequency
error of up to 4% giving a "room temperature error" of up to
50 deg.C. All materials will show some degree of hysteresis
under subsequent thermal cycling due to structural changes
occurring in the material. The materials with the lowest
hysteresis are the single crystal ceramics e.g. sapphire
(see figure 5.13, also Southgate 1966). These materials are
the best because there are no grain size effects and in
addition, they have a much lower dislocation concentration.
Polycrystalline metals have moderate amounts of hysteresis
particularly when the temperature is raised above say 1/3 of
the melting point (Seth 1974). From the experiments done on
stabilised zirconia and alumina (Seth 1974) it appears that

polycrystalline ceramics are rather poor in this respect. Possibly this is due to the formation of microcracks on cooling which sinter together again at higher temperatures.

A further consideration is the long term stability of Young's modulus. In the case of the elements or compounds of stable stoichiometry this is unlikely to be a problem. In the case of alloys some evaporation or rearrangement of atoms of the alloying element could cause long term changes in Young's modulus. For this reason the experimental work was directed at pure materials rather than alloys.

6.3 Internal Friction

For precise frequency measurements the Q of the probe must be high. If the crossover method is to be used then $Q_m^{-1} < \frac{1}{2} Q_c^{-1}$ to give a good signal. Thus if $nx = 10$, $Q_c^{-1} = 45 \times 10^{-3}$ and Q_m^{-1} must not exceed 22×10^{-3}. If five oscillations to crossover are used (the smallest practical number) then Q_m^{-1} must not exceed 44×10^{-3}. If the decrement is used to measure the frequency, then these upper limits for Q_m^{-1} do not apply, but the higher the total Q the better the sensitivity (see 4.4a). If Q_T^{-1} is 100×10^{-3} then 0.15% mistuning is required for 10% reduction in signal amplitude. No ordinary grain boundary peak gives a Q_m^{-1} larger than 100×10^{-3}. To summarise it is desirable that Q_m^{-1} should be less than 20×10^{-3} and in no case should it exceed 100×10^{-3}.

The use of the Arrhenius plot of internal friction against

temperature makes it easy to predict the performance of a
particular resonator at different temperatures, and also
allows a certain amount of extrapolation. For example,
considering the case of iridium using the graph in figure
6.3 and the relationships $Q_T^{-1} = Q_m^{-1} + Q_c^{-1}$, $n_o = Q_c/4.55$
the following results can be deduced:-

n_o	max. temperature for $Q_m^{-1} < \frac{1}{2} Q_T^{-1}$	temperature for complete loss of crossover
20	1350	1450
10	1450	1580
5	1580	-

The general internal friction behaviour of materials has
already been described in Chapter 3. Figure 6.2 shows
the internal friction-temperature curves for some refractory
materials. In general the materials with the best Young's
modulus properties have also the best internal friction
properties. The materials can be classified in decreasing
order as follows:

single crystal ceramics

single crystal metals

doped polycrystalline metals

polycrystalline metals

polycrystalline ceramics

The other factors which can affect internal friction are
less important. The amplitude, provided it is less than
10^{-4} does not have an appreciable affect at high temperatures.

An experiment was performed in conjunction with T. N. Seth to check that the high temperature internal friction was independent of amplitude. A molybdenum tuning fork resonator was heated up in a furnace till $n_x = 1.5\ n_o$ (about 1450°C). The transducer coil drive was then reduced from 30 V pk-pk to 10 V pk-pk. There was no perceptible change in n_x showing that there was no significant amplitude dependence of internal friction.

Frequency does not have any gross effects, particularly if the temperature is not near the grain boundary peak temperature, as the frequency dependence is normally weak. There is some evidence to suggest (Seth 1974) that the tuning fork gives rather higher values of Q_m^{-1} than the longitudinal resonators. There are also indications that the larger tuning forks have lower internal friction than the smaller ones — this could be a grain size effect.

It must be remembered that near the melting point the background internal friction is increasing sharply and even if the internal friction was reduced by 50% over the whole range it would provide a relatively modest improvement in performance. For example, in the iridium case mentioned earlier a good crossover would be maintained till 1450°C rather than 1350°C if this was done. In other words, the most important factor is the choice of probe material.

6.4 Other considerations

Some other considerations in selecting a probe material
will be discussed in this section with reference to the
table in figure 6.1.

One obvious requirement is a high melting point. The most
refractory element is carbon (sublimes at 3300°C) and then
tungsten (mpt 3410°C). Of the oxide ceramics the highest
melting is thoria (mpt 3300°C). Stabilised zirconia and
hafnia have melting points of about 2500°C.

A vital requirement is low vapour pressure. The boiling
point gives an indication of this, but for exact data vapour
pressure curves (see Kohl 1962 for the elements) should be
referred to. If the vapour pressure is high then weight
loss will occur, increasing the frequency of the resonator
and therefore affecting long term stability. At vapour
pressures of above 10^{-6} torr the rate of weight loss could
become serious. The rate of weight loss will be reduced
when the probe is enclosed in a gas rather than a vacuum.
A possible way to reduce weight loss would be to surround
the probe with a tube of the probe material, thus keeping
the probe in dynamic equilibrium with its saturated vapour.

The subject of chemical stability must now be considered,
but only probe-gas contact will be discussed here. The
metals oxidise:

$$M + O_2 \longrightarrow M_nO_m \quad \text{(solid or gas)}$$
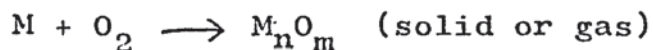
If the oxide is volatile then weight loss will occur. If the oxide is not volatile, then it may form a protective coating, or oxidation inside the solid may occur via cracks causing embrittlement (e.g. tantalum). It is important to realise that there is a continuum of oxidising and reducing conditions and that even traces of oxygen, water or carbon dioxide will cause oxidation in many cases and this will not be prevented by the presence of the reducing agent hydrogen. This is discussed in 4.5. Tungsten and rhenium are protected by hydrogen but tantalum and carbon are not. (See Swalin(1962) for graphs of heats of formation of the oxides).

The oxide ceramics are most stable to oxygen because the equilibrium lies well to the right in the equation:

$$M + O_2 \longrightarrow M_n O_m$$

Under conditions of low oxygen pressure decomposition can occur, particularly with magnesia which can be reduced above 1700°C.

Nitrogen affects some refractories, but less drastically than oxygen, with the exception of tantalum.

At high temperatures some instability can occur in the solid phase if there are impurities present. For example precipitates could dissolve or alternatively segregation of impurities could occur.

Other considerations such as thermal shock, neutron stability and behaviour in carbonising atmosphere have been described by Seth (1974).

6.5 Practical details

In this section the practical details will be discussed in relation to the two probes shown in figures 6.4 -6.6. One is made of iridium and the other of sapphire. These materials were chosen because they were capable of operation in both oxidising and reducing atmospheres up to high temperatures. The sapphire can be used up to 1800°C and iridium up to 2000°C.

One important feature which governs the probe design is the length, which in this case was set at 1 metre. The length criterion formula (see 4.1b) was used.

$$\sum \frac{l_i}{c_i} \geq \frac{1.5n_o}{f}$$

$$\text{or} \quad 1 \geq \frac{1.5n_o C}{f}$$

For the iridium the frequency was made low (about 70 kKz) to reduce the echo from the rod-strip joint. Therefore, n_o had to be small to fulfill the criterion.

Using a mild steel transmission line ($c = 5000$ m s^{-1}) and making $n_o = 7$, $f = 70$ kHz then $l \geq 0.85$m. For the sapphire it was difficult to achieve a small n_o, so the parameters chosen were $n_o = 15$, $f = 170$ kHz then $l \geq 0.85$ m. However, as the crossover does not move out due to the low internal friction at high temperatures, the length can be rather shorter.

Should it be difficult to construct a probe short enough in

mild steel then the use of copper with a velocity of
4000 m s^{-1} will give a 20% reduction in length.

Normally, a joint will have to be made between the probe
material and the transmission line. This has already
been discussed in 4.1c. For the thermometer the junction
echo must be less than 10% and preferably much less than
this. Large junction echoes give signals which affect the
temperature readings and would require individual calib-
ration of each probe unit rather than each material.

The probe units were constructed as shown in figures 6.4-
6.6. The transducer units are rather large because of the
large horshoe bias magnets used. There is an external
knurled wheel to adjust the mechanical tuning.

The units were tested by heating in an oxygen-gas flame
capable of reaching a temperature in excess of 2000°C and
using a 'pyrowerk' optical pyrometer to measure the
temperature (see 4.5d). The calibration curves are
shown in figure 6.2. The sapphire characteristic is
fairly linear being a single crystal but the iridium,
having a grain boundary peak has a knee in the curve.
Polynomial equations were fitted to these results using
a computer package (see Appendix C) with the following
results:

$$\text{sapphire} \quad f = f_0(1.001 - 5.28 \times 10^{-3}\theta - 1.238 \times 10^{-6}\theta^2)$$

$$\text{iridium} \quad f = f_0(1.003 - 9.482 \times 10^{-3}\theta + 2.756 \times 10^{-7}\theta^2$$
$$- 2.962 \times 10^{-10}\theta^3)$$

An important property of a thermometer probe is its long

term stability. When the probe is held at a high temp-
erature evaporation could occur giving a progressive
increase in frequency with time. Some preliminary tests
were done to determine the extent of this in the flame
and the effect was found to be significant above about
1800°C for sapphire and 1900°C for iridium. In other
atmospheres the results would be different, the sapphire
being most stable under conditions of high oxygen pressure
and the iridium most stable at low oxygen pressures.

Another aspect is the "room temperature error". When an
annealed probe is heated to a high temperature and cooled
the temperature reading will be different from the previous
one. This reading will fluctuate in a random manner, as
opposed to the long term changes already referred to, and
is caused by minor structural changes caused by successive
temperature cycles. Sapphire is very good in this respect
and produces fluctuations of up to ±3 deg.C on successive
runs. The iridium probe being polycrystalline gives rather
larger fluctuations of up to ±15 deg.C. It must be
remembered that the high temperature errors are unrelated
to the room temperature errors and may be lower. The
sensitivity in terms of Hz deg.$^{-1}$C is generally better at
high temperatures.

Another test was done under industrial conditions in con-
junction with T.N. Seth. This took the form of a test in
a Dart jet engine combustion chamber at Rolls Royce, Derby,
(see Pelmore 1973, Salt 1973). The purpose was to try the
thermometer under extreme conditions of vibration. Some

slight amplitude modulation of the signal was all that was noticeable. A platinum "Bell" resonator probe, enclosed in a platinum aspirated sheath was heated up to 1300°C. The temperature readings were very satisfactory as compared with a sheathed thermocouple and a gas analysis method.

Material	mpt °C	bpt °C	Temperature for vapour pressure of 10⁻⁶ torr °C	CHEMICAL STABILITY			Young's modulus stability	internal friction	General Remarks
				high oxygen pressure	low oxygen pressure	behaviour with hydrogen			
Carbon (graphite)	(3550)	3800	1900	unstable	v.good	unprotected	good	low	possibly useful for reactor applications
Tungsten	3410	6700	2450	unstable	v.good	protected	good	grainboundary peak	good
Rhenium	3180	5630	2250	unstable	v.good	protected	good	"	good
Tantalum	2996	6100	2250	v.unstable	good	unprotected	good only if pure	"	too good a getter for most applications
Iridium	2442	5300	1850	good	v.good	unprotected	good	"	very good, can be used in flame
Sapphire (Al₂O₃)	2000	2980		v.good	fair	stable	excellent	v.low	very good, can be used in flame
Stabilised Zirconia	2500 (appx)	4000 (appx)		v.good	fair		poor		unsuitable
Zirconium silicate (single crystal)	2500 (appx)			v.good	fair	reduction possible		v.low	a very promising material
Stabilised thoria	2500 (appx)	4000 (appx)		v.good	fair				expected to be similar to stabilised zirconia
Magnesia single crystal	2800	2825		v.good	poor	reduction possible			subject to thermal shock

FIGURE 6.1 - Table of properties of some refractory materials. The materials above the line have been tested by the author.
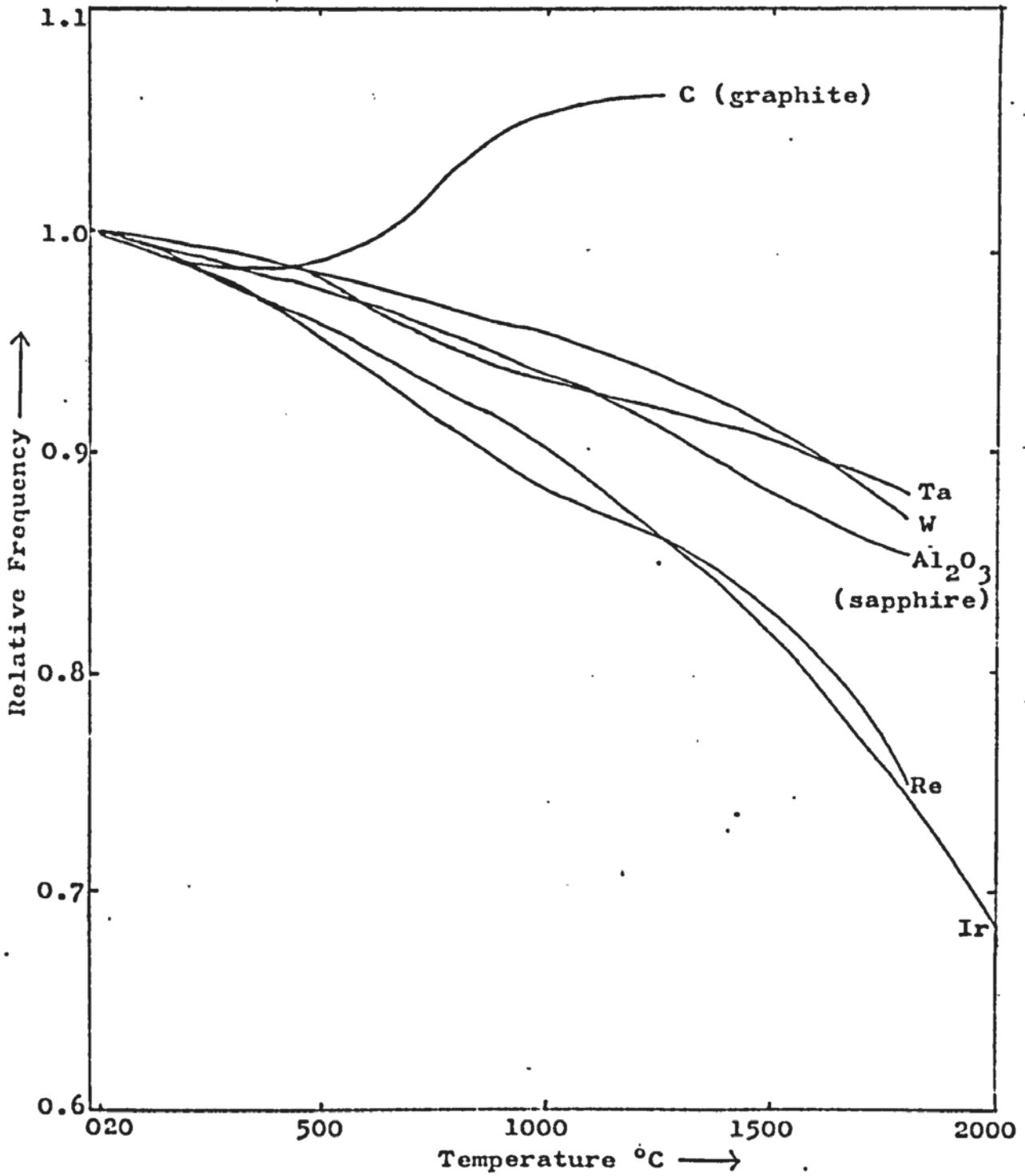
FIGURE 6.2 - Frequency - temperature characteristics
for some materials (Results from Chapter 5).
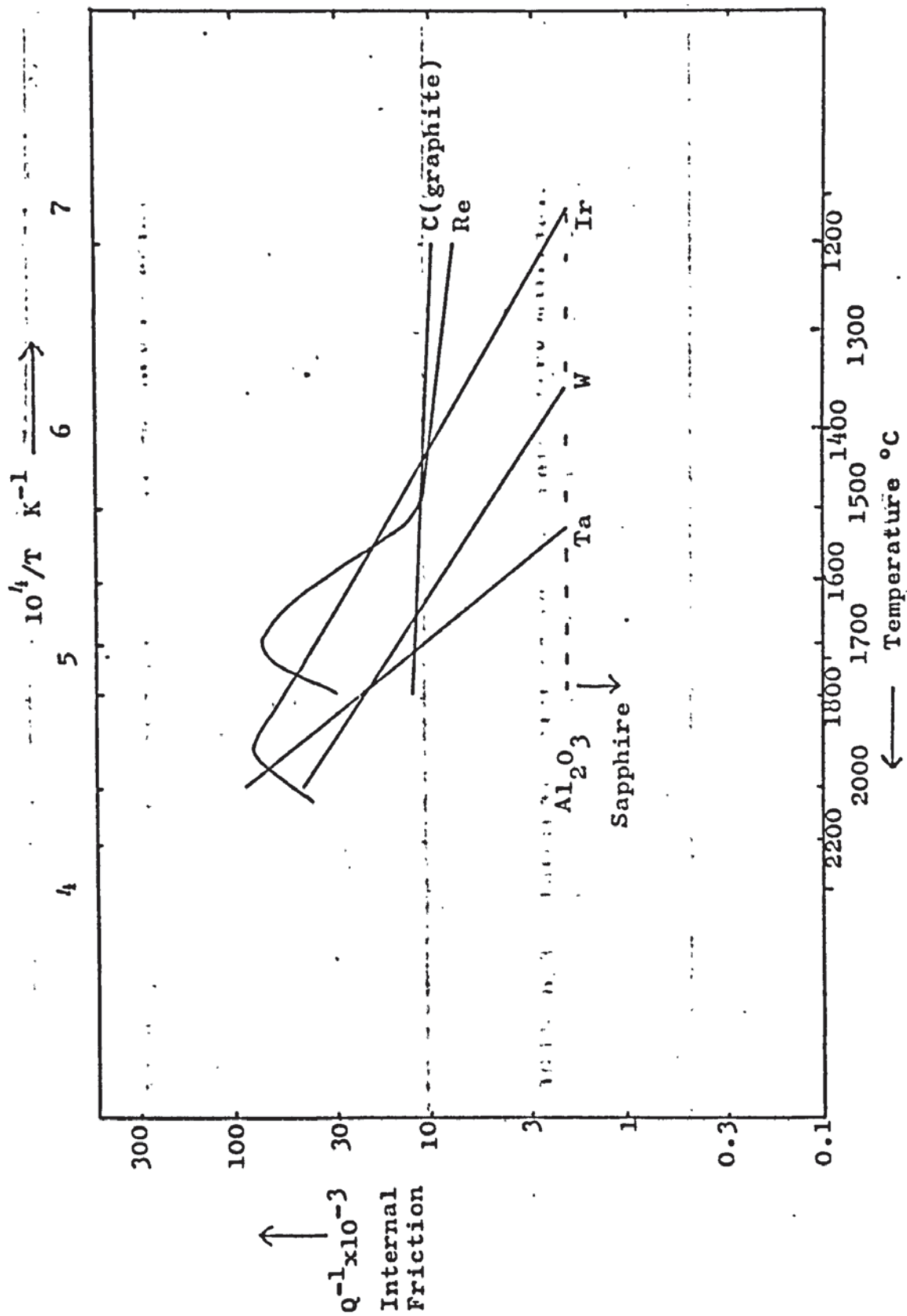
FIGURE 6.3 - Internal friction in some refractory materials (Results from Chapter 5) (Arrhenius plot).
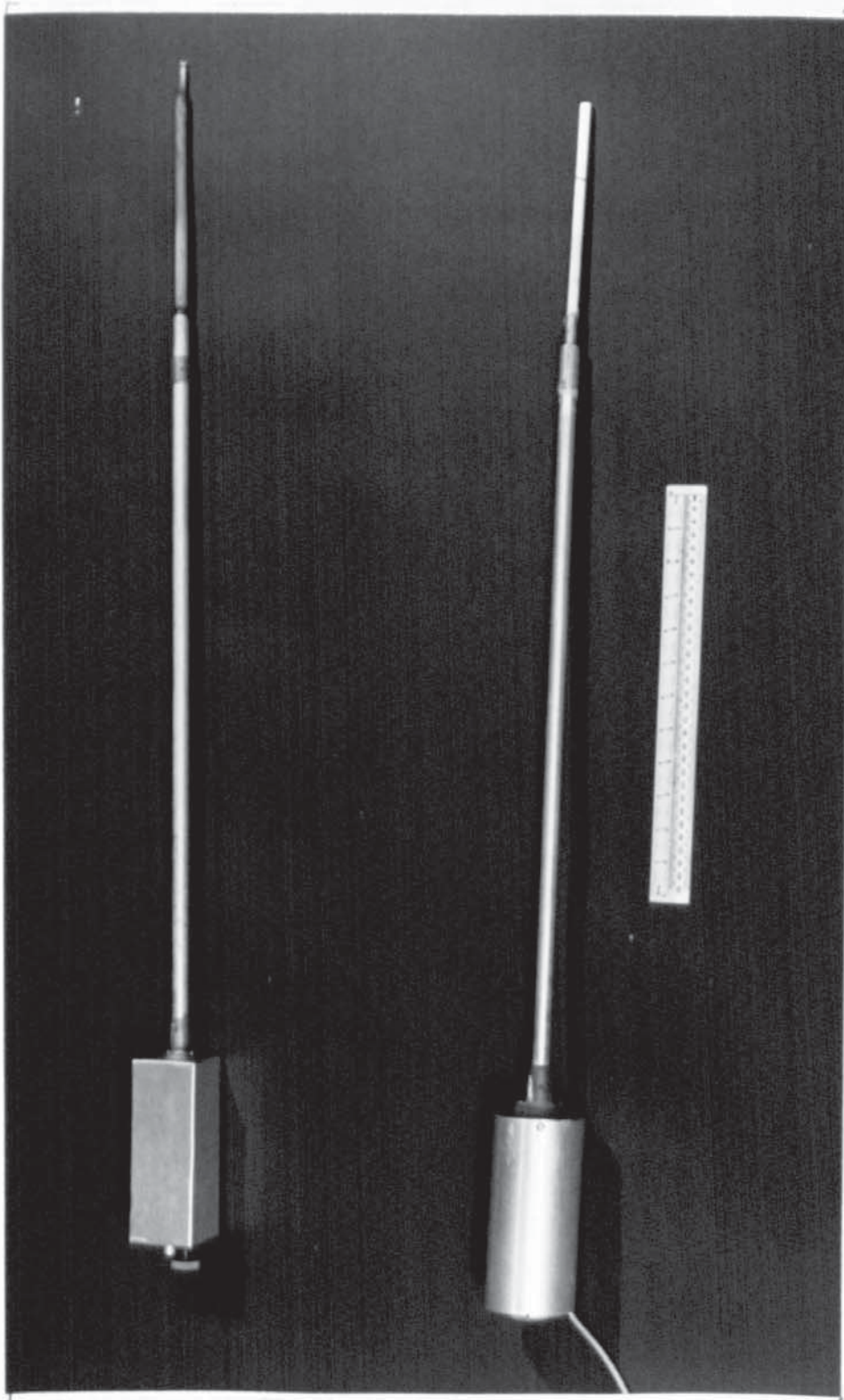
FIGURE 6.4 - The iridium (upper) and the sapphire (lower) ultrasonic thermometer probes. The iridium probe can be used up to 2000°C and the sapphire up to 1900°C. The sapphire probe is sheathed in alumina to protect it from uneven heating and possible melting in a flame.
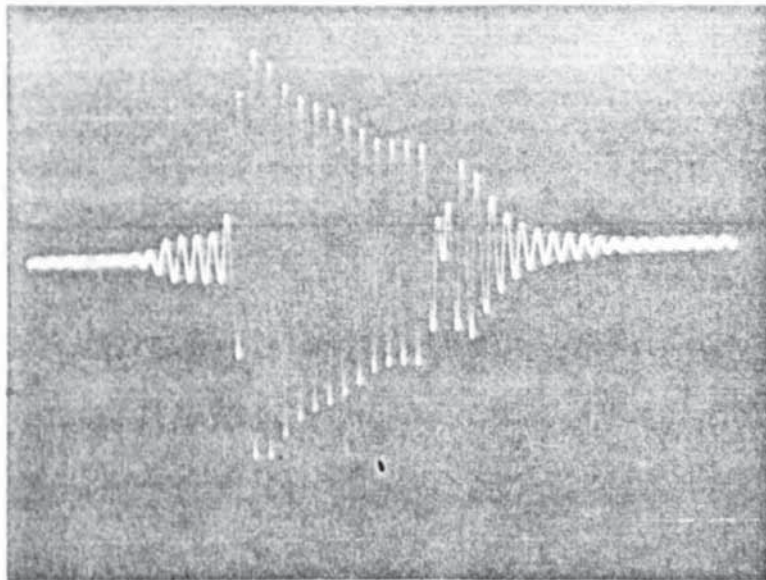
FIGURE 6.5A - Echo signal from
iridium probe at 1750 °C
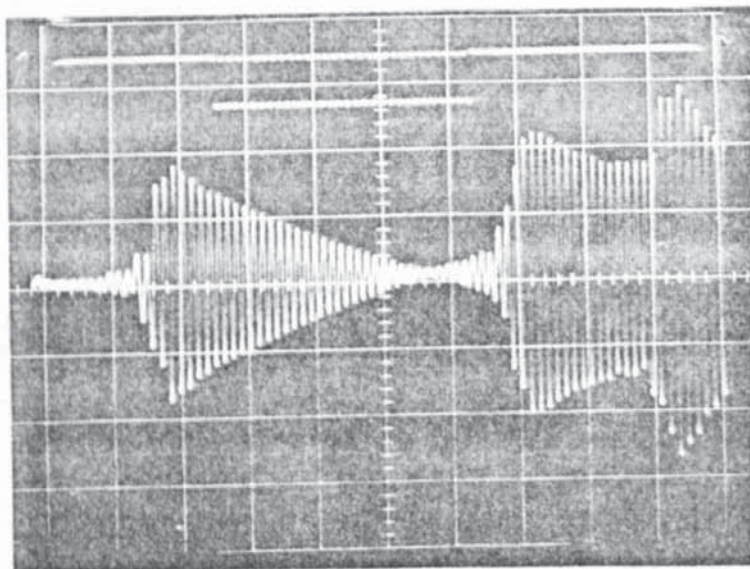
FIGURE 6.5B - Echo signal from
sapphire probe at 1800 °C

1 metre

50 mm

150mm

silver solder

steel end tapered
to 3.0mm x 2.9mm

3.2mm dia
mild steel

50mm

4.8mm
x1.0mm

a = 1.5mm
b = 1.5mm
c = 1.2mm
d = 2.4mm
e = 1.5mm

$f20°C = 70$ kHz $nx = .17$

$f2000°C = 0.68f_{20} = 47.5$ kHz

FIGURE 6.6 - Iridium probe

a = 1.1mm
b = 0.60mm
c = 0.70mm
d = 1.80mm
e = 0.6mm

3mm dia.
Sapphire rod

Recrystallised Al_2O_3
tube 6.5mm OD/4mm ID

soldered joint
max.temp.150°C

silver solder

mild steel
3.2mm dia.

$f_{20°C}$ = 167 kHz n_x = 15
$f_{1800°C}$ = 0.855 f_{20} = 143 kHz

12.5mm OD
aluminium tubing

permendure 3mm dia.

transducer unit mounted
in aluminium tube

150mm

50mm

1 metre

FIGURE 6.7 - Sapphire probe

CHAPTER 7: THE MEASUREMENT OF IMPURITIES IN LIQUID SODIUM

7.1 Introduction

In a sodium cooled reactor hot liquid sodium flows round a
circuit of stainless steel pipes. Impurities in the liquid
sodium, particularly oxygen can cause serious corrosion and
it is important to monitor their concentrations.

There are three main methods available for measuring oxygen
levels of several ppm. In the first, a sample of sodium is
taken, followed by removal of sodium metal by distillation or
amalgamation and chemical analysis of the oxide residue. A
second electrochemical method has the advantage of being
direct reading. A solid electrolyte tube of thoria-yttria
is used and the liquid sodium acts as one half of an oxygen
concentration cell giving an output dependent on the oxygen
concentration (Smith C.A. 1973). However, the electrochemical
stability is rather poor and furthermore, the electrolyte tubes
tend to fracture. In the third type of method a piece of
vanadium is put in the sodium. Oxygen partitions preferentially
in the vanadium with a coefficient in the range 10^3 to 10^5.
The vanadium which will now have a concentration of up to 1%
oxygen can then either be analysed by vacuum fusion (Smith D.L.
1971) or by measurement of the Snoek peak height. The internal
friction can be measured by a torsion pendulum but the use of
the Bell method offers the possibility of a direct 'in situ'
reading instrument because the vanadium resonator can be immersed
in the liquid sodium while an internal friction reading is
being taken.

7.2 Theory

The chemical aspects have been described by Glover (1975) and Smith (1973). The presence of dissolved interstitial gas in the bcc metals vanadium, niobium, tantalum and iron give an internal friction peak (see 2.4) whose amplitude increases with the gas concentration. The relationship is linear for low concentrations but not for high concentrations. The variation of peak temperature with frequency is shown in figure 2.6. To obtain rapid equilibration of oxygen in vanadium, the temperature must be greater than 700°C for a thickness of 0.5mm, otherwise the time taken will be several hours. It can be seen from the diagram that a frequency of 10MHz is required to give an oxygen peak at this temperature, which is beyond the range of the resonant technique. It is envisaged that the vanadium sample would be held in an arm of the sodium circuit whose temperature could be set to 700°C for equilibration and 400°C for taking the reading. Vanadium was chosen as the sensor material for this study because its behaviour with oxygen has been well documented and it gives the highest peak temperature but the metals niobium and tantalum would also be feasible.

One of the complications that might occur with this method is that other sources of internal friction could give a false reading of the peak height. Background damping should be small at temperatures of around 500°C and the grain boundary peaks should occur at much higher temperatures. There is, however, a possibility of interference from the carbon and nitrogen peaks. For vanadium the carbon and oxygen peaks occur at almost the same temperature in the 100 kHz region.

The carbon effect is not expected to be very serious because
vanadium carbide tends to precipitate out, thus not giving
a peak and also the amount of carbon in the sodium may not
be very high. The formation of a carboxide has been discussed
by Glover (1975) who concludes that this would not appreciably
affect the sodium-oxygen equilibrium. For niobium and tantalum
the oxygen peak is well away from the other peaks so this
problem would not arise, but nitrogen and carbon could not be
measured because the two peaks are close and the carbon peaks
are stable. A more serious effect is the interaction between
separate peaks - for example nitrogen and oxygen can give an
interaction peak which will alter the 'background' on the
main peak (Powers 1959).

7.3 Experimental

The experimental determination of the Snoek peaks of oxygen
and nitrogen have already been reported in 5.4.

It remains here to describe the investigation of the effect
of liquid immersion on the resonator technique. When a
normal resonator is in air the damping due to the air is
negligible but when placed in a liquid the damping can be
severe - of the order of 10^{-2} to 10^{-1} or more. Resonators
constructed in the form of a strip vibrating in the plane
have very low coupling to the surrounding medium and corres-
ingly low damping (see Seth 1974 for same data on strip tuning
forks). Some tests were performed to check that the damping
would be low enough to make the project feasible. To avoid
the inconvenience of using liquid sodium, water was used
which has very similar physical properties (density, viscosity

and impedance) and is commonly used in preliminary experiments on liquid sodium technology. Tests were performed with both the strip vanadium longitudinal resonator used for the Snoek peak experiments and a strip tuning fork. The results are tabulated below:

| | Frequency kHz | | oscillations to crossover nx | | liquid damping $Q^{-1} \times 10^{-3}$ | Frequency shift % |
	air	water	air	water		
vanadium strip	51.22	50.98	8	8	<3	0.6
longitudinal	100.84	100.41	17	17	<1.5	0.6
resonator (ρ = 6.3)	146.49	145.36	27	27	<1	0.6
iridium strip	90.2	89.1	5	5	<5	1.2
tuning fork (ρ = 22.4)						

These experiments show that the damping is low enough compared to the Snoek peak height (100 x 10^{-3} 'full scale') to make the method feasible. In all cases the damping was too low to measure with the particular resonator and only an upper limit could be placed on it. It is interesting to note also the small effect on the frequency. The damping decreases proportionally with increasing density ratio.

$$\text{damping} \quad \propto \frac{\text{density of liquid}}{\text{density of resonator}}$$

Liquid sodium has a density of 0.98, while vanadium has a density of 6.3, niobium 8.6, and tantalum 16.6, so that the other two metals under consideration would have even lower damping.

7.4 Discussion of Results

The internal friction data is tabulated in figure 7.1 The
oxygen peak occurred at 390°C using a 97 kHz frequency as
compared to the extrapolated value of 420°C. This peak has
no direct interference from the nitrogen peak at 560°C (see
figure 5.5).

The sensitivity at the low end of the range is approximately
1×10^{-3} for 500 ppm of oxygen in the vanadium, thus giving
a minimum sensitivity of 2×10^{-3} per ppm of oxygen in the
sodium (using Powers + Doyle's data on the relaxation strength
and assuming a partition coefficient of 10^3). The background
damping corresponds to about 1 ppm of oxygen which is quite
acceptable. The grain boundary peak gives no interference at a
temperature of 400°C.

In a final version of the instrument it might be desired to
make the measuring temperature nearer the equilibration
temperatures. Two steps could be taken to secure this.
Firstly, raising the operating frequency to 300 kHz would
raise the peak temperature by 50°C. Secondly, with the
sacrifice of some accuracy readings could be taken on the
side of the peak giving a further 30°C. This would give a
measuring temperature of 470°C as compared to an equilibrium
temperature of 700°C. To raise the measuring temperature up
to 700°C a frequency of 10 MHz is required. This is beyond
the range of the resonator technique but the single pulse tech-
nique could easily be applied in view of the large damping
involved. There might be a problem with background scattering
loss when using this frequency.

The mounting of the probe in the liquid sodium requires some consideration. It is difficult to lead the acoustic signals into a pressure vessel and, therefore, it would be best to mount the transducer inside the vessel. Furthermore, it would be best to have the transducer immersed in the liquid as the use of a gas pocket would cause problems of condensation of sodium vapour. A suggested scheme is shown in figure 7.2. The transducer is at a temperature of 200°C which is quite feasible as a transducer operating at this temperature has already been used for ultrasonic thermometry in the Dragon reactor.

Finally, a few comments will be made about the electronic system. Due to the high damping involved measurements must be made on the decrement. The direct observation method used in this thesis would be unsatisfactory for this application. The measurements could be made semi-automatically by using an adjustable logarithmic timebase on the oscilloscope display. The operator would set a calibrated control knob to give a trapezoidal display. There are two approaches to complete automation (see 4.4e). A completely analogue system could be used to recognise the trapezoidal condition and used to feed a control loop to adjust the logarithmic amplifier time constant. Alternatively, successive pulse heights in the decrement could be measured and the damping computed from this. As the operating frequency would be fixed it would seem unnecessary to control the transmitter frequency though this could be done using the method of Fathimani (1974).

Summary Table   Vanadium   mpt. 1920°C   purity 99.7% (Koch Light)

	Experimental data from this thesis					Data from or calculated from Powers and Doyle (1959)		
	frequency kHz	T_p °C	ΔE from $W_{\frac{1}{2}}$ kJ	Q^{-1} max $\times 10^{-3}$	calc atom %	ΔE kJ	T_p calc from 1Hz data °C	Δm at 220°C zero conc. per atom %
Exp.1 oxygen				<2	<0.01	121	420	1250
nitrogen	133	580	202	18	0.42	143	560	330
Exp.2 oxygen	97	390	92	12	0.060	121	420	
nitrogen	96	570	–	5.4	0.13	143	560	
carbon						114	420	–
hydrogen						38	130	–
Exp.1 grain boundary	133	>800°C				800 expected ($\frac{1}{2}$ mpt) Q^{-1} max		
2 background		400°C		3		Q^{-1} max " 0.1		
		600°C		3-6				

FIGURE 6.1 – <u>Summary table of internal friction in Vanadium</u>
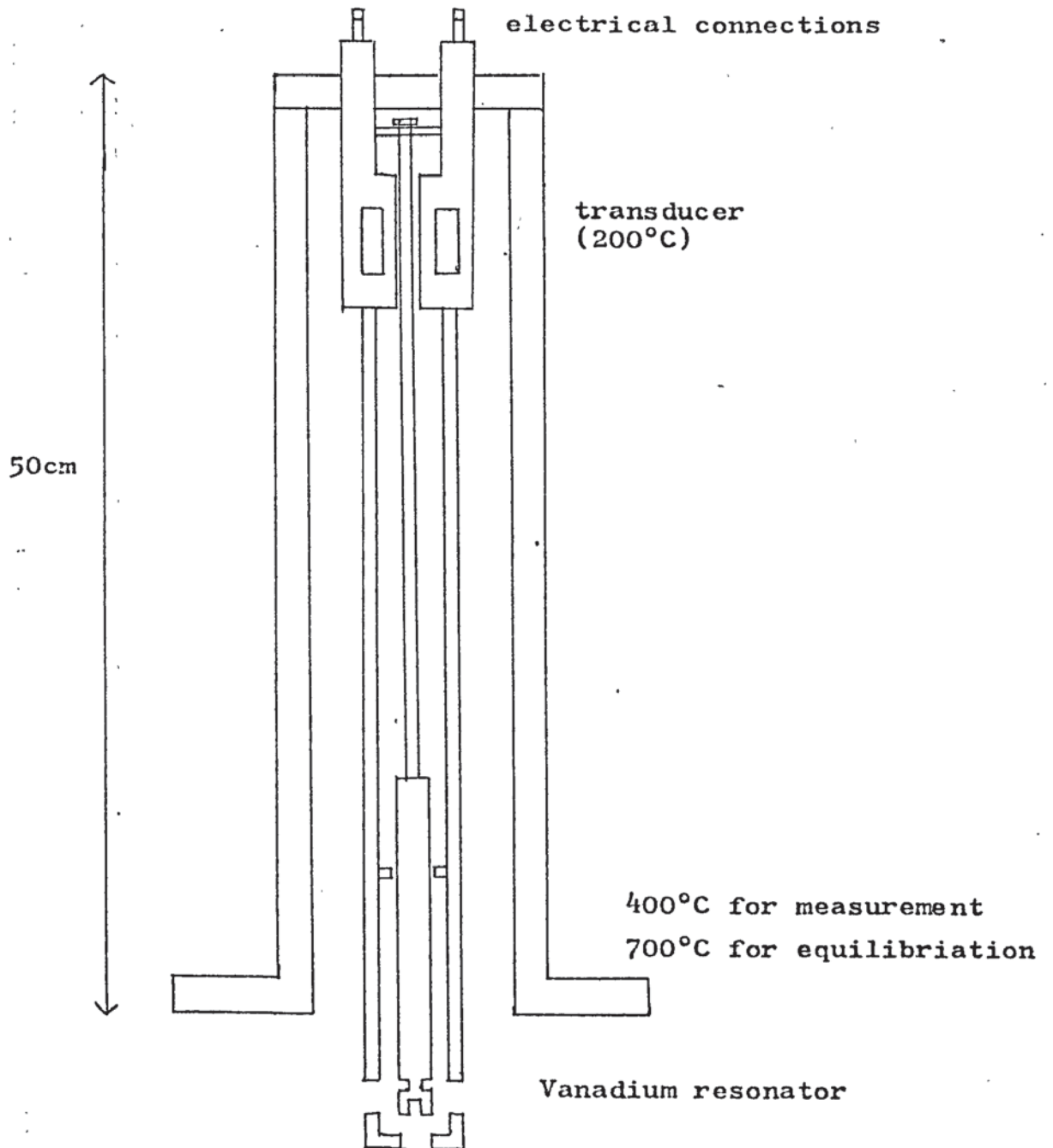
FIGURE 6.2 - Proposed system for mounting Vanadium
probe in liquid sodium circuit.

CHAPTER 8: SUGGESTIONS FOR FURTHER WORK

The metallurgical aspects and technical applications have already been dealt with and comments in this section will be confined to the instrumentation.

Some useful acoustic improvements would be:

1. An integral line type resonator that is capable of operating in several modes for frequency dependence work.

2. A good method of joining strip and rod transmission lines.

3. Modifications to the transducer so that the frequency can be changed more readily. One approach is to use an 'absorbing back', making all the tuning electrical and more easily usable in a totally automatic system.

On the measurement side a useful innovation would be more accurate measurement of the decrement, without recourse to photography which is expensive for a large number of readings. The use of amplitude marker signal would help here. Even more valuable would be complete automation of the internal friction measurement. The decrement part of the echo should be used because it is always available. A digital method would be to measure the peak values of successive oscillations and to compute the Q factor from the results. A possible analogue method might be to make use of a swept gain amplifier to maintain the decrement at constant amplitude via a control loop. The internal friction could then be computed from the amplifier control signal and the frequency.

APPENDIX A: Acoustics

1.   Joints in transmission lines

The theory of a transmission line containing a thin layer of different impedance such as occurs in a soldered or adhesive joint is given below:-

$$Z_2 \text{ thickness } t = \lambda \frac{\theta}{2\pi}$$
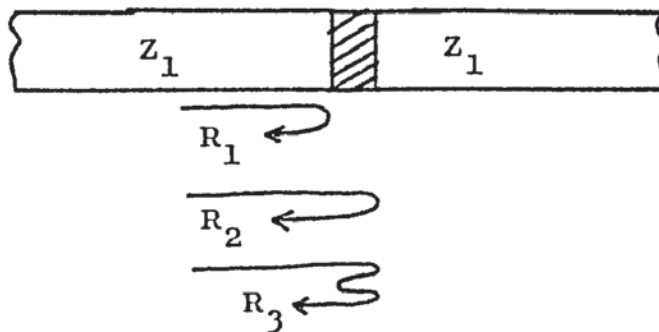
For the successive reflections shown on the diagram,

$$R_1 = -J \qquad R_2 = +JT^2 e^{i\theta} \qquad R_3 = J^3 T^2 e^{i2\theta}$$

$$R_n = J^{(2n-3)} e^{i(n-1)\theta}$$

where, $J = \dfrac{Z_1 - Z_2}{Z_1 + Z_2}$ reflection coefficient

transmission coefficient $T = 1 - J^2$

Hence:

junction echo amplitude $E = -J + JT^2 e^{i\theta}(1 + J^2 e^{i\theta} + J^4 e^{2i\theta}$

$$+ \cdots)$$

This geometric progression sums to give;

$$E = -J + \frac{JT^2 e^{i\theta}}{1 - J^2 e^{i\theta}}$$

Separating the real and imaginary parts;

$$E = -J + \frac{JT^2(\cos\theta - J^2) + iJT^2 \sin\theta}{1 - 2J^2 \cos\theta + J^4}$$

when θ is small $\sin \theta \simeq \theta$ $\cos \theta \simeq 1 - \tfrac{1}{2} \theta^2$

$$E \simeq -J + \frac{JT^2(1-J^2-\tfrac{1}{2}\theta^2) + iJT^2\theta}{1 - 2J^2 + J^4 + J^2\theta^2}$$

If we neglect θ^2 terms, the real part can be neglected and

$$|E| \simeq \frac{J\theta}{(1-J^2)}$$

putting the impedance ratio $Z_2/Z_1 = \beta$

$$J = (1-\beta)/(1+\beta)$$

$$E \simeq \frac{1-\beta^2}{4\beta} \theta$$

We may use this to calculate the echo at a silver solder and an araldite joint.

For silver solder $\rho = 9400 \ \mathrm{kg \ m^{-3}}$, $c = 3000 \ \mathrm{ms^{-1}}$

    steel $\rho = 7800 \ \mathrm{kg \ m^{-3}}$ $c = 5200 \ \mathrm{ms^{-1}}$

$$\beta \ \therefore \ Z_2/Z_1 = 0.70$$

To make $E = 0.01$, $\theta = \dfrac{0.04\beta}{1 - \beta^2} = 5.5 \times 10^{-4}$

    at 100 kHz in the solder $\lambda = 30\mathrm{mm}$

    so $t = 0.26 \ \mathrm{mm}$

This is quite a feasible thickness in practice and this level of performance corresponds to a carefully made joint.

Now consider the araldite joint;

For araldite $c \simeq 1800 \ \mathrm{ms^{-1}}$ $\rho \simeq 1200 \ \mathrm{kg \ m^{-3}}$

$$\beta = Z_2/Z_1 = 0.053$$

Following through the same steps as before;

$t = 6.1\mu m$ for $E = 0.01$ at 100 kHz.

This is not a physically realisable thickness for a metal ceramic joint. In practice, the thickness is likely to be about twenty times this ($t \sim 0.1mm$) giving a 20% echo as was reported in 4.1c.

2. Seth tuning fork resonators

Details of the Seth resonators are given below. The first table shows the designs in dimensionless form and the second table shows the physical dimensions of the resonators used in the experiments described in chapter 5. Generally fixed dimensions of the slot widths b, e were used for easy machining.
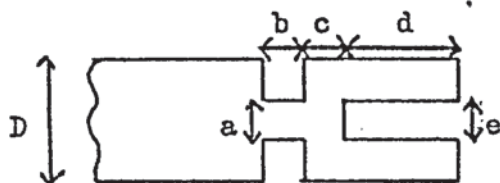
R = rod   S = strip   D = diameter of rod or width of strip

TABLE 1

Ref. letters	a/D	b/D	c/D	d/D	e/D	frequency parameter $(fD/C)\times 10^2$	coupling n_o
RA	0.345	0.188	0.225	0.560	0.315	3.57	15
RB	0.345	0.188	0.320	0.660	0.200	5.70	25
SA	0.315	0.315	0.250	0.610	0.315	5.02	10
SB	0.370	0.315	0.245	0.475	0.315	7.75	10
SC	0.370	0.315	0.168	0.675	0.315	6.50	30
SD	0.400	0.275	0.665	0.365	0.275	10.0	10
SE	0.315	0.211	0.375	0.545	0.211	7.60	6

TABLE 2

Material	Co ms^{-1}	type	D mm	a mm	b mm	c mm	d mm	e mm	f kHz	no.
Graphite	2800	R	3.0	1.0	0.60	1.03	2.80	0.60	89	7
Sapphire	9900	R	3.0	1.1	0.60	0.70	1.80	0.60	167	15
Iridium	4850	S	4.75	1.50	1.50	1.16	2.20	1.50	83	10
Tantalum	3300	S	4.75	2.73	0.50	1.81	2.00	1.2	85	7
Rhenium	5000	S	4.75	1.50	1.50	1.16	2.3	1.50	66	6
Silicon nitride	~5700	S	4.0	1.58	1.10	1.45	2.66	1.07	130	10

FIGURE A.3. - STRIP-ROD JOINTS

Silicon nitride   5.5mm Al rod Si_3N_4 4mm x 0.8mm

3mm steel rod

top view
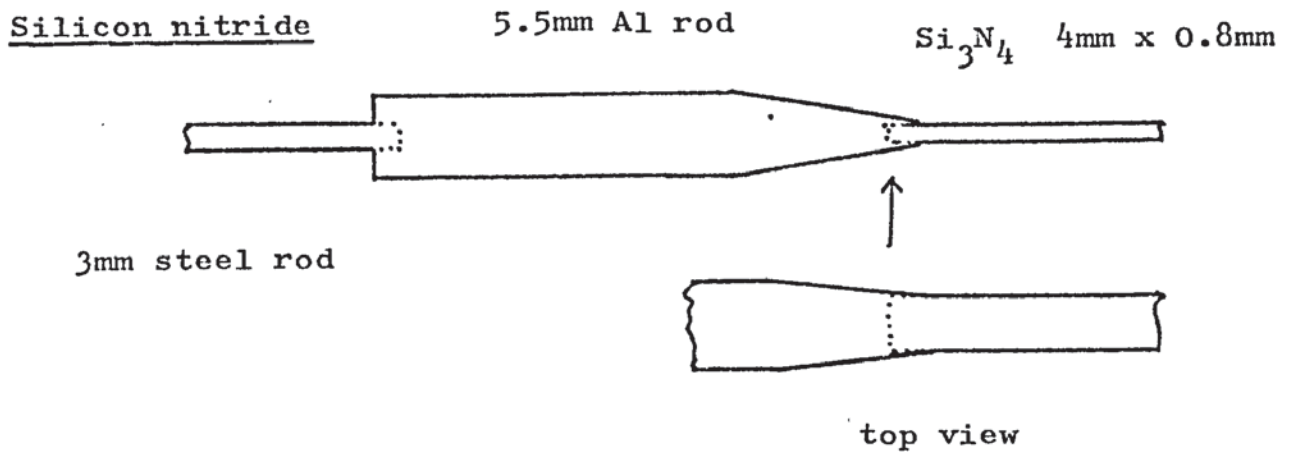
Suggested rod-strip matching section

constant area of cross section
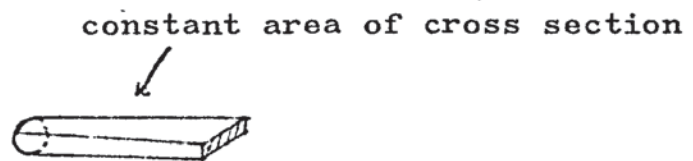
APPENDIX B - ELECTRONICS

The principles of the electronic design have been discussed elsewhere (e.g. Pelmore 1971, Seth 1974, Sharp 1974). The full circuit diagrams are shown on the following pages.

Some instruments use a presettable number of oscillations in the burst but this only allows counting of oscillations to crossover. In this instrument a separate reference signal with a variable number of oscillations was used so that oscillations in the decrement can be counted. Some important practical points are:

1. The supply to the oscillator must be very stable to give good frequency stability. Therefore, the supply should be derived via a separate line.

2. To avoid oscillator crosstalk on 'receive' attention should be paid to decoupling and earth returns. As an additional precaution the oscillator may be switched off on 'receive'.
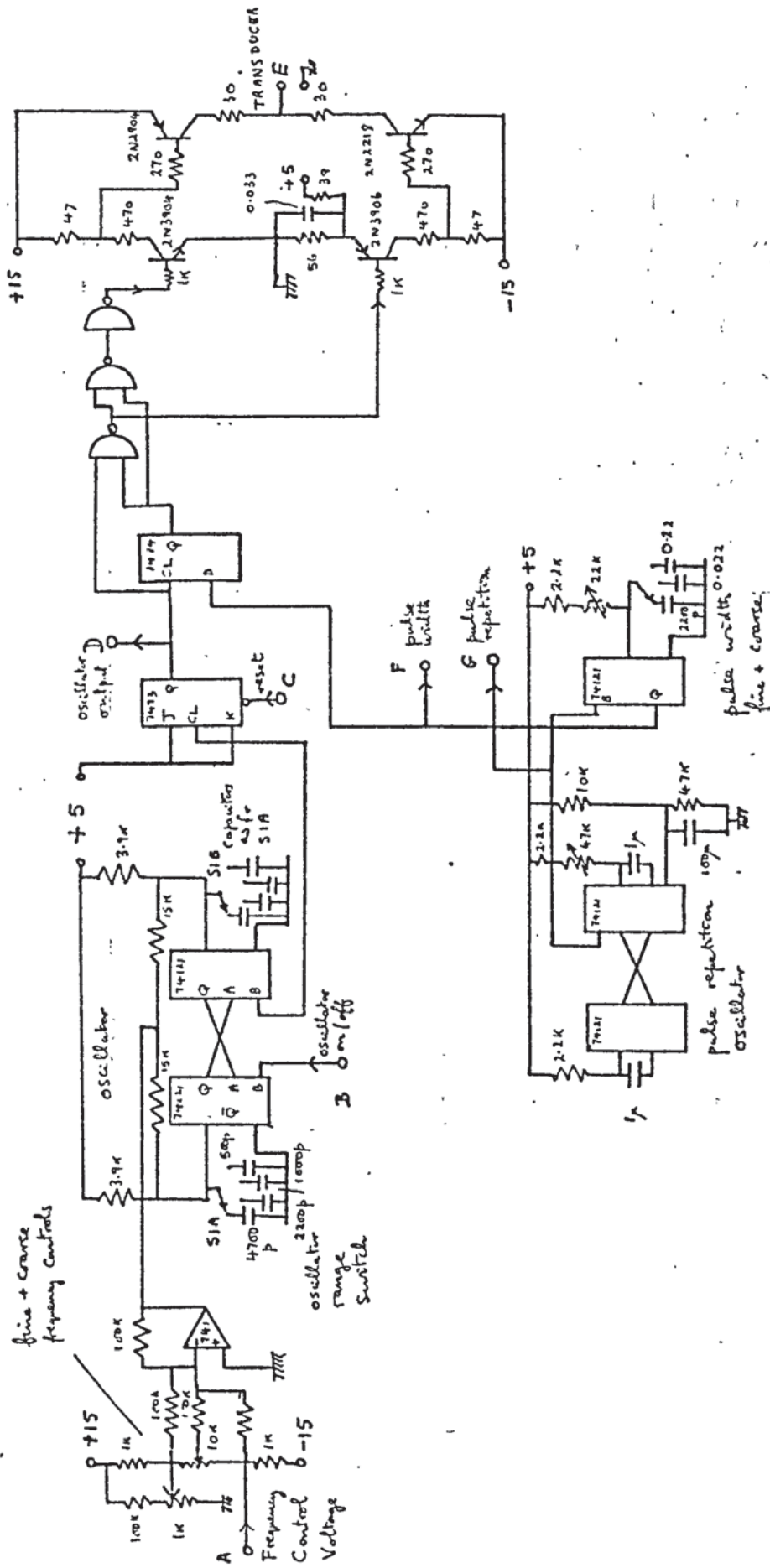
FIGURE B1 - THE TRANSMITTER CIRCUIT
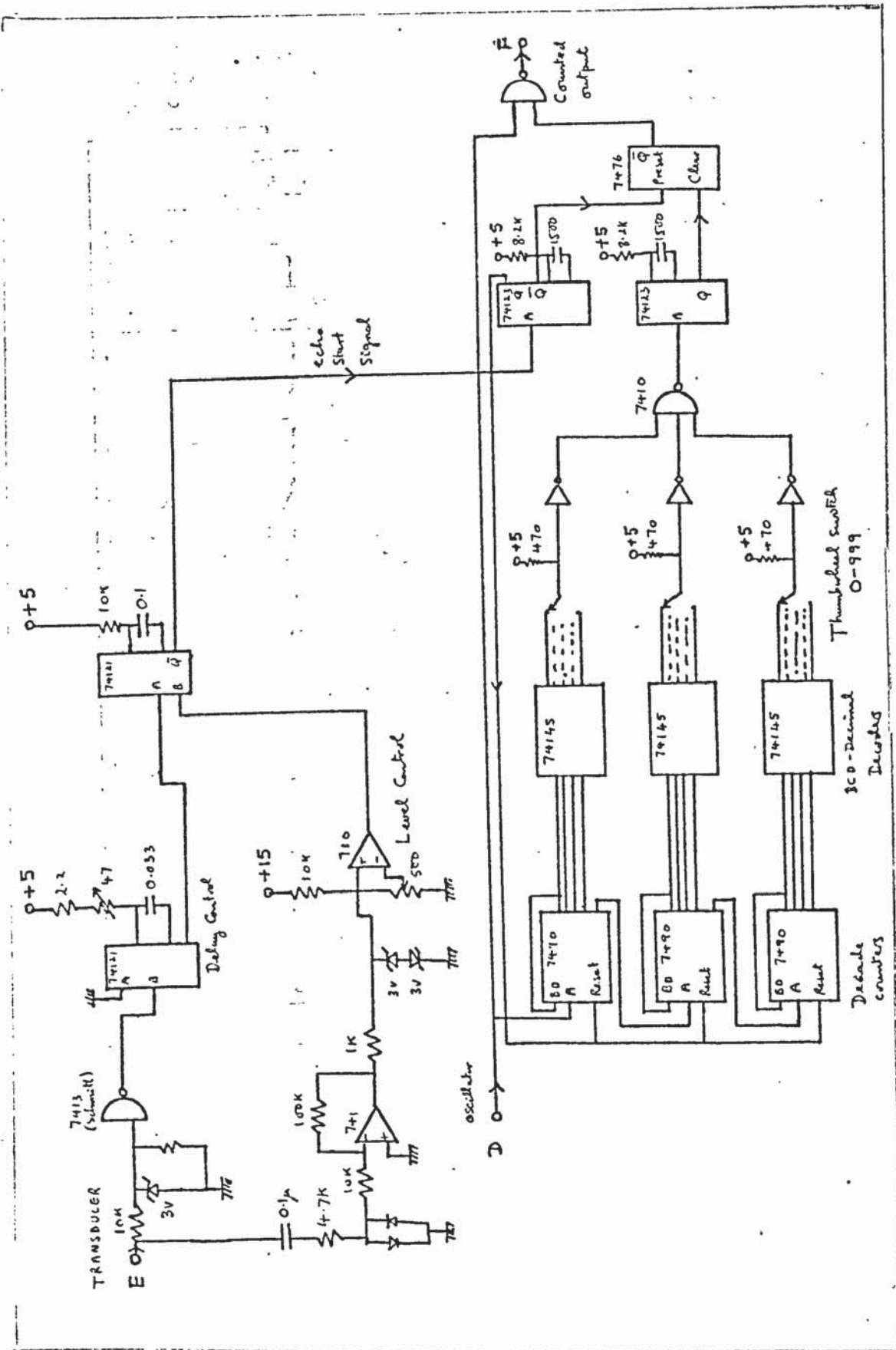
FIGURE B2 — THE REFERENCE COUNTER CIRCUIT
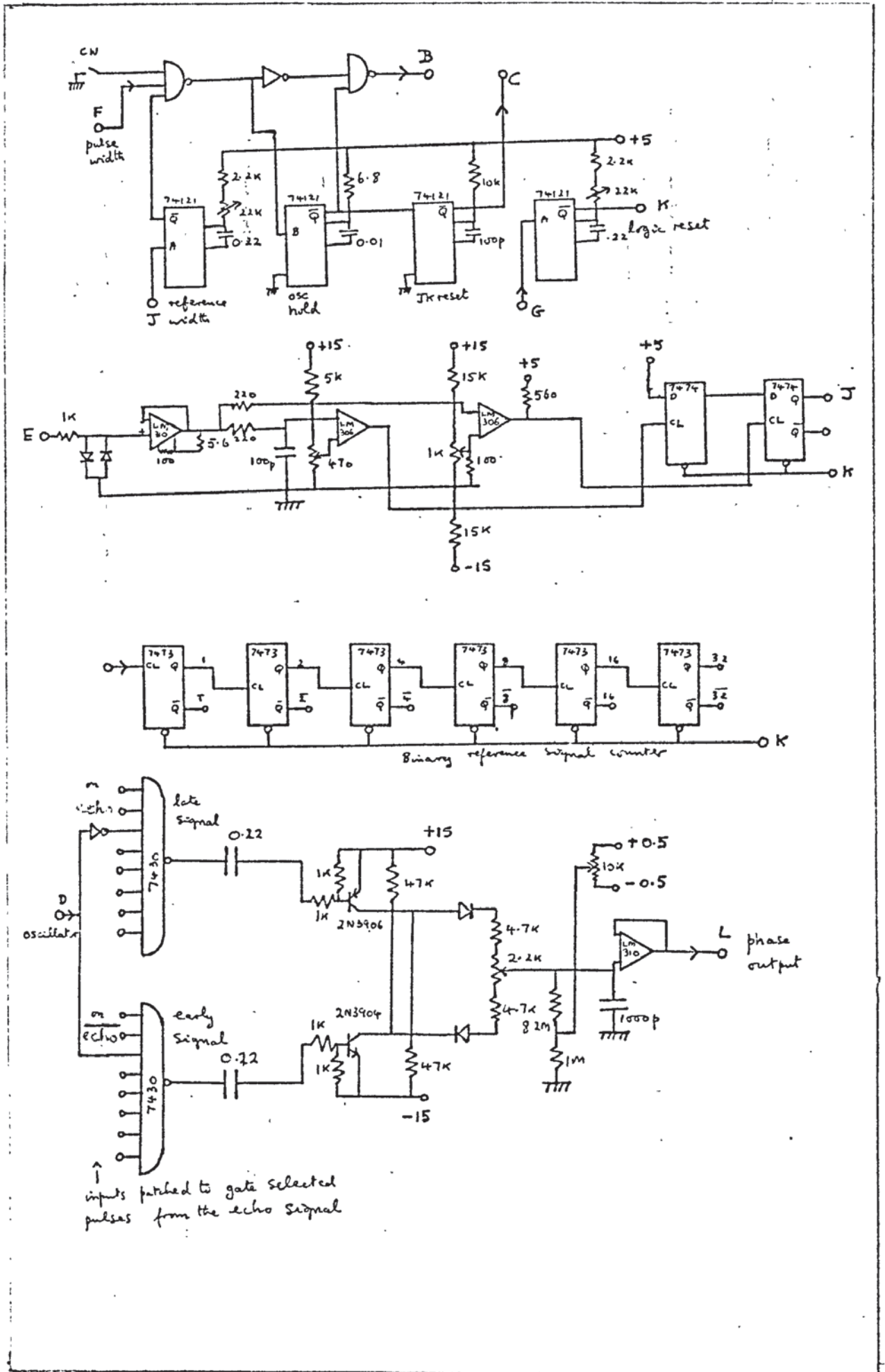
FIGURE B3 — THE PHASE DETECTOR AND AUTOMATIC TRACKING CIRCUIT

APPENDIX C - MATHEMATICS NOTES

The calibration graphs in figure 4.12 were calculated from equations 3.12-3.14. By feeding in values of Q_m^{-1} for set values of Q_c^{-1} the values of nx, Q_T^{-1} can be calculated. From this (Q_T^{-1} - nx/4.55) can be calculated for the values of Q_m^{-1}. The other calibration graphs were calculated in a similar way.

The curve fitting for the ultrasonic thermometer was done using University of Aston Application Program UA01. This program fits a polynomial using the method of least squares.

BIBLIOGRAPHY

Note:

The bibliography was compiled from Nowick and Berry (1972),
De Batist (1972), Mason (1964-1966), Boodson (1972) and
various other sources.

The following abstracting journals were found useful:

> Ceramics Abstracts
> High Temperature Bulletin
> Metals Abstracts (key words internal friction,
> grain boundary)

The use of the indexing term 'ultrasonic attenuation' did not
produce much useful material. The Science Citation Permuterm
Index was used to some extent but was laborious as it produced
much unwanted information ('noise').

ASHCROFT, W. 1973 Proc.Brit.Ceram.Soc. No.22, 169-179. Mechanical
properties of silicon nitride at elevated
temperatures.

BAKER, G. S. 1962 J.Appl.Phys. 33, 3366-3368. Dislocation motion
and asymmetric resonance peaks.

BARRAND, P. 1966 Acta.Met. 14, 1247-1256. Grain boundary
relaxations in iron chromium alloys.

BELL, J.F.W. 1957 Phil.Mag. 2, 1113-1120. The velocity of sound
in metals at high temperatures.

BELL, J.F.W. 1960 Dragon Report No.5, Elastic properties of graphite.

BELL, J.F.W., DOYLE, B.P., SMITH, B.S. 1966, J.Sc.Inst. 43, 28
An instrument for the measurement of acoustic
pulse velocity and attenuation in a solid probe.

BELL, J.F.W., U.K. Patent No.54637/66.

BELL, J.F.W., 1968 Ultrasonics, 6, 11-14. A solid acoustic
thermometer.

BELL, J.F.W., PELMORE, J.M. 1971 Wireless world, 77, 532 (1971).
Digital method of obtaining frequency difference.

BELL, J.F.W., NOBLE, A.E., SETH, T.N. 1973. Ultrasonics, 11, 178-181.
Graphical displays of acoustic properties of solids.

BELL, J.F.W., PELMORE, J.M. 1974 Proc. 8th International Congress on Acoustics (Abstract only) Elasticity and internal friction measurements on refractory materials at high temperatures.

BELL, J.F.W., SHARP, J.C.K. 1974 Proc. Thermophysical properties at high temperatures. Orleans. The precision measurement of elastic constants over wide temperature ranges.

BELL, J.F.W., FATHIMANI, A. 1974, International Colloquium on high temperature in pile thermometry. Patten, Holland. Ultrasonic thermometry using resonance technique.

BELL, J.F.W., SETH, T.N. 1974 Patent applied for (Tuning fork).

BELL, J.F.W., JOHNSON, A.C., SHARP, J.C.K. 1975 JASA, 57, 1085 1093. A pulse echo method of investigating the properties of mechanical resonators.

BELYAKOV, A.A. et al, 1967 Phys. Metal Metallog. 23, 306-312.

BERLEC, I. 1970 Met. Trans. 1, 2677-2688. The effects of impurities and heat treatment on the internal friction of tungsten at high temperatures.

BESHERS, D. N. 1967 Advances in materials research 1, 193-214. Anelastic techniques: Iron, a case history.

BOODSON, K. 1972 Non ferrous metals: A bibliographical guide. MacDonald technical and scientific.

BRANDON, D. G. et al, 1964 Acta. met. 12, 813-821. A field ion microscope study of atomic configuration at grain boundaries.

BRIGGS, J.Z., BEER, R. 1971 High temperature-high pressure 3, 363-409. Arc Cast molybdenum base TZM alloy, properties and applications.

BROWN, H.L., ARMSTRONG, P.E. 1963, J.Sci. Inst. 34, 636-639. Young's modulus measurements above 2000°C.

BROZEL, M.R., LEAK, G.M. 1973 5th Int. Congress on internal friction and ultrasonic attenuation in solids (abstract only) Zener relaxations in alloys.

CARNAHAN, R. D., BRITTAIN, J.O. 1963 J. Appl. Phys. 34, 3095-3104. Point defect relaxation in rutile single crystals.

CAMPBELL, I.E., SHERWOOD, E.M. ed. 1967 Wiley. High temperature materials and technology.

CHICK, B.B. et al. 1960 JASA, 32, 186-193. Ultrasonic attenuation unit and its use in measuring attenuation in alkali halides.

CLARK, C. A. 1961 JASA 33, 7. Magnetostrictive transducer.

CORDEA, J. N., SPRETNAK, J. W. 1966 Trans. Met. Soc. AIME 236, 1685. Grain boundary relaxation in four high purity fcc metals.

DATSKO, O.I., PAVLOV, V.A. 1963 In 'relaxation phenomena in metals and alloys' p.174. Consultants bureau, New York.

DE BATIST, R. 1972 North Holland, Internal friction and structural defects in crystalline solids.

DE MORTON, M.E., LEAK, G.M. 1966, Acta Met. 14, 1140-1142. High temperature relaxation peaks in copper and gold.

DEN BUURMAN, R., WEINER, D. 1971 Scrip Metall. 5, 753-756. Internal friction in annealed copper between 150 and 1500 Hz.

DETWILER, D. P. et al. 1968. Rev.Sc.Inst. 39, 1727-30. Apparatus for precision measurement of internal friction.

DIGNUM, R. 1964 Am. J. Phys. 32, 507-519. Brief review of ultrasonic attenuation with some emphasis on work at ultra high frequency.

DREYFUS, R. W., LAIBOWITZ, R. B. 1964 Phys. Rev. 135, A1413-1422 Anelastic and dielectric relaxation due to impurity vacancy complexes in NaCl crystals.

DYKSTRA, L. J. 1947 Philips research report 2, 357.

ELYUTIN V. P. et al. 1968 Vysokotempartum Materialy 218-229. The temperature dependence of the internal friction of molybdenum wire at moderate and elevated temperatures.

FATHIMANI, A. 1974 Internal report.

FELTHAM, P. 1971 Scrip Metall. 5, 395. On the background internal friction in crystalline solids.

FIRLE, T. E. 1969 Carbon 7, 595. Torsional damping in pyrolytic graphite.

FOEX, M. 1968 Science of ceramics 3, 217-245 (Academic press) Investigations of structure transformations in refractories above 2000°C.

FOX, C. W., SLAUGHTER, G. M. 1964 Welding Journal, 43, 591-597. Brazing of ceramics.

FLOCKTON, S. J., HICKMAN, T. J. 1974 8th Int. Cong. on Acoustics. 2, 722. Comparison of the transient and steady state behaviour of acoustic resonators, (summary only).

FRIEDEL, J. Metaux Corr- Irid. 36, 148.

GALKIN, A. A. et al. 1969 Phys. Metal Metallog. 28, 187-189. Internal friction of recrystallising aluminium.

GLOVER, G. M. 1975 CERL report no.RD/L/N48/75. An ultrasonic method for the measurement of oxygen in sodium: An experimental investigation.

GRANATO, A., LÜCKE, K. 1956 J. Appl. Phys. 27, 583-593. Theory of mechanical damping due to dislocations.

GRANATO, A., LÜCKE, K. 1967 In 'Physical Acoustics' 4A.
Ed. W.P. Mason. Acad. Press. Vibrating string
model of dislocation damping.

GUBERMAN, H. D., BESHERS, D. N. 1968 Acta Metall. 16, 167-176.
Amplitude dependent internal friction and
induced modulus defect in purified iron.

HALL, I. H. 1968 Nelson Deformation of solids.

HENNICKE, H. W., SCHLEUSSLER, H. 1968 Ber. Deut. Keram. Ges. 45
234-238. High temperature rheology of ceramic
materials II. Temperature dependence of internal
friction and modulus of elasticity of basic re-
fractories.

HEARMAN, R.F.S. 1946 Rev. Mod. Phys. 18 The elastic constants
of anisotropic materials.

HOFFMAN, R. A., WERT, C., 1966 J. Appl. Phys. 37 237-240.
Anisotropy of the Snoek phenomenon in niobium.

HOPKINS, I. L., KURKJIAN, C. R. 1965 In Physical Acoustics 2B
Ed. Mason, W.P. Acad. Press. Relaxation spectra
in solid polymers and glasses.

HORNSTRA, J. 1965 Science of ceramics 2, 191-202 (Academic press).
Dynamic properties of grain boundaries.

HUB, D. R. 1962 Proc 4th Int. Conf. Acoustics (Copenhagen).
Measurement of velocity and attenuation constant
of sound in iron up to the melting point.

HU, H. (Ed) 1972 The Nature and behaviour of grain boundaries.
Plenum.

JOHNSON, A.C.J. 1971 M.Sc. Thesis. University of Aston.
Apparatus for ultrasonic measurement.

KALUGIN, B. A., MIKHAILOV, I. G. 1961 Sov. Phys. Acoust. 7,
154-158. A new ultrasonic method of measuring
the elastic properties of solids at high
temperatures.

KALUGIN, B. A., MIKHAILOV, G. 1966 Sov. Phys. Acoust. 12, 91-92.
Ultrasonic method for measuring the elastic
moduli of metals at temperatures up to 3000°K.

KAYE, G.W.C., LABY , 1974 Longmans. Tables of physical and
chemical constants.

KÊ, T. S. 1947 Phys. Rev. 71, 533-546. Experimental evidence
for the viscous behaviour of grain boundaries
in metals.

KÊ, T. S. 1948 Phys. Rev. 74, 9. Internal friction of carbon
and oxygen in tantalum.

KÊ, T. S. 1950 J. Appl. Phys. 21, 414. Internal friction of
metals at very high temperatures.

KÊ, T. S., ZENER, C. 1950 Symposium on the plastic deformation of crystalline solids, p.185, Mellon Inst., Pittsburgh.

KIKUCHI, Y. 1969 Magnetostrictive transducers. Sendai, Japan.

KLEIN, M. J. 1967 J. Appl. Phys. 38, 167-170. Diffusion coefficient of nitrogen in chromium.

KOHL, W. H. 1967 Reinhold; Handbook of materials and techniques for vacuum devices.

KOLSKY, H. 1967 Dover Stresswaves in solids.

KOSTER, W. 1948 Z. Metallk. 39, 1-9. The temperature dependence of the modulus of elasticity of pure metals.

LEAK, G. M. 1961 Proc. Phys. Soc. 78, 1520. Grain boundary damping. I Pure Iron.

LLOYD, D. E. 1968 Special Ceramics 4, 165 (Brit. Ceram. Res. Assoc.) High temperature properties of reaction sintered and hot pressed silicon nitride and their relation to fabrication conditions.

LÜCKE, K., ROTH, G. 1971 Scrip Metall. 5, 757-758. Comments to internal friction in annealed copper between 150 and 1500 Hz.

LYNNWORTH, L. C. 1967 NASA report no.CR-72395.

MAHIL, K. S. 1975 Ph.D. Thesis. University of Aston.

MASON, W. P. 1950 Academic Press. Piezo electric crystals.and their application to ultrasonics.

MASON, W. P. 1958 Physical acoustics and the properties of solids.

MASON, W. P. 1964-1974 Academic Press. Physical Acoustics;
        1A Methods and devices (1964)
        2B Properties of polymers and non linear acoustics
        3A Effects of imperfections (1966)   (1965)

McCLEAN 1957 OUP Grain boundaries in metals.

McCRUM, D. et al. 1967 Wiley. Anelastic and dielectric effects in polymeric solids.

MERLIN, J. et al. 1969 J. Nucl. Mat. 24, 300-309 (in French) Internal friction in graphites.

MORSE, P. M. 1948 McGraw Hill. Vibration and sound.

MOSBY, E. G. 1969 Ultrasonics 7, Practical acoustic thermometer.

MURRAY, M. J. 1968 J. less common metals. 15, 425-435. Mechanical
relaxations in polycrystalline molybdenum,
tantalum and iridium at high temperatures and
low frequencies.

NOWICK, A. S., BERRY, B. S. 1972 Academic Press. Anelastic
relaxation in crystalline solids.

PELMORE, J. M. 1971 M.Sc. Thesis, University of Aston. An instrument
to measure elastic properties at high temperatures.

PELMORE, J. M. 1973 University of Aston, Elec.Eng.Dept.
Report on ultrasonic thermometer test at
Rolls Royce Ltd.

PETERS, D. T. et al. 1964 Trans. AIME 230, 530-540. Some
observations of grain boundary relaxation in
copper and copper-2pct cobalt.

PINES, B. Ya., KARMAZIN, A. A. 1966 Phys. Metal. Metallog. 22,
172-174. Activation energy of the 'high
temperature background' of internal friction
in various metals.

POLDER, D. 1945 Philips Res. Rep. 1, 5.

POPE, M. et al. 1973 5th Int. Congress an internal friction
and ultrasonic attenuation in crystalline
solids. Internal friction associated with
substitutional interstitial solute atom
clusters in Fe-Va-N alloys and other ternary
nitrogen ferrites. (Abstract only).

POSTNIKOV, V. S. 1957 Phys. Metal. Metallog. 4, 344-351. The
temperature dependence of internal friction
in several pure metals.

POSTNIKOV, V. S. 1971 Ind. Lab. USSR, 37, 1608. High temperature
system for continuous recording of internal
friction and elastic modulus.

POWERS, R. W., DOYLE, M. V. 1957 J. Appl. Phys. 28, 255-258.
Carbon tantalum internal friction peak.

POWERS, R. W., DOYLE, M. V. 1959 J. Appl. Phys. 30, 514-524.
Diffusion of interstitial solutes in Gp V
transition metals.

PUGH, J.W., 1967 In 'High temperature materials and technology'.
Campbell Ed. Wiley. Mechanical properties
at high temperatures.

REED-HILL, R. E. 1964 Van Nostrand. Physical metallurgy principles.

SADOLAH, M. 1974 M.Sc. thesis, University of Aston.

SALT, D. 1973 Rolls Royce (Derby) report. Physics section.

SCHNITZEL, R. H. 1959 J. Appl. Phys. 30, 2011-2012. High temperature damping of tantalum, rhenium and tungsten.

SCHOEK, G. et al. 1964 Acta Met. 12, 1466-1468. The activation energy of high temperature internal friction.

SETH, T. N. 1974 Ph.D. Thesis, University of Aston. Ultrasonic pyrometer for industrial applications.

SHAFFER, 1964 Plenum, New York. High temperature materials.

SHAPOVAL, B. I. 1964 Phys. Metal. Metallog, 18, 142 Internal friction of metals at high temperatures.

SHARP, J.C.K. 1974 Ph.D. Thesis, University of Aston. A theoretical and experimental investigation into the spectra of selected resonators.

SHESTOPAL, V. O. 1967 Phys. Metal Metallog. 25, 148-155. Frequency dependence of the internal friction of tungsten at high temperatures.

SHESTOPAL, V. O. 1968 Phys. Metal Metallog. 26, 176-180. High temperature rheological properties of platinum.

SMITH, D. L. 1971 Nuclear Technology 11, 115-119. An equilibration method for neasuring low oxygen activities in liquid sodium.

SMITH, C. A. 1973 J. less common metals, 31, 345-358. Solubility of oxygen in vanadium.

SMITHELLS, C. J. 1967 Butterworth. Metals reference book.

SNOEK, J. L. 1941 Physica 8, 711-733. Effect of small quantities of iron on the elastic and plastic properties of iron.

SOCINO, G. et al. 1967 Proc. Brit. Ceram. Soc. 9, 73-81. Relaxation processes in single crystal UO_2.

SOUTHGATE, P. D. 1959 J. Sci. Inst. 36, 284-287. Measurement of low values of internal friction at elevated temperatures.

SOUTHGATE, P. D. 1966, J. Phys. Chem. Solids 27, 1263-69, Internal friction due to Cr, Fe in magnesium oxide.

SPRIGGS, R. M. 1969 In 'Mechanical and thermal properties of ceramics', NBS. Inelastic deformation of oxide ceramics.

SPRIGGS, R. M. et al. 1964 J. Amer. Ceram. Soc. 47, 323-327. Mechanical properties of pure dense alumina as a function of grain size.

STARR, C. D. et al 1953 Trans. Amer. Soc. Metals, 45, 275-285.
Effect of alloying elements on grain boundary
relaxation in alpha solid solutions of aluminium.

STEPHENS, R.W.B., BATE, A. E. 1966 Arnold. Acoustics and
vibrational physics.

SWALIN, R. A. 1962 Wiley. Thermodynamics of solids.

SYRE, R. 1968 Technivision Services. A bibliography of refractory
metals.

TIETZ, T. E., WILSON, J. W. 1967 Arnold. Behaviour and properties
of refractory metals.

THREADER, R., FELTHAM, P. 1973 5th Congress on internal friction
and ultrasonic attenuation in crystalline solids.
The Bauschinger effect in polycrystalline copper
and α brasses in the temperature range 90-300°K.

TOULOUKIAN, Y. S. 1967 Macmillan. Thermophysical properties of
high temperature solid materials 1.

TRUELL, R., ELBAUM, C., CHICK, B. B. 1969. Academic Press.
Ultrasonic methods in solid state physics.

VAN HOUTEN, G. R. 1959, Bull Amer. Ceram. Soc. 38, 301-307.
A survey of ceramic to metal bonding.

WACHTMAN, J. B., LAM, D. G. 1959, J. Am. Ceram. Soc. 42, 254-266.
Young's modulus of various refractory materials
as a function of temperature.

WACHTMAN, J. B., CORWIN, W. C. 1965 J. Res. Nat. Bur. Std. 69A,
457-460 Internal friction in ZrO_2 containing CaO.

WEGEL,R,L., WALTHER, H. 1935 Physics, 6, 141-157. Internal friction
dissipation in solids for small cyclic strains.

WERT, C., MARX, J. 1953 Acta Meta. 1, 113-115. A new method for
determining the heat of activation for
relaxation processes.

WILLIAMS, T. M., LEAK, G. M. 1967 Acta. Metal. 15, 1111. High
temperature relaxation peaks in copper and
aluminium.

ZENER, C. 1941 Phys. Rev. 60, 906-908. Theory of the elasticity
of polycrystals with viscous grain boundaries.

ZENER, C. 1948 U. of Chicago Press. Elasticity and anelasticity
of metals.